k - version of finite element method: A new mathematical and computational framework for BVP and IVP

by

K.S.Surana

Dean E. Ackers Distinguished Professor

University of Kansas, Department of Mechanical Engineering

3013 Learned Hall, Lawrence, KS, 66046, USA

Ph: (785) 864-2988; Fax: (785) 864-5254; email: kssurana@ku.edu

J.N.Reddy

Distinguished Professor and Wyatt Chair

Texas A & M University, Department of Mechanical Engineering

210 Engg./Physics Building Office Wing, College Station, TX, 77843, USA

Ph: (979) 862-2417; Fax: (979) 862-3989; email: jnreddy@shakti.tamu.edu

A progress report submitted to

DEPARTMENT OF THE AIR FORCE

Air Force Office of Scientific Research (AFRL)

Directorate of Mathematics & Space Sciences

Computational Mathematics Program

Attn: Dr.Fariba Fahroo, AFOSR/NM

4015 Wilson Blvd, Room 713

Arlington, VA 22203-1954

Under Grant number: F49620-03-1-0298 and F49620-03-1-0201

for the work completed during the Third and last year of the grant

REPORT DOCUMENTATION PAGE

Form Approved
OMB No. 0704-0188

1. REPORT DATE *(DD-MM-YYYY)*	2. REPORT TYPE	3. DATES COVERED *(From - To)*
22-01-2007	Research	(Sept. 2005) - (Sept. 2006)

4. TITLE AND SUBTITLE
k-Version of Finite Element Method : a New Mathematical and Computational Framework for BVP and IVP

5a. CONTRACT NUMBER

5b. GRANT NUMBER
F-49620-03-1-0298 and F-49620-03-1-0201

5c. PROGRAM ELEMENT NUMBER

6. AUTHOR(S)
Karan. S. Surana
J.N.Reddy
Peter. W. TenPas

5d. PROJECT NUMBER

5e. TASK NUMBER

5f. WORK UNIT NUMBER

7. PERFORMING ORGANIZATION NAME(S) AND ADDRESS(ES)
University of Kansas, Dept. of Mechanical Engineering, Lawrence, KS, 66045
Texas A &M University, Dept. of Mechanical Engineering, College Station, TX, 77843

8. PERFORMING ORGANIZATION REPORT NUMBER

9. SPONSORING/MONITORING AGENCY NAME(S) AND ADDRESS(ES)
Air Force Office of Scientific Research, Computational Mathematics Program
Dr. Fariba Fahroo, 4015 Wilson Blvd, Room 713, Arlington, VA 22203-1954

10. SPONSOR/MONITOR'S ACRONYM(S)
AFOSR

11. SPONSOR/MONITOR'S REPORT NUMBER(S)

12. DISTRIBUTION/AVAILABILITY STATEMENT
UU Approved for public release. Distribution is unlimited

AFRL-SR-AR-TR-07-0087

13. SUPPLEMENTARY NOTES

14. ABSTRACT

Work performed during the third year of the Grant: (i) Preliminary research on fluid-solid interaction, development of mathematical models, computational methodology in hpk framework. (ii) Preliminary research towards development of concepts for a priori and a posteriori error estimation in hpk mathematical and computational framework. (iii) Re-discretizations, moving meshes and solution mapping strategies and associated computational infrastructures for BVPs and IVPs in hpk framework (Appendix A contains technical report on this work).

15. SUBJECT TERMS
hpk framework, variational consistency, variational inconsistency, higher order global differentiability, fluid-solid interaction, error estimation, re-discretization, moving meshes

16. SECURITY CLASSIFICATION OF:			17. LIMITATION OF ABSTRACT	18. NUMBER OF PAGES	19a. NAME OF RESPONSIBLE PERSON
a. REPORT	b. ABSTRACT	c. THIS PAGE			Karan S. Surana
U	U	U	UU	126	19b. TELEPHONE NUMBER *(Include area code)* 785-864-2988

1 Summary

This report summarizes the work completed during the third year of the three year AFOSR Grant no. F 49620-03-1-0298 to the University of Kansas, Lawrence, KS (K.S.Surana, PI) and Grant no. F 49620-03-1-0201 to Texas A & M University, College Station, TX (J.N.Reddy, PI). The development of *hpk* mathematical and computational framework for all boundary value problems (BVPs) and initial value problems (IVPs) regardless of their origin or fields of application has been the main thrust of this research. Previous two reports have presented the mathematical and computational developments for BVPs and IVPs in *hpk* framework in which the order of approximation space k defining global differentiability of order $(k-1)$ has been pointed out as an independent computational parameter in addition to h and p. Successful applications of this new *hpk* framework have been presented in various areas of continuum mechanics to demonstrate the benefits of using this framework as apposed to h, p framework used currently in the finite element processes.

The thrust of the work completed during the third year of these grants have been in the following areas:

(I) Preliminary research towards development of mathematical models for fluid-solid interaction and associated computational infrastructure in *hpk* mathematical framework

(II) Preliminary research work towards development of concepts for *a priori* and *a posteriori* error estimation in h, p, k mathematical and computational framework

(III) Rediscretization, moving meshes and solution mapping strategies and associated computational infrastructure for BVPs and IPVs in *hpk* framework

While the works in (I) and (II) are aimed towards preliminary concepts and methodology developments, the research in (III) is at a higher maturity level and has already been applied to many BVPs and IVPs, but some work is needed to streamline the algorithms for applications to practical problems of interest. Details for each of the three areas of research are presented in the following.

2 Fluid-solid interaction

The preliminary work dealing with general methodology and development of mathematical models for fluid-solid interaction problems (BVPs and IVPs) is presented in this section.

2.1 Introduction

The thrust of this research is to develop basic concepts and methodologies towards development of a new mathematical and finite element computational framework based on h, p, k for fluid-solid interaction BVPs and IVPs. For all fluid-solid interaction problems, a single mathematical model describing all phases of the physics (i.e. solid, liquid, or

gas) is essential in the development of a rigorous mathematical framework that naturally translates into a sound computational infrastructure in which no additional ad-hoc adjustments and treatments are needed. The interface behaviors are intrinsic in the mathematical models hence, details at solid-liquid, liquid-gas or solid-gas interfaces are resolved naturally and accurately. This methodology eliminates the need for constraint equations at the interfaces to couple the behaviors of diverse media in complex interaction problems. It also eliminates inter-element flux problems and problem dependent treatments associated with moving meshes and re-discretizations.

While the mathematical models are generally derived using conservation laws, constitutive equations, and equations of state, the specific forms of the governing differential equations (GDEs) vary significantly. First-order systems derived using auxiliary variables and auxiliary equations, decomposition of total stress into elastic and viscous parts for polymer flows, use of vorticity and stream functions are a few examples of commonly used approaches. When using the Galerkin method with weak form, some forms of GDEs may be advantageous over the others. The current mathematical framework based on h, p finite element processes employs local approximations of class C^0 in space as well as in time. Convergence of the numerical errors is measured in terms of Lebesgue measures or L_2-type global norms. Consequently, the differentiability requirements may be violated at sets of measure zero in the discretizations. This results in flexibility but at the expense of local (inter-element) accuracy and local convergence. The proposed framework utilizes the theory of continuous and differentiable functions in conjunction with Sobolev spaces and hence it is possible to incorporate the desired global differentiability in the design of the computational process due to k, the order of the approximation space.

In this research it is demonstrated that the GDEs in their strong forms (higher order systems) are highly meritorious over all others. Additionally, use of fundamental variables such as density, velocities, temperature is preferred over others (mathematical quantities) in that such variables naturally lead to simplicity in defining boundary and initial conditions. Use of the strong form of GDEs also eliminates redundancies and inconsistencies that may arise when constructing local approximations. Higher order systems of GDEs, however, require approximations in higher-order spaces that have many additional benefits [1-4] as shown subsequently.

In Section 2.2, we present a brief summary of currently used finite element approaches, followed by the development of mathematical models, mathematical and computational approach in Sections 2.3-2.5.

2.2 Background

2.2.1 Methods of Approximation

In designing finite element processes one utilizes mathematical models to construct integral forms [5-7]. For example, consider the operator equation $A\varphi - f = 0$ in Ω, where A is a differential operator, φ is the dependent unknown, and f is the data. We assume that the solution φ exists and is unique. We construct $\int_\Omega (A\varphi - f)v \; d\Omega = 0$. Here v is an arbitrary weight (test) function that vanishes on the part Γ_1, where $\varphi = \varphi_0$. Utilizing this integral form we can distinguish between the following weighted-residual methods:

1. *Petrov-Galerkin method (PGM)*: In this method the weight function is an independent function $v = \psi \neq \delta\varphi_h$, with $v = 0$ on Γ_1 if $\varphi = \varphi_0$ on Γ_1.

2. *Galerkin method (GM)*: If φ_h is an approximation of φ, the Galerkin method seeks φ_h such that $\int_\Omega (A\varphi_h - f)v \, d\Omega = 0$ with $v = \delta\varphi_h$. This can be written as $B_g(v, \varphi_h) = l_g(v)$.

3. *Galerkin method with weak form (GMWF)*: In this approach, we set $v = \delta\varphi_h$ and transfer some of the differentiation from φ_h to $\delta\varphi_h$ to obtain $B_{gw}(\delta\varphi_h, \varphi_h) = l_{gw}(\delta\varphi_h)$.

4. *Least squares method (LSM)*: In this approach we define the residual E by $E = A\varphi_h - f$, construct a functional $I(\varphi_h) = (E, E)_\Omega$, and determine φ_h by minimizing $I(\varphi_h)$. Thus, $\delta I(\varphi_h) = 0$ provides the necessary condition from which φ_h is determined, and $\delta^2 I(\varphi_h) > 0$ provides the sufficient condition.

2.2.2 Variationally Consistent Finite Element Processes

The methods of approximation described above are classical methods in which the domain of definition Ω is not discretized. The major drawback of these methods is that it is very difficult to construct global approximation functions for arbitrary domains and boundary conditions [7-10]. In FEM, we utilize these methods over a discretized domain $\Omega^T = \cup_e \bar{\Omega}^e$ in which $\bar{\Omega}^e$ is a closure of Ω^e, an element. In this approach, the global approximation $\varphi_h = \cup_e \varphi_h^e$, where φ_h^e is the restriction of φ_h over Ω^e, and is referred to as the local approximation. While the local differentiability of φ_h can be controlled by the degree of local approximation p, the global differentiability of φ_h depends entirely on the order k of the approximation space. Thus, k is an independent parameter in finite element processes in addition to h and p. The need for global differentiability arises from the requirements of continuity and differentiability of φ over Ω which is intrinsic in the physics (see Figure 1 and Sections 3.2 and 3.3). The issues of non-smooth data and applied disturbance often leading to singular BVP and IVP can also be easily resolved in h, p, k framework [11].

In the GM, GMWF and PGM, we convert a system of differential equations into an algebraic system using integral forms and the approximation φ_h. In the current mathematical framework, we must establish, on a problem by problem basis, as to which possible choices of h and p ensure well-posedness. This issue is resolved in the current research by establishing a link between the integral forms and the elements of the calculus of variations. Calculus of variations deals with extrema of functionals which are often integrals.

Let $I(\varphi_h)$ be a functional. Then based on calculus of variations [5-7], $\delta I(\varphi_h) = 0$ provides the necessary condition from which φ_h is determined and $\delta^2 I(\varphi_h)$ provides an extremum principle or sufficient condition that establishes uniqueness of φ_h obtained from $\delta I(\varphi_h) = 0$. One can show that a φ_h that yields a unique extrema of $I(\varphi_h)$ is also a unique solution of the differential equation $A\varphi_h - f = 0$, which is often referred to as the Euler equation. Thus, we have a link between the solution φ_h of the differential equation and calculus of variations. We note that integral forms in the GM, GMWF, and PGM

are equivalent to $\delta I(\varphi_h) = 0$. In these integral forms, existence of $I(\varphi_h)$ is not always guaranteed. Even when $I(\varphi_h)$ exists, $\delta^2 I(\varphi_h)$ may not yield a unique extremum principle.

To distinguish well-posedness of the integral forms, the concepts of variational consistency (VC) and variational inconsistency (VIC) are introduced. If there exists a functional $I(\varphi_h)$ such that $\delta I(\varphi_h) = 0$ and $\delta^2 I(\varphi_h)$ yields a unique extremum principle then the integral form under consideration is termed *variationally consistent.* Obviously, VC integral forms always ensure unique φ_h. Integral forms that are not VC are called *variationally inconsistent.* In such cases the resulting computations may not be unconditionally stable or may fail all together. It has been shown by Surana et. al [1-4] that the concepts of VC and VIC permit us to decide whether integral forms would yield unconditionally positive-definite algebraic systems and hence unconditional numerical stability. This is an issue of paramount importance in adaptive processes in which one often begins with very coarse discretizations and very low p-levels. Variationally inconsistent integral forms in such cases may not even permit computations without the use of ad-hoc approaches and upwinding methods. The PGM and GM are always VIC regardless of the differential operators; GMWF is variationally consistent when the bilinear functional is continuous and satisfies the so-called Inf-Sup condition which is only possible for self-adjoint operators; LSM, on the other hand, is always VC for all three types of differential operators. These conclusions are significant and helpful in assessing the current finite element computational technology and associated deficiencies as well as in designing a new computational framework in which the computational processes always remain numerically stable and nondegenerate.

2.2.3 Mathematical Models and Currently Used Finite Element Methods

The mathematical models for fluid-solid interaction problems are diverse. The mathematics of performing finite element computations depends on whether the models are continuum based. In the proposed research we only consider fluid-solid interaction mathematical models that are based on continuum mechanics. The solid medium could be elastic, elasto-plastic, visco-elastic or even energetic material. The fluid can be an incompressible Newtonian, Generalized Newtonian or a polymeric liquid with elasticity as well as viscosity. The fluid medium can also be a gas with complex properties requiring real gas models and temperature dependent transport properties. The combined fluid-solid problems may be non-isothermal with large motions, large strain rates, moving interfaces, and/or moving boundaries. In addition, the problems may involve chemical kinetics if the materials are energetic or reacting. Towards obtaining numerical solutions of such interaction problems, we present a comprehensive review of currently used mathematical and finite element models. This is followed by details of the concepts developed in the present methodology.

The mathematical models of fluid-solid interactions often result in non-linear partial differential equations in space coordinates (BVP) or space cordinates and time (IVP).The most prevalent finite element computational methodologies for obtaining their numerical solutions is based on GMWF which results in integral forms that are VIC. Such integral forms yield computational processes that are not unconditionally stable or nondegenerate. Thus, one must establish for each problem, the ranges of computational and

physical parameters for which the computations will remain stable. This often leads to unreasonable and impractical dicretizations and p-levels. The desire to compute with coarser dicretizations and lower p-levels has lead to the developments of upwinding methods [12-26]. Amongst many other drawbacks, the most disturbing aspect of such methods is that they are problem dependent. Hence, they cannot be considered as a general computational methodology for all BVP and IVP. In the proposed research we only consider VC integral forms. We therefore, eliminate the need and use of problem dependent approaches all together.

The fluid-solid interaction problems most naturally can be viewed as initial-value problems (IVP). Current computational approaches for IVP can be broadly classified into two groups: space-time decoupled methods and space-time coupled methods. Space time methods with time marching (as opposed to space-time meshes) offer many advantages [4, 27]. Most significant features of space-time coupled methods are: (i) concurrent dependence of the solution on space and time, (ii) possibility of making mathematical classifications of space-time differential operators and hence developing a general mathematical framework for all IVP, (iii) possibility of assessing VC or VIC of space time integral forms, and (iv) VC integral forms lead to unconditionally non-degenerate computations (no issues of stability). None of these features exist in space-time decoupled methods. In the present work, we only utilize space-time integral forms that are space-time variationally consistent.

The mathematical models of fluid-solid interaction problems can be established either using Lagrangian approach or Eulerian approach. In the Lagrangian approach, most commonly used in solid mechanics, all quantities of interest are measured in a fixed frame of reference embedded in the body. In contrast, in the Eulerian description all quantities of interest are measured and referred to a reference frame fixed in space and material particles move through the space. In the currently used approaches for fluid-solid interaction problems, each medium of the process is mathematically modeled and discretized using the most suitable strategy for each medium and then interfaced through constraint equations to the neighboring media. In this approach: (1) The interface behavior, which is often of great interest is highly dependent on the nature of constraint equations describing the coupling. Their legitimacy in relation to the true physical behavior may be difficult to ascertain. (2) Often the variables from each medium at the interface boundaries are different. This results in significant difficulties in describing constraint equations at the interfaces. (3) The most disturbing feature of this approach is that the integration of the different media of the process at the interfaces is only established numerically after discretizations. (4) Inaccuracies in the constraint equations at the interfaces may also contaminate the solutions in the entire media. Such approaches are problem dependent and can not viewed as a general methodology for all fluid-solid interaction problems. *In the approach presented here, all media of fluid-solid interaction problems are mathematically modeled under one mathematical umbrella.* This approach completely eliminates the necessity of applying interface constraint equations but requires the development of rigorous mathematical models. Details of this approach are described in Section 2.3. In summary, the mathematical models in Lagrangian frame of reference for solids and those for fluid in Eulerian frame of reference with constraint equations at the interfaces describing their coupling remains the current methodology for fluid-solid interaction processes.

2.2.4 Moving Fronts, Boundaries, Meshes, and Rediscretizations

Accurate and practical numerical simulations of fluid-solid interaction problems may require a representation of moving interfaces, fronts and/or moving boundaries that can be tracked accurately. The discretizations in other regions are kept intact but moved to different locations. This requires a mathematical infrastructure in which front tracking and moving mesh capability is transparent during computations. In other instances a total re-discretization may be required. The mathematical framework to support these features are of critical significance in interaction problems. It requires the results of one discretization to be mapped onto a new dicretization. It is well known that in the h, p framework based on global approximations of class C^0, the mapping of solutions from one discretization to another may suffer severe damage in the solution derivatives, referred to as the *flux problem* in the published literature (discontinuity of normal derivative to the inter-element boundaries, see Figure 1). Many problem dependent remedies are available [27] to circumvent these difficulties to some extent. Due to the C^0 nature of the global approximation used, the inter-element flux discontinuity remains. Thus, within h, p framework with C^0 global approximations, a general methodology for moving fronts, moving meshes and re-discretization that is free of flux problem is not possible.

Moving interfaces, fronts and boundaries can be tracked using the level set theory. The h, p, k framework maintains sharpness of the fronts during all stages of the evolution. Since the global differentiability of the approximation is controlled through k, flux problems are totally absent in the present approach. Mapping of the solutions from one discretization to another with desired global differentiability and measures of their accuracy remain totally transparent (See Section 4 on Rediscretization,moving meshes and solution mapping).

2.3 Development of Mathematical Models

This is one of the most important phases of the present research. We recognize that the fluid description in Eulerian frame of reference is essential due to large motions of the fluid particles. In the present work, we construct the mathematical model of the entire fluid-solid system in the Eulerian frame of reference.

The mathematical model for the fluid medium are constructed using the Eulerian frame of reference and conservation of mass, momentum and energy, constitutive equations, and equations of state. The fluid may be Newtonian, generalized Newtonian (power law, Carreau-Yasuda, Bingham etc.), or viscoelastic liquid (Maxwell, Oldroyd, Giesekus, PTT, etc.), or a gas with complex constitutive models and temperature dependent transport properties. The process can be non-isothermal with chemical kinetics. The variables in the formulation may include density, velocities, pressure, stresses, and temperature, among others. For the equations of state describing relationships between density, pressure and temperature, we consider ideal gas as well as real gas models such as Van der waals, Redlich-Kwong, Beattie-Bridgeman, Benedict-Web-Rubin, and virial models. Transport properties such as viscosity, thermal conductivity, specific heat will be considered to be temperature and possibly strain-rate dependent. Models such as power law, Southerland law are utilized for this purpose.

For a linear or non-linear elastic solid medium as well as the solid medium undergo-

ing large deformation and strain rates with plasticity, the mathematical models are also derived in the Eulerian frame of reference. While the basic conservation laws: continuity, momentum and energy remain the same as in the case of fluids, some modifications are needed for solids. Additionally, the constitutive equations for solids require more careful considerations. The solid medium may be elastic, elasto-plastic, viscoelastic, heterogeneous (i.e.,laminated composite) or even energetic. The Cauchy stress tensor σ is decomposed into deviatoric and hydrostatic parts. With this decomposition, deviatoric stress components in solids have the same physical meaning as viscous stress in case of fluids after using the Stokes hypothesis. Density, velocities, pressure, deviatoric part of Cauchy stress, and temperature are the variables of choice in the mathematical models of both fluid and solid media.

Use of velocities in the conservation laws requires that the constitutive equations for the solid medium be derived in terms of strain rates as opposed to strains used in the Lagrangian frame of reference. For this purpose, we employ rate constitutive models based on stress tensors of Jaumann, Truesdell, Green-Nagdi, and convected stress tensor [28-31]:

$$\frac{^{j}D\sigma}{Dt} = {}^{j}\mathbf{C} : \mathbf{D}; \quad \frac{^{t}D\sigma}{Dt} = {}^{t}\mathbf{C} : \mathbf{D}; \quad \frac{^{gn}D\sigma}{Dt} = {}^{gn}\mathbf{C} : \mathbf{D}; \quad \frac{^{c}D\sigma}{Dt} = {}^{c}\mathbf{C} : \mathbf{D}$$

where $\frac{D\sigma}{Dt}$ with superscripts j, t, gn and c are Jaumann, Truesdell, Green-Nagdi, and convected rates of Cauchy stress σ. Here ${}^{j}\mathbf{C}$, ${}^{t}\mathbf{C}$, ${}^{gn}\mathbf{C}$ and ${}^{c}\mathbf{C}$ are the corresponding material tangent moduli tensors and $\mathbf{D}$ is the symmetric part of the rate of deformation tensor. The rate constitutive equations are invariant of rotations. Note that the choice of one rate equation over other is material dependent and there is no consensus on their choice. In the present research, we consider all four rate equations and investigate their ranges of applications for various materials. When the solid medium is compressible (as in case of high strain rate plasticity) appropriate equations of state (i.e., [32] and others) are utilized to define relationships between density, pressure and temperature.

When these mathematical models are discretized and solved numerically, the interaction of the solid medium with the fluid medium at the interfaces is intrinsic in the mathematical models and hence completely eliminates the use of constraint equations at the interfaces. Since the mathematical models are in Eulerian frame of reference, the computations for these models are on a fixed discretization hence eliminating re-discretizations and mapping of solutions as integral part of the numerical computational methodology.

2.4 Higher-Order Global Differentiability of Approximation Functions

Theoretical solutions of the mathematical models may be of higher-order global differentiability in space as well as in space and time. When considering numerical solutions of these governing differential equations using FEM, the higher-order global differentiable approximations in space as well as in space and time are meritorious over solutions of class C^0 [1-4].

Surana et. al [1-4] have shown that the order k of the approximation space $H^{k,p}$ establishes global differentiability of order $(k-1)$ of the numerical solutions, and is an

independent parameter in all finite element computations in addition to h and p. They have developed a k-version of the finite element method and associated hp, pk and hpk processes. Authors also shown that even the most prudent hp-adaptive processes cannot alter the order k of the approximations. Adaptive control of higher-order global differentiability allows control of continuity and differentiability of any quantity of interest in the design of a computational process. The higher-order globally differentiable approximations in space and time for initial-value problems (IVP) require the use of $H^{k,p}$ spaces in which $k = (k_1, k_2)$ and $p = (p_1, p_2)$ with $p_1 \geq 2k_1 - 1$ and $p_2 \geq 2k_2 - 1$; here k_1 and k_2 denote the orders of the approximation spaces in spatial coordinates and time, respectively, and p_1, p_2 are the corresponding degrees of approximations. Higher-order global differentiability of the approximations is necessary when the theoretical solution is of a higher class and therefore has higher-order global derivatives. In the case of singular data, boundary or initial conditions and their approximations in $H^{k,p}$ space using interpolants permit one to resolve the desired behaviors as a suitable k is adapted [11]. Use of $H^{k,p}$ scalar product spaces for space-time approximations has been extensively investigated by Surana et. al [1-4, 11] and they have shown that very high accuracy is achievable.

For illustrative purposes, we consider the steady state convection-diffusion equation (BVP) for Peclet number of 100 shown in Figure 1. The theoretical solution is of class C^∞. Numerical solutions of classes C^j, $j = 0, .., 4$ (corresponding to $k = 1, ..., 5$) are computed using least squares finite element formulation (VC) for a uniform discretization of ten p-version 1D elements. In most engineering applications, at least the first derivative of the solution is of considerable interest. Figure 1 shows $d\varphi_h/dx$ versus x at and in the neighborhood of $x = 0.9$ (inter-element boundary) for the solutions of various classes and a comparison with the theoretical solution. Discontinuity of $d\varphi_h/dx$ for the solutions of class C^0 ($k = 1$) at $x = 0.9$ and its influence, causing oscillations in the neighboring elements is clearly observed. The discontinuity of $d\varphi_h/dx$ is also observed at all other inter-element boundaries, however the magnitude decreases moving from $x = 1.0$ toward $x = 0.0$ due to decreasing magnitude of $d\varphi/dx$ (theoretical value). Solutions of classes C^1 to C^4 show dramatically improved behavior of $d\varphi_h/dx$ with lower degrees of freedom (dofs) compared to those used to obtain the C^0 solution. Solution of class C^4 is almost in perfect agreement with the theoretical solution for only 108 dofs compared to 120 dofs used to obtain the C^0 solution that is grossly in error. Progressive reductions in total dofs for progressively higher classes of approximations are more dramatic for 2D and 3D problems. We note that the L_2 norm of the error in the first derivative for C^4 solution is two orders of magnitude lower than that for C^0 solution. Ability of the approximations of higher classes in approaching theoretical solutions efficiently is clearly observed. In this research, we propose to construct the space and space-time approximations of higher order global differentiability in the $H^{k,p}$ spaces for obtaining finite element solutions of the mathematical models.

2.5 h, p, k Finite Element Processes: VC Integral Forms

The governing equations of non-linear processes in the fluid-solid interaction considered here are naturally non-linear partial differential equations. In case of IVP all quantities of interest are simultaneously dependent on space coordinates as well as time. We solve these

GDEs for both BVP and IVP using h, p, k finite element processes in which approximations in space as well as in space and time are of higher-order global differentiability. The space as well as space-time integral forms are always variationally consistent. The significant features of this methodology are summarized below.

- For BVPs, finite element processes based on variationally consistent integral forms are considered so that unconditional stability of the resulting computational processes is ensured.

- For IVPs, space-time coupled FE processes [4] are used as opposed to space-time decoupled approaches [27]. Space-time coupled methods are consistent with the physics of the IVPs.

- Only for space-time coupled finite element processes with space-time integral forms it is possible to establish a link between the integral forms and the calculus of variations. Surana et. al [4] have shown that space-time variationally inconsistent integral forms yield computational processes in which the coefficient matrices are always non-symmetric. Such computational processes are only conditionally stable and may even become totally degenerate for some choices of h, p and k. Space-time variationally consistent integral forms always yield symmetric coefficient matrices that are positive-definite and the computational models are unconditionally stable and non-degenerate regardless of the choice of h, p, k as well as the parameters of the physics. The space-time differential operators in the mathematical models of fluid-solid interactions are naturally non-linear. Surana et. al [4] have shown that for such differential operators only the space-time integral forms derived using space-time least squares processes are VC and hence are computationally meritorious over all others. Therefore, these are be utilized in the present research.

- The space-time least squares processes are also completely free of numerical dispersion [33] for appropriate choices of h, p and k. This feature permits computations that are time-accurate for IVPs.

- Commonly encountered limitations of CFL number and stability issues in space-time decoupled methods are totally absent in the present methodology due to variational consistency of the integral forms.

- When GMWF is used to obtain numerical solutions, the resulting integral forms are VIC, and it becomes necessary to use upwinding techniques such as SUPG, SUPG/DC, SUPG/DC/LS [12-26] and so on to stabilize the computations. In the current methodology, VC of the least squares integral forms eliminates the use of problem dependent upwinding methods all together. This is a significantly advantageous characteristic of the computational methodology presented here.

- Surana et. al [4] and others [27] have shown that space-time marching techniques are advantageous over the space-time meshes in terms of computational efficiency as well as control over the solution errors during evolution of the solution. The numerical solution is computed for one strip at a time, and only when the desired

solution accuracy is achieved then marched in time until the target time is reached. In space-time meshes, the problem size is significantly larger than that in the space-time strip approach, and since the solution is computed simultaneously for all values of time, error control as in space-time strip is not possible.

- While much is published in the numerical analysis of fluid-solid interaction problems, the solutions independent of the computational parameters (referred to as mesh independent solutions) are generally not available. In h, p, k framework proposed here, numerical simulations are sought that are independent of h and p for a chosen k. The proximity of such solutions to the theoretical solutions are established through appropriate measures.

- For a numerical solution of a BVP to be valid it must correspond to the stationary state of the corresponding IVP. In many instances in polymer flows in which the constitutive equations are highly complicated and are empirical (Maxwell, Oldroyd, Giesekus, PTT, models etc.). This aspect is essential in establishing the legitimacy of the solutions of the BVP.

- Time accurate evolutions for fluid-solid interaction problems are generally not reported. Numerical solutions of such processes available in the literature are obtained using GMWF (VIC) with upwinding techniques. In the present work, we establish time accurate evolutions of fluid-solid interaction problems.

- In the following we present the basic steps of LSM for non-linear BVP and IVP [3-4] that are encountered in fluid-solid interactions. Let $A\varphi - f = 0$ be a BVP or an IVP in Ω, φ_h be an approximation of φ and $A\varphi_h - f = E$ be residual in Ω. Then we construct a functional,

$$I(\varphi_h) = (E, E) \tag{1}$$

and the necessary condition for its minimum is

$$\delta I(\varphi_h) = (E, \delta E) = g(\varphi_h) = 0 \tag{2}$$

The second variation yields

$$\delta^2 I(\varphi_h) = (\delta E, \delta E) + (E, \delta^2 E) \tag{3}$$

We note that $\delta^2 I(\varphi_h)$ is not unconditionally greater than zero and does not represent a unique extremum principle unless $(E, \delta^2 E)$ in (3) is neglected [3-4,33], which amounts to correcting the search direction. However, we still seek the solution of (2). Thus we use

$$\delta^2 I(\varphi_h) = (\delta E, \delta E) \tag{4}$$

Note that $\delta^2 I(\varphi_h)$ defined by (4) is always greater than zero; hence, a unique extremum principle and a φ_h obtained from (2) minimizes $I(\varphi_h)$ in (1). The system of non-linear equations in (2) are solved using Newton's method with line search. Let ${\varphi_h}^0$ be a starting solution, then, we have the following:

$$\varphi_h = {\varphi_h}^0 + \alpha \Delta {\varphi_h}^0; \quad \Delta\varphi_h = -[\delta^2 I(\varphi_h)]^{-1}_{\varphi_h^0} \{g(\varphi_h)\}_{\varphi_h^0} \tag{5}$$

The factor α is determined such that $I(\varphi_h) \leq I(\varphi_h^0)$. We remark that the LSM based on (1), (2), (3), and (5) is VIC, while the LSM based on (1), (2), (4), and (5) is VC. Rationale of deriving (4) from (3) has been established in [3,34]. We consider the steady state Burgers equation in (0,1) with $\varphi(0)$=1.0 and $\varphi(1)$=0.0. Figure 2 shows numerical solutions obtained using VC and VIC least squares formulations. At $p =$ 7, VIC formulation produces spurious solution, though criterion for the convergence of the Newton's method with line search is satisfied and the least squares functional is of the same order of magnitude as in case of VC integral form. Additionally, convergence of the iterative solution method slows down significantly in case of a VIC integral form for all p levels, requiring over 50 iterations, whereas VC formulation always converges in less than 10 iterations for all p levels. This example demonstrates the potential of failure of VIC integral form for some choice(s) of computational parameters (p level in this case). Consequences of VIC integral forms in GAL/WF are far more serious if upwinding methods are not used.

2.6 Preliminary Results

Figure 3 shows preliminary results of evolutions for 1D axial stress wave propagation in media containing bimaterial interfaces obtained using computational methodology discussed in this research. The mathematical models for both fluid and solid media are in Eulerian frame of reference. Interface coupling equations and upwinding methods are not used at all. The integral forms are space-time variationally consistent, hence ensure unconditionally stable computations during all stages of the evolution. In all cases wave propagation, transmission, reflection and interface behavior is simulated easily. Interface behaviors are oscillation free and wave motions are in conformity with the impedences of the media and their transport properties.

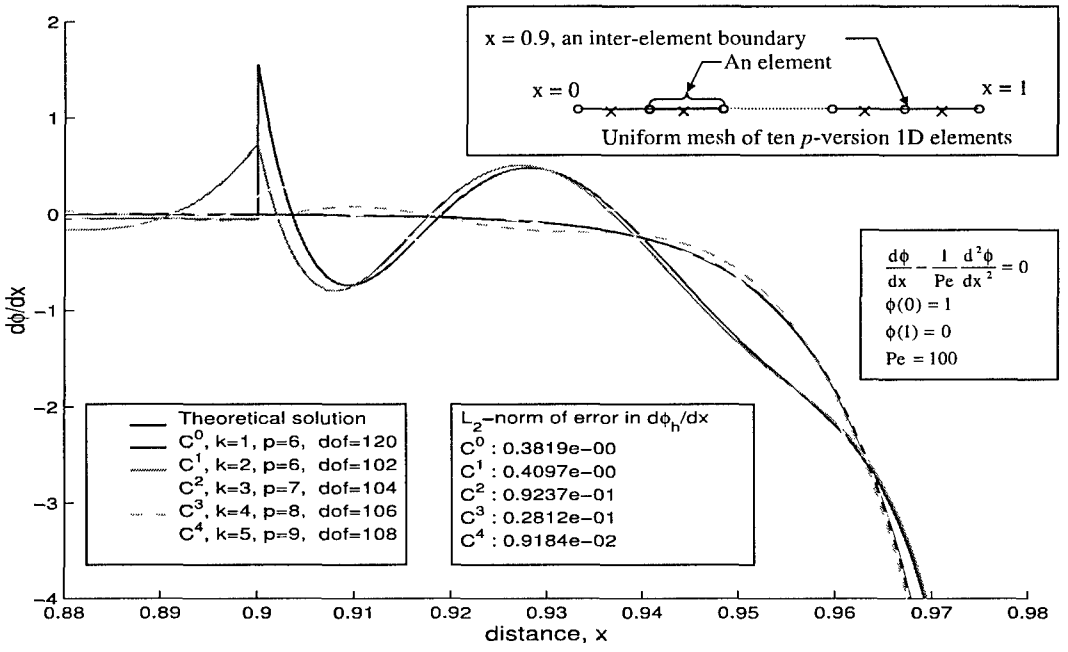

Figure 1 ***dφ/dx*** **versus** ***x*** **for steady state convection diffusion equation : Solutions of various classes (exploded view at x = 0.9, an inter-element boundary)**

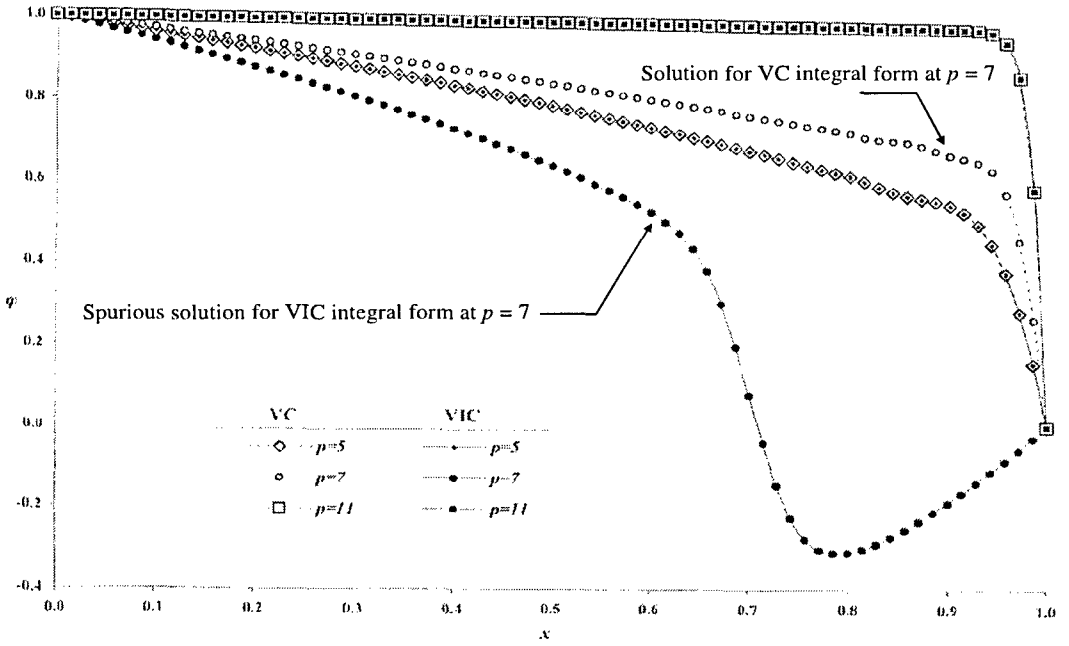

Figure 2 Solution φ versus *x* for steady state Burgers equation for different *p*-levels : VC and VIC formulations

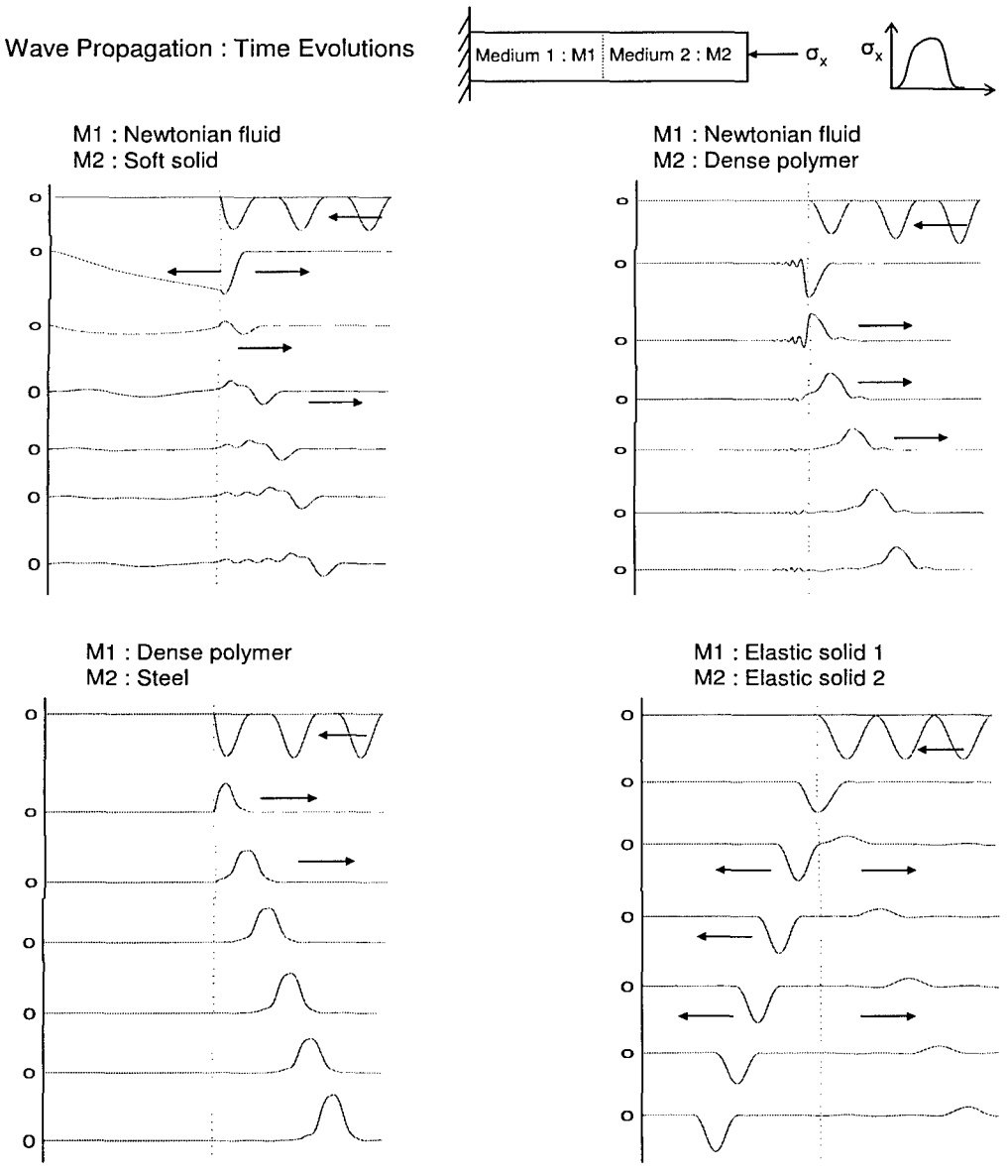

Figure 3 Stress wave propagation, transmission and reflection in bimaterial media.

3 A priori and a posteriori error estimation : Preliminary work

3.1 Introduction

In recent works, Surana et.al. [1-4] have shown that order k of the approximation space defines global differentiability of order $(k-1)$ of the approximations and is an independent parameter in all finite element computations. Authors have established k- version of finite element method and associated hk, pk, hpk processes in addition to h, p-versions and h, p, hp processes used currently. Under the AFOSR grants F 49620-03-1-0298 and F 49620-03-1-0201, Surana et.al. [1-4] proposed and developed hpk mathematical and computational framework for finite element processes for solving BVP and IVP. Due to the fact that h, p and k are independent parameters in the new mathematical framework, all quantities of interest in the finite element computations within this framework are naturally dependent on h, p and k as opposed to only h and p.

A-priori and a posteriori error estimates are intrinsically important aspects of a mathematical framework for finite element computations. A priori and a posteriori error estimates derived and used currently are strictly based on h and p. The global approximations are almost always assumed to be of class C^0. The purpose of this research is to examine the methodology for a priori and a posteriori error estimates for 1-D, 2-D and 3-D BVP and IVP that are dependent on independent computational parameters h, p and k.

The work is basic and fundamental in that it: (i) requires a closer examination of the global behaviors of approximations to assess and determine the intrinsically important approximation features dependent on k that are ignored in the currently used methodologies. (ii) requires development of fundamental approaches through with approximation aspects dependent on k can be incorporated in the a priori and a posteriori error estimates. Our preliminary investigations show that inter-subdomain behaviors of the approximations (normal derivatives of dependent variables) ignored in the currently derived estimates are dependent on k. These behaviors must be incorporated in the error estimates of the quantities of interest so that the resulting estimates will hold globally in the pointwise sense.

A priori and a posteriori estimates for BVP and IVP must be considered in h, p, k framework in which approximations are in higher order scalar product spaces $H^{k,p}$ (k being the order of the space). For initial value problems, such estimates must consider $k = (k_1, k_2), p = (p_1, p_2)$ in which $p_1 \geq 2k_1 - 1, p_2 \geq 2k_2 - 1$ in which k_1 and k_2 are the orders of the approximation spaces in space and time and p_1, p_2 are the degrees of local approximations in space and time. The importance of these estimates in adaptive process, estimation of theoretical convergence rates achievable, and rigor of the mathematical framework for finite element processes has been well recognized. The concepts discussed here will bring the mathematical foundation for finite element computations in h, p, k framework to a more complete stage in which adaptive processes in h, p, k framework can

be initiated and designed for optimality of computational efficiency and appropriate error control.

3.2 A review of current methodology and development of concepts in *hpk* framework

In this section we present some preliminaries and a short review of currently used methodology of deriving the estimates and demonstrate the need for new research in this area. The finite element approximations in Sobolev space (generally of order 1) and the associated infrastructure leading to the theory of generalized solutions or theory of distributions forms the mathematical backbone of a priori and posteriori error estimations. To demonstrate the features of the currently used mathematical framework, we consider the following 1-D simple boundary value problem,

$$-\frac{d^2\varphi}{dx^2} = f \quad \text{in} \quad \Omega = [0, L] \tag{1.1}$$

with

$$\varphi|_0 = \varphi_0 \quad \text{and} \quad \frac{d\varphi}{dx}|_L = q \tag{1.2}$$

Galerkin method with weak form yields the following integral form,

$$B(v, \varphi)_\Omega = l(v)_\Omega \tag{1.3}$$

in which

$$B(v, \varphi)_\Omega = \int_\Omega \frac{d\varphi}{dx}\frac{dv}{dx} d\Omega \tag{1.4}$$

$$l(v)_\Omega = (f, v)_\Omega + qv(L) \tag{1.5}$$

$$\text{and} \quad v = \delta\varphi; \tag{}$$

Let $\Omega^T = (\cup_e \bar{\Omega}_e)$ be a discretization of Ω in which $\bar{\Omega}^e$ is a typical subdomain 'e' of $\bar{\Omega}^T$ and let $\varphi_h = \cup_e \varphi_h^e$ be an approximation of φ in $\bar{\Omega}^T$ where φ_h^e approximates φ_h over an element 'e'. The φ_h would be a solution of

$$B(v, \varphi_h) = l(v) \quad ; \quad v = \delta\varphi_h \tag{1.6}$$

For the discretization Ω^T, we obtain

$$\sum_e B^e(v, \varphi_h^e) = \sum_e l^e(v) \quad ; \quad v = \delta\varphi_h^e \tag{1.7}$$

In (1.7), $B^e(v, \varphi_h^e)$ is obviously from (1.4). However, $\sum_e l^e(v)$ requires a closer examination. Using (1.5), we obtain

$$\sum_e l^e(v) = \sum_e (f, v)_{\Omega^e} + \sum_e (v(x_1^e)P_1^e + v(x_2^e)P_2^e)) \tag{14}$$

where x_1^e and x_2^e are nodal coordinates of the two end nodes of the element.

Remarks

(1) If φ_h and hence φ_h^e are of class C^0, i.e. in $H^{1,p}(\bar{\Omega}^e)$ scalar product space, then $\frac{d\varphi_h}{dx}$ is discontinuous at the inter-element boundaries and (1.7) from (1.3) is not possible in the strict sense of calculus of continuous and differentiable functions.

(2) However, based on theory of distributions, (1.7) from (1.3) is valid in $H^{1,p}(\bar{\Omega}^e)$ space in which φ_h is of class C^0. In such approach it is well known that inter-element behavior is ignored.

(3) Furthermore, when computing for nodal degrees of freedom in φ_h (or φ_h^e i.e. constants in the linear combination) using (1.7), one must impose the condition that sum of secondary variables at the inter-element boundaries is zero (assuming no external disturbance is applied at such nodes). This condition is not supported by the local approximations φ_h^e over $\bar{\Omega}^e$ when φ_h^e are of class C^0, due to the fact that $\frac{d\varphi_h}{dx}$ is discontinuous at the interelement boundaries. Thus when φ_h^e are of class C^0, we have a computational process in which there are inconsistencies at all inter-element boundaries. If one involves h, p, hp-adaptive processes with φ_h^e of class C^0, then a vast amount of resources are spent in overcoming the inconsistency described here.

(4) When φ_h^e are of class C^1, i.e. in $H^{2,p}(\bar{\Omega}^e)$ scalar product space: (a) (1.7) from (1.3) conforms to the calculus of continuous and differentiable functions due to the fact that φ_h and $\frac{d\varphi_h}{dx}$ are continuous everywhere in $\bar{\Omega}^T$ including inter-element boundaries, and hence the integrand in (1.3) is continuous in $\bar{\Omega}^T$ (b) the conditions on the sum of the secondary variables is enforced correctly at the inter-element nodes due to the fact that local approximations φ_h^e in $H^{2,p}(\bar{\Omega}^e)$ space support this condition. Hence, there is no inconsistency in the computational process when φ_h^e are of class C^2 in $H^{2,p}(\bar{\Omega}^e)$ space. The issues discussed here become far more serious and damaging in two and three dimensions

This simple model BVP, its finite element formulation and the remarks presented here demonstrate how one ignores the inter-element behaviors and creates inconsistency in the resulting computational process in one approach (current approach) and how simply these are avoided all together in the *hpk* framework. Since, the a priori and posteriori error estimation techniques are based on weak forms such as (1.6) or (1.7) in which φ_h^e are of class C^0 in $H^{1,p}(\bar{\Omega}^e)$ spaces, it is rather straightforward to observe that in these methodologies inter-element behaviors are ignored (just like it is in (1.6) or (1.7) where φ_h^e is of class C^0). A priori and a posteriori error estimates used currently are derived in terms of Lebesgue measures that do not incorporate the inter-element behaviours. Such estimates thus naturally are only functions of h, p and smoothness of the theoretical solution in each element. In view of the fact that all finite element computations are actually dependent on h, p and k, the need for the new research in h, p, k framework is quite clear.

(5) Our preliminary work shows that inclusion of inter-subdomain behaviors in the a priori and posteriori error estimates is important and crucial. This can be demonstrated by considering a simple 1-D case (like described above) in which the discretization

is uniform with characteristic length h and the degree of local approximation is p. Let the local approximation be of class C^0. We wish to establish a bound on $\| \frac{d\varphi}{dx} - \frac{d\varphi_h}{dx} \|_{L_2}$. In this case $\frac{d\varphi_h}{dx}$ exhibits discontinuity (jump) at the inter-element boundaries. One finds that the rate of convergence of the error in the jumps of $\frac{d\varphi_h}{dx}$ is lower than the rate of convergence of the errors in $\frac{d\varphi_h}{dx}$ over the interiors of the subdomains. The same holds true for other measures as well. Thus the measures based strictly on the open domains of the elements are in fact over estimates of the local features of the solution that are often of great interest to the analyst (such as stresses or fluxes across the interfaces)

(6) A clear demonstration of how the inter-element behaviors of the solution derivatives is ignored in the presently used estimates is presented in this section. For simplicity, consider a one-dimensional problem similar to one described earlier. Let h and p be the characteristic length and degree of local approximation. Let φ_h be of class C^0. Then, for each Ω^e the estimates of $\| \frac{d\varphi}{dx} - \frac{d\varphi_h}{dx} \|_{L_2}$ only depend upon h and p. Hence estimates of $\| \frac{d\varphi}{dx} - \frac{d\varphi_h}{dx} \|_{L_2}$ over $\bar{\Omega}^T$ if derived solely based on $\| \frac{d\varphi}{dx} - \frac{d\varphi_h}{dx} \|_{L_2}$ over Ω^e, will naturally depend on h and p only as well as the smoothness of the theoretical solution φ. In this process inter-element behaviors of $(\frac{d\varphi}{dx} - \frac{d\varphi_h}{dx})$ has been completely ignored. Currently derived estimates are based on this methodology.

(7) A global estimate of $\| \frac{d\varphi}{dx} - \frac{d\varphi_h}{dx} \|_{L_2}$ that holds true for entire $\bar{\Omega}^T$ requires that we incorporate measures of $(\frac{d\varphi}{dx} - \frac{d\varphi_h}{dx})$ at the inter-element boundaries in $\| \frac{d\varphi}{dx} - \frac{d\varphi_h}{dx} \|_{L_2}$ i.e. the estimates must be derived over $\bar{\Omega}^T$. Inter-element behaviors of the solution derivatives normal to the inter-element boundaries is a function of h, p as well as k. If the local approximations are of class C^0 (k=1), then $\frac{d\varphi_h}{dx}$ (i.e. derivative of order k=1) is discontinuous at the inter-element boundaries. When φ_h^e are of class C^1, then $\frac{d^2\varphi_h}{dx^2}$ (i.e. derivatives of order k=2) exhibit discontinuity at the inter-element boundaries. That is a measure of $(\frac{d^k\varphi}{dx^k} - \frac{d^k\varphi_h}{dx^k})$ at the inter-element boundaries is a function of k (as well as h and p), the order of the approximation space.

Thus, a priori and posteriori error estimates must be in h, p, k framework in which the estimates will incorporate inter-element behavior and thereby including k, the order of the approximation space in the estimates in addition to h and p.

4 Rediscretizations, moving meshes and solution mapping strategies and associated computational infrastructure for BVPs and IVPs in *hpk* framework

Appendix A contains a research report issued under 'Computational Mechanics Laboratory' of the Department of Mechanical Engineering of the University of Kansas, Lawrence, KS. This report describes the research work done in this area during the third year of the grants.

5 Future work

The fluid-solid interaction and error estimation work presented here is preliminary. At present, many Ph.D students are engaged in utilizing the concepts presented here to develop a complete infrastructure in these two areas in which 1D, 2D and 3D BVPs and IVPs will be treated rigorously without bias to their origin or fields of application. *hpk* adaptive processes are also currently an area of focus. This research will utilize the developments in a priori and a posteriori error estimation for developing methodologies and algorithms for h, p, k adaptive processes.

The research work presented here on rediscretizations, moving meshes and solution mapping is of critical significance in solid mechanics areas of large deformation, large strain utilizing Lagrangian mathematical models. In such cases discretizations become excessively distorted during evolution (IVPs) or load incrementing (BVPs) and hence it becomes necessary to rediscretize and obtain a map of the existing solution onto the rediscretization. Moving mesh approach permits efficient computations in which moving micro fronts can be resolved in a macro domain. The future work in this area consists of some algorithm developments but largely of applications in various areas of continuum mechanics that may necessitate specific developments related to those areas. As an example, mapping strategies for fracture, plasticity and damage mechanics in general in which the quantities of interest are generally accumulated on incremental basis are generally history dependent and hence may require specific developments.

References

1. K.S.Surana, A.R.Ahmadi and J.N.Reddy, The k-Version of Finite Element Method for Self-adjoint Operators in BVP, Int.J.Comp.Eng.Sci, Vol. 3, No. 2, pp 155-218, 2002.

2. K.S.Surana, A.R.Ahmadi and J.N.Reddy, The k-Version of Finite Element Method for Non-self-adjoint Operators in BVP, Int.J.Comp.Eng.Sci, Vol. 4, No. 4, pp 737-812, 2003.

3. K.S.Surana, A.R.Ahmadi and J.N.Reddy, The k-Version of Finite Element Method for Non-linear Operators in BVP, Int.J.Comp.Eng.Sci, Vol. 5, No. 1, pp 133-207, 2004.

4. K.S.Surana, S.Allu and J.N.Reddy, The k-Version of Finite Element Method for Initial Value Problems: Mathematical and Computational Framework, in review, 2006-2007.

5. M.Gelfand, S.V.Fomin, Calculus of Variations, Dover Publications, New York, 2000.

6. G.Mikhlin, Variational Methods in Mathematical Physics, Pergamon press, New York, 1964.

7. J.N.Reddy, Applied Functional Analysis and Variational Methods in Engineering, McGraw Hill Company, 1986.

8. J.T.Oden and G.F.Carey, Finite Elements: Mathematical Aspects, Prentice Hall, Engleood Cliffs, N.J.,1983.

9. C.Johnson, Numerical Solutions of Partial Differential Equations by Finite Element Method, Cambridge University Press, 1987.

10. J.N.Reddy, An Introduction to The Finite Element Method,McGraw-Hill, Third Edition, 2006.

11. K.S.Surana, J.Kane, J.N.Reddy and P.W.Tenpas, Higher Order Global Differential Evolutions of Initial Value Problems in h,p,k, Mathetatical and Computational Framework, Presented at the China Conference, 2006.

12. G.DeVahl Davis and G.Mallinson, An Evaluation of Upwind and Central Difference Approximations by a Study of Recirculating Flow, Computers and Fluids 4 (1976) pp. 29-43.

13. P.M.Gresho and R.L.Lee, Don't Supress the Wiggle - They're Telling You Something!, in: T.J.R.Hughes ed., Finite Element Methods for convection Dominated Flows, AMD Vol. 34 (ASME, New York, 1979).

14. B.P.Leonard, A Survey of Finite Differences on Numerical Modeling of the Incompressible Convection-Diffusion Equation, in: T.J.R.Hughes, ed., Finite Element Methods for Convection Dominated Flows, AMD Vol. 34 (ASME, New York, 1979).

15. I.Christie, D.F.Griffiths, A.R.Mitchell and O.C.Zienkiewicz, Finite Element Methods for Second Order Differential Equations with Significant First Derivatives, Int. J. Num. Meth. Engr. 10 (1976) pp. 1389-1396.

16. J.C.Heinrich, P.S.Huyakorn, O.C.Zienkiewicz and A.R.Mitchell, An 'Upwind' Finite Element Scheme For Two-Dimensional Convective Transport Equation, Int. J. Num. Meth. Engr., 11 (1977) pp. 134-143.

17. T.J.R.Hughes, A Simple Scheme for Developing 'Upwind' Finite Elements, Int. J. Num. Meth. Eng., 12 (1978) pp. 1359-1365.

18. T.J.R.Hughes and J.Atkinson, A Variational Basis for 'Upwind' Finite Elements, IUTAM Symposium on Variational Methods in the Mechanics of Solids, Northwestern University, Evanston, IL, 1978.

19. T.J.R.Hughes and A.Brooks, A Multidimensional Upwind Scheme With no Crosswind Diffusion, in: T.J.R.Hughes, ed., Finite Element Methods for Convection Dominated Flows, AMD Vol. 34 (ASME, New York, 1979).

20. T.J.R.Hughes and A.Brooks, Galerkin/Upwind Finite Element Mesh Partitions in Fluid Mechanics, in: T.J.H.Miller, ed., Boundary and Interior Layers-Computational and Asymptotic Methods, (Book, Dublin, 1980) pp. 103-112.

21. T.J.R.Hughes and A.Brooks, A Theoretical Framework for Petrov-Galerkin Methods with Discontinuous Weighting Functions: Application to the Streamline Upwind Procedure, R.H.Gallagher, ed., Finite Elements in Fluids, Vol. 4 (Wiley, London).

22. Alexander N. Brooks and T.J.R.Hughes, Streamline Upwind/Petrov-Galerkin Formulation for Convection Dominated Flows with Particular Emphasis on the Incompressible Navier-Stokes Equations, Comp. Meth. in Applied Mech. and Eng. 32 (1982) pp. 199-259. references.

23. A.Mizukami and T.J.R.Hughes, A Petrov-Galerkin Finite Element method for Convection-Dominated Flows: An Accurate Upwinding Technique for Satisfying the Maximum Principle, Comp. Meth. in Applied Mech. and Eng. 50 (1985) pp. 181-193.

24. T.J.R.Hughes, M.Mallet and A.Mizukami, A New Finite Element Formulation for Computational Fluid Dynammics: II. Beyond SUPG, Comp. Meth. in Applied Mech. and Eng. 54 (1986) pp. 341-355.

25. T.J.R.Hughes and M.Mallet, A New Finite Element Formulation for Computational Fluid Dynamics: III. The Generalized Streamline Operator for Multidimensional Advective-Diffusive Systems, Comp. Meth. in Applied Mech. and Eng. 58 (1986) pp. 308-328.

26. T.J.R.Hughes and M.Mallet, A New Finite Element Formulation for Computational Fluid Dynamics: IV. A Discontinuity-Capturing Operator for Multidimensional Advective-Diffusive Systems, Comp. Meth. in Applied Mech. and Eng. 58 (1986) pp. 329-336.

27. T. Belytschko and T.J.R.Hughes(ed.),Computational Methods for Transient Analysis, North-Holland, 1992.

28. G.Jaumann,Grundlagen der Bewegundslehre, Leipsiz, 1905.

29. C.Truesdell, J. Ratl.references. Mech. Anal. 2, 593, 1953.

30. W.Prager,An Elementary Discussion of Defititions of Stress Rates, Quat. Appl. Math. Vol.18, pp 403-407, 1961.

31. R.B.Bird, R.C.Armstrong and O.Hassager, Dynamics of Polymeric Liquids, Volume 1, Fluid Mechanics, Second Edition, John Wiley and Sons , 1987.

32. M.A.Meyers, Dynamic Behavior of Materials, Wiley, New York, 1994.

33. K.S.Surana and J.S.Sandhu, Investigation of Diffusion in p-version 'LSFE' and 'STLSFE Formulations, Comp. Mech. 16 (1995) 151-169.

34. B.C.Bell and K.S.Surana, A Space-Time Coupled p-Version Least Squares Finite Element Formulation for Unsteady Fluid Dynamics Problems, Int. J. Num. Meth. Eng., Vol.37, (1994), pp. 3545-3569.

35. K.S.Surana, S.R.Petti, A.R.Ahmadi and J.N.Reddy, On p-Version Hierarchical Interpolation Functions for Higher Order Continuity Finite Element Models, Int. J. Comp. Eng. Sci.,Vol.2, No.4, 2001, pp. 653-673.

36. A.R.Ahmadi, K.S.Surana and J.N.Reddy, Higher Order Continuity 2D p-Version references.tex Approximation Functions, 7th World Congress on Computational Mechanics, July 16 - 22, 2006, Los Angeles, California.

Appendix A

KU THE UNIVERSITY OF KANSAS
School of Engineering

REPORT NO. CML/ME-07-01

REDISCRETIZATIONS, MOVING MESHES AND SOLUTION MAPPING IN *h, p, k* FRAMEWORK FOR BVPs AND IVPs

Karan S. Surana
The University of Kansas

Tyler Stone
The University of Kansas

January, 2007

COMPUTATIONAL MECHANICS LABORATORY

DEPT. OF MECH. ENGG.
3124 LEARNED HALL
1530 W. 15th St
LAWRENCE, KS 66045

ABSTRACT

Rediscretization, moving mesh and solution mapping approaches are presented for boundary value problems (BVPs) and initial value problems (IVPs). When BVPs are solved using mathematical models in Lagrangian frame of reference, the discretizations often become excessively distorted during load incrementing. Rediscretization and a total map of the solution from the original discretization is beneficial in such cases. In the case of IVPs, using space-time strips with time marching, the moving mesh approach permits accurate evolutions of high solution gradient moving fronts using computationally practical spatial discretizations. Both the rediscretization and moving mesh procedure require mapping of the geometry of the new discretization (whole or part of the boundary) onto the original discretization and then mapping of the solution using this geometry map.

Rediscretization and moving mesh approaches for 1D and 2D cases are considered for local approximation of C^0,$C^{0,0}$ Lagrange type, C^0,$C^{0,0}$ p-version hierarchical as well as C^i,$C^{i,j}$ approximations of higher order global differentiability. Merits of higher order global differentiability approximations in h, p, k mathematical and computational framework are demonstrated for rediscretizations as well as moving meshes. Inter-element flux problems present in currently used procedures are examined for C^0 local approximations. Remedies are presented and their absence is clearly shown when the local approximations are of higher classes than C^0. Introduction, literature review and scope of work is presented in Chapter 1. Chapter 2 contains developments of methodologies, approaches and procedures. Numerical studies are presented in Chapter 3. Summary and conclusions are given in Chapter 4.

Contents

List of Figures

List of Tables

Chapter 1

Introduction and Proposed Research

Moving mesh and rediscretization strategies are important and an integral part of practical and accurate computational methodologies. The need for such approaches arise in boundary value problems (BVP) as well as initial value problems (IVP). These strategies must be considered and evaluated for mathematical models constructed in Lagrangian frame of reference as well as Eulerian frame of reference.

In Lagrangian frame of reference the reference frame and the observer both are stationary and all quantities of interest are measured in the fixed frame of reference. In this approach, the material particles and the discretization are the same and hence as the material particles undergo large motion and large strain the discretization become progressively distorted due to which the computations deteriorate and may eventually cease. In order for the computations to proceed and to be reliable and accurate, rediscretization is often necessary when the mesh distortion becomes excessive and the current state of the solution must be mapped accurately onto the rediscretization. The mathematical models in Lagrangian frame of reference are most commonly used for solid continua.

When the mathematical models are constructed in Eulerian frame of reference and simulated numerically, the discretization remains fixed and the material particles flow through it. This approach is ideally suited for arbitrary large motion and large strain rates and hence is the preferred strategy of constructing mathematical models for fluid flow, gas dynamics, polymer flow, etc. The

most significant advantage of this approach is that since the mesh remains fixed, there is no mesh distortion. Hence, in the case of BVPs, there is very little need for rediscretizations if any. However, in many instances IVPs contain high localized gradient moving fronts such as in the case of Riemann shock tube, combustion process with flame propagation, etc. In such cases, severe mesh grading may be required in the zones containing the fronts but a relatively coarser discretization can be employed elsewhere. Since the fronts propagate as time evolution proceeds, the high fidelity of the solution in the local zone containing fronts necessitates the same level of discretization ahead of the fronts. This often results in discretizations that are computationally impractical. For such applications a space-time time marching approach is highly meritorious [1]. In this approach one constructs a space time strip or a slab for an increment of time and computes a converged space-time solution for it through h,p,k adaptivity. The solution state at the open boundary ($t = t_0 + \Delta t$), t_0 being initial time) serves as the initial condition for the second space-time strip or slab for which a converged solution is obtained. This process is continued until the desired time is reached. In this strategy it is obvious that the discretization in space for the second space-time strip needs to be of the same level of refinement as that for the time t_o containing the front if high fidelity of the fronts is to be maintained. The same holds true for subsequent stages of the evolution.

An alternative to the uniformly fine discretization in the zones containing fronts and ahead of the front is to move the discretization at time t_0 with the same speed as the speed at which the fronts are moving. This automatically provides the needed refinement for the front to evolve accurately during the subsequent time steps. An advantage to this approach is that the total degrees of freedom (dofs) at each space-time strip or slab remain approximately the same.

From the standpoint of mathematical treatment the rediscretization and moving mesh approaches are almost identical. In both cases the following features are common.

(1) There is an existing discretization with numerical results, i.e. numerical values of all dofs and the complete solution state are known.

(2) There is a new discretization which may be arbitrary (for the sake of generality) compared to the existing discretization for which the numerical solution is not known.

(3) The geometry of the new discretization needs to be mapped on to the existing discretization

(4) The complete state of the numerical solution needs to be mapped from the existing discretization onto the new discretization.

(5) In the case of BVPs a total map is required for the entire new discretization.

(6) In the case of IVPs with a space-time strip or slab and space-time time marching, only the solution at the open boundary of the previous space-time strip needs to be mapped as the initial condition for the new space-time strip.

(7) Development of measures to ensure that the solution mapping from the existing discretization onto the new discretization accurate.

In principle, the rediscretization and moving mesh methodologies appear rather simple and straightforward. However, their success depends upon the accuracy of the solution mapping.

1.1 Basic Concepts, Methodologies and Literature Review

Functional analysis in Sobolev spaces and approximation theory basically constitute the mathematical foundation of the currently used finite element method. In this approach, local approximations over subdomains (elements) of class C^0 and Galerkin method with weak form have primarily dominated the research over the past forty years. The problems in the computational processes associated with Galerkin method with weak form when the differential operators (for both BVP and IVP) are non-self-adjoint and non-linear have been reported by Surana et. al. [2-4] and are not a subject of study in the present work. However, the role of C^0 local approximations in rediscretization and moving mesh strategies is of critical importance and its consequences need to be examined in detail.

First, we note that when the local approximations are of class C^0, the global approximation for the whole discretization is also of the class C^0. Such local approximations exhibit discontinuity in the first derivatives of the dependent variables normal to the inter-element boundaries which cannot be quantified in the sense of L_2-norms due to the fact that such discontinuities occur

on sets of measure zero. Instead, their influence can only be measured in terms of how they affect the L_2-norms over the interiors of the subdomain. This is referred to as inter-element flux discontinuity problem. When solutions with such inter-element flux discontinuities are mapped onto a new discretization in which the inter-element boundaries do not coincide with those in the existing discretization, new inter-element flux discontinuities are created at different locations. Furthermore, the jump discontinuity magnitude in the map may be quite different than those in the original discretization. This problem is well recognized [5] and there are many published work that present various procedure to minimize such problems. Nonetheless, it is well recognized and agreed upon that such flux problems always exist in almost all rediscretization and moving mesh procedures. Some pertinent published work is discussed in the following.

As described above, a need for rediscretization or moving mesh method typically arises when solving BVPs with a Lagrangian description or IVPs with an Eulerian description. A purely Lagrangian approach is limited by its ability to maintain reliable computations when the material and hence, the mesh undergo large distortion. It has been suggested by Hughes et. al [5] to combine the best features of both approaches in the Arbitrary-Lagrangian-Eulerian (ALE) method. The ALE method employs continuous rezoning of the mesh to provide both flexibility for dealing with large distortions in the material and resolution for capturing details in the solution. This proves especially useful when applied to fluid-structure interaction problems. The difficulty in the ALE method is the difficulty in finding algorithms to prescribe the appropriate nodal displacements during rezoning. The authors have noted the need for studies regarding the accuracy for such an algorithm.

The Moving Finite Elements (MFE) of Miller [6, 7] has been developed to maintain resolution for IVPs with sharp solution gradients or "near-shocks". In such generalized methods, nodes automatically move to critical areas where finer resolution is needed to accurately describe the solution. The usefulness of MFE has been demonstrated in the solution of transient Burgers equation in which the nodes rapidly accumulate where the solution is steepest. A concern of MFE is the possibility of overturned solutions or shocks, as discussed for convection diffusion phenomena by Baines [8]. Baines has reported great success in solving difficult problems when employing

appropriate penalty functions. The inter-element flux problems inherent in these procedures due to C^0 local approximations remain unresolved.

1.2 Scope of Present Research

In the present work, rediscretization and moving mesh procedures are developed, evaluated and numerically demonstrated in h,p,k mathematical and computational framework [1-4]. In this framework, the order k of the approximation space is an independent computational parameter in addition to h, the characteristic discretization length and p, the degree of local approximation. The parameter k defines global differentiability of the approximation. Thus, the local approximations are considered in $H^{k,p}(\bar{\Omega}^e)$ scalar product spaces containing approximation functions of degree p yielding global differentiability of order $(k-1)$, i.e. global approximations of class C^k. Methodologies and procedure are developed (Chapter 2) for: (1) mapping the new discretization onto the existing discretization (2) mapping of the solution from the existing discretization onto the rediscretization (3) measures that ensure the accuracy of the mapped solution for 1D and 2D BVPs as well as IVPs in h,p,k framework. Numerical studies for 1D and 2D BVPs and 1D IVPs are presented in Chapter 3. A summary of the work, conclusions and some directions for future work are presented in Chapter 4.

Chapter 2

Rediscretization and Moving Mesh Methodology: Mathematical and Computational Developments

This chapter contains development of mathematical and computational methodologies for rediscretization and moving meshes as well as developments of the measures to assess the validity and accuracy of the proposed approach. First, we consider rediscretizations associated with BVPs. For the sake of simplicity, we consider a BVP in one dependent and independent variable (an ordinary differential equation). One-dimensional axial deformation of an elastic rod, convection-diffusion equation and Burgers equation are a few examples of such BVPs.

2.1 Approximations of Class C^0, Lagrange Functions, 1D Case

Let

$$A\phi - f = 0 \quad in \quad \Omega = (0, L) \tag{2.1}$$

be the BVP (with some boundary conditions). Let the differential operator be of order $2m$ and also let the theoretical solution of (2.1) be of class $C^k(\Omega)$, $k \geq 2$. A finite element formulation of (2.1) may be constructed using any appropriate integral strategy based on the nature of the differential

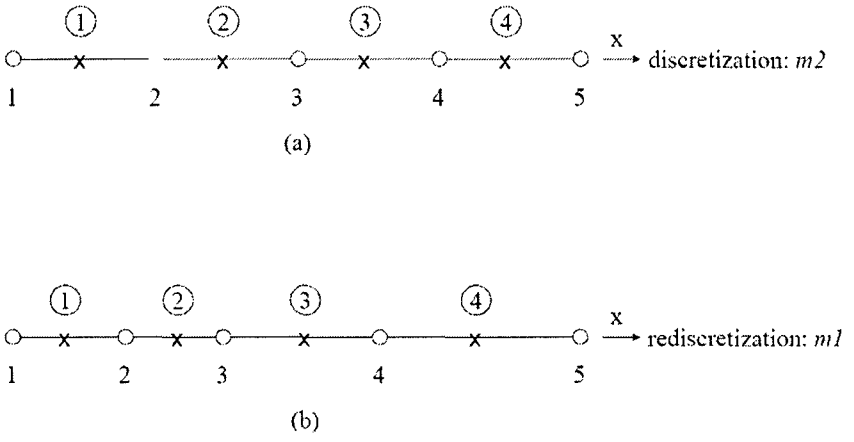

Figure 2.1: Discretization $m1$ (a): current mesh and rediscretization $m2$ (b): new mesh

operator A [2]-[4]. Let $\bar{\Omega}^T_{m1}$ be a four-element discretization: m_1 (Figure 2.1) for obtaining a numerical solution of (2.1), in which $\bar{\Omega}^e_{m1}$ is a subdomain (or an element) such that

$$\bar{\Omega}^T_{m_1} = \bigcup_e \bar{\Omega}^e_{m_1} \tag{2.2}$$

Let ${}^{m1}\phi_h(\bar{\Omega}^T_{m1})$ be the global solution (approximation) for $\bar{\Omega}^T_{m1}$. Then:

$${}^{m1}\phi_h(\bar{\Omega}_{m1}) = \bigcup_e {}^{m1}\phi^e_h(\bar{\Omega}^e_{m1}) \tag{2.3}$$

in which ${}^{m1}\phi^e_h(\bar{\Omega}^e_{m1})$ is the local approximation for a subdomain $\bar{\Omega}^e_{m1}$. For the sake of simplicity we assume the p-level to be two and the approximation functions to be of standard Lagrange type implying the function values at each node are the nodal degrees of freedom and ${}^{m1}\phi_h$ and ${}^{m1}\phi^e_h$ are of class C_0. Let each element of the discretization be mapped in the natural coordinate space ξ with local node numbers 1,2 and 3 and let ${}^{m1}x^e_i$; $i = 1, 2, 3$ to be the global coordinates of the nodes of the element (Figure 2.2). Let

$${}^{m1}\chi^e(\xi, \eta) = \sum_{i=1}^{3} \bar{N}_i(\xi, \eta) {}^{m1}\chi^e_i \tag{2.4}$$

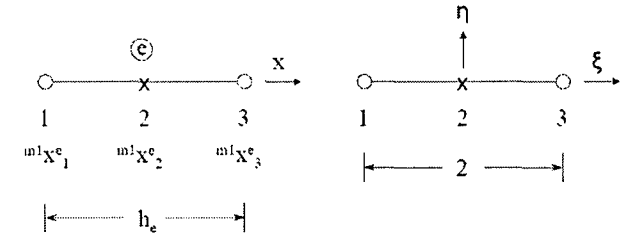

(a) element ⓔ of $\bar{\Omega}^T_{m1}$ in physical coordinate space

(b) map of element ⓔ of $\bar{\Omega}^T_{m1}$ in natural coordinate space

Figure 2.2: Element e and its map in natural coordinate space

define the mapping of element e of $\bar{\Omega}^T_{m_1}$ with domain $\bar{\Omega}^e_{m_1}$ in the natural coordinate space.

Figure 2.1 (b) shows a four element rediscretization ($m2$) of the domain $\bar{\Omega}$ in which the interior nodes (including inter-element boundaries) do not coincide with the original discretization m_1 (for the sake of generality).

Let $^{m2}\phi_h(\bar{\Omega}^T_{m2})$ be the map of $^{m1}\phi_h(\bar{\Omega}^T_{m1})$ over the discretization $m2$ such that

$$^{m2}\phi_h(\bar{\Omega}^T_{m2}) = \bigcup_e {}^{m2}\phi^e_h(\bar{\Omega}^e_{m2}) \tag{2.5}$$

in which $^{m2}\phi_h(\bar{\Omega}^e_{m2})$ is the approximation of ϕ over Ω^e_{m2}, an element e of the discretization $m2$. Determination of $^{m2}\phi_h(\bar{\Omega}^T_{m2})$ over $\bar{\Omega}^T_{m2}$ from $^{m1}\phi_h(\bar{\Omega}^T_{m1})$ over $\bar{\Omega}^T_{m1}$ is a two step process. First we determine the locations of the nodes of mesh $m2$ onto mesh $m1$. We refer to this step as mapping of rediscretization $m2$ onto discretization $m1$. In the second step we determine $^{m2}\phi_h(\bar{\Omega}^T_{m2})$ from $^{m1}\phi_h(\bar{\Omega}^T_{m1})$ using the mapped geometry. Details are described in the following.

2.1.1 Mapping of Rediscretization ($m2$) onto Original Discretization ($m1$)

First, we note that the Cartesian coordinates of nodes of rediscretization $m2$ are known. Secondly, our ultimate goal is the determination of $^{m2}\phi_h(\bar{\Omega}^T_{m2})$ from $^{m1}\phi_h(\bar{\Omega}^T_{m1})$. This essentially requires the determination of the numerical values of the nodal degrees of freedom for each node of $m2$. Once

the nodal dofs for $m2$ are known, ${}^{m2}\phi_h^e(\bar{\Omega}^e_{m2})$ is defined through local approximations and hence ${}^{m2}\phi_h(\bar{\Omega}^T_{m2})$ by (2.5). We proceed as follows.

(a) Consider an element e of $\bar{\Omega}^T_{m2}$ with domain $\bar{\Omega}^e_{m2}$ and nodal coordinates ${}^{m2}\chi^e_i$.

(b) Determine the elements in discretization $m1$ containing these nodes. Let ${}^{m2}\chi^e_i, i = 1, 2, 3$ lie in elements p, q and r of $\bar{\Omega}^T_{m1}$ respectively.

(c) Determine the ξ coordinates in elements p, q, r for the locations ${}^{m2}\chi^e_i, i = 1, 2, 3$. Using the geometry mapping for elements p, q, r of $\bar{\Omega}^T_{m1}$, we have the following in which ${}^{m2}\chi^e_i$, ${}^{m1}\chi^p_i$, ${}^{m1}\chi^q_i$, ${}^{m1}\chi^r_i$ are known x-coordinates.

$$ {}^{m2}\chi^e_1 = \sum_{i=1}^{3} \bar{N}_i(\xi) {}^{m1}\chi^p_i \tag{2.6} $$

$$ {}^{m2}\chi^e_2 = \sum_{i=1}^{3} \bar{N}_i(\xi) {}^{m1}\chi^q_i \tag{2.7} $$

$$ {}^{m2}\chi^e_3 = \sum_{i=1}^{3} \bar{N}_i(\xi) {}^{m1}\chi^r_i \tag{2.8} $$

Each of the (2.6)-(2.8) are quadratic expressions in ξ and hence we can determine a pair of ξ values from each of (2.6)-(2.8). Let $({}^{m1}\xi^p)_i, i = 1, 2$; $({}^{m1}\xi^q)_i, i = 1, 2$; and $({}^{m1}\xi^r)_i, i = 1, 2$ be the pair of values of ξ determined from (2.6)-(2.8) respectively. Discarding those outside the range $[-1, 1]$, we obtain the ξ coordinates $({}^{m1}\xi^p_1)^e$, $({}^{m1}\xi^p_2)^e$ and $({}^{m1}\xi^p_3)^e$ for the x-locations.

(d) Using the procedure described in (c), we can determine the elements of $\bar{\Omega}^T_{m1}$ containing each node of the elements of $\bar{\Omega}^T_{m2}$ and their corresponding ξ locations in the elements of $\bar{\Omega}^T_{m1}$.

2.1.2 Mapping of ${}^{m1}\phi_h(\bar{\Omega}^T_{m1})$ onto $\bar{\Omega}^T_{m2}$, i.e. Determination of ${}^{m2}\phi_h(\bar{\Omega}^T_{m2})$

For an element e of $\bar{\Omega}^T_{m2}$ with the map of its nodes in elements p, q and r of $\bar{\Omega}_{m1}$ and their ξ-coordinates determined in (c) of Section 2.2.1, we proceed as follows. For elements p, q and r of

$\bar{\Omega}^T_{m1}$ the local approximations are given by

$$ {}^{m1}\phi^i_h(\bar{\Omega}^i_{m1}) = \sum_{i=1}^{3} N_j(\xi)\, {}^{m1}\phi^i_j; \quad i = p, q, r \tag{2.9} $$

where ${}^{m1}\phi^i_j$; $j = 1, 2, 3$ are nodal dofs for element i of discretization $m1$ (known function values in this case). We note that

$$ {}^{m1}\phi^p_h(\bar{\Omega}^p_{m1})|_{\xi=({}^{m1}\xi^p_1)^e} = {}^{m2}\phi^e_1 \tag{2.10} $$

$$ {}^{m1}\phi^q_h(\bar{\Omega}^q_{m1})|_{\xi=({}^{m1}\xi^q_2)^e} = {}^{m2}\phi^e_2 \tag{2.11} $$

$$ {}^{m1}\phi^r_h(\bar{\Omega}^r_{m1})|_{\xi=({}^{m1}\xi^r_3)^e} = {}^{m2}\phi^e_3 \tag{2.12} $$

Using (2.9)-(2.12) numerical values of the nodal dofs ${}^{m2}\phi^e_1$, ${}^{m2}\phi^e_2$, ${}^{m2}\phi^e_3$ of element e of discretization $\bar{\Omega}^T_{m2}$ are obtained. This procedure is repeated for each element and thus eventually all numerical values of the dofs for each node of the discretization $\bar{\Omega}^T_{m2}$ are determined. Now using local approximations for each element $\bar{\Omega}^T_{m2}$ the solution ${}^{m2}\phi^e_h$ is established and we have

$$ {}^{m2}\phi^e_h(\bar{\Omega}^e_{m2}) = \sum_{i=1}^{3} N_i(\xi)\, {}^{m2}\phi^e_i \tag{2.13} $$

and

$$ {}^{m2}\phi_h(\bar{\Omega}^T_{m2}) = \bigcup_e {}^{m2}\phi^e_h(\bar{\Omega}^e_{m2}) \tag{2.14} $$

Thus we have the map ${}^{m2}\phi_h(\bar{\Omega}^T_{m2})$ onto $\bar{\Omega}^T_{m2}$ from ${}^{m1}\phi_h(\bar{\Omega}^T_{m1})$ onto $\bar{\Omega}^T_{m1}$.

Remarks

(1) Many issues need to be addressed regarding the validity and accuracy of the solution mapping procedure described above.

(2) Extension of this procedure to the C^0 p-version hierarchical local approximations is needed.

(3) Extension to higher order continuity local approximations is required.

(4) Measures to assess the accuracy of the mapping procedure need to be established.

(5) Extensions to 2D and 3D.

2.1.3 Measures of the Accuracy of the Mapping

In the development presented here, there are some specific points to be noted that may be helpful in further understanding the behaviors of ${}^{m1}\phi_h$ and ${}^{m2}\phi_h$ and development of the measures of accuracy of ${}^{m2}\phi_h$.

(1) ${}^{m1}\phi_h^e(\Omega_{m1}^e)$ and ${}^{m2}\phi_h^e(\Omega_{m2}^e)$ are of class C^2 due to p-level of 2, however ${}^{m1}\phi_h^e(\bar{\Omega}_{m1}^e)$ and ${}^{m2}\phi_h^e(\bar{\Omega}_{m2}^e)$ are of class C^0. Thus, ${}^{m1}\phi_h(\bar{\Omega}_{m1}^T)$ and ${}^{m1}\phi_h(\bar{\Omega}_{m1}^T)$ are of class C^2 over $\Omega_{m1}^T = int(\bigcup_e \bar{\Omega}_{m1}^e)$ and $\Omega_{m2}^T = int(\bigcup_e \bar{\Omega}_{m2}^e)$ but of class C^0 at the inter-element boundaries.

(2) Since ${}^{m1}\phi_h^e$ and ${}^{m2}\phi_h^e$ are of class C^0 globally, inter-element discontinuities (jumps) exist in their first derivatives normal to the inter-element boundaries in both discretizations. Locations of the jump discontinuities are different in $m1$ and $m2$. The magnitudes of the jump discontinuities may also differ between $m1$ and $m2$.

(3) Based on (1) and (2), $\left\| \frac{d^i({}^{m1}\phi_h)}{dx^i} \right\|_{L_2}$ and $\left\| \frac{d^i({}^{m2}\phi_h)}{dx^i} \right\|_{L_2}$; $i = 0, 1$, in general may be the first good indicators regarding the reliability of mapping. Their agreement between $m1$ and $m2$ discretizations indicate a good mapping. Lack of agreement, on the other hand, points out the existence of flux discontinuity problems.

(4) When to map: (3) raises a very significant question, i.e. when to map. We elaborate on this point in the following and provide some clear guidelines.

(a) Since in the above discussion the approximations are of class C^0, the inter-element jumps in the first derivatives exist. However, if the theoretical solution is sufficiently smooth we expect weak convergence of the class C^0 to C^1 upon h, p refinements. In such converged solutions, the jump discontinuities are no longer significant hence we expect $\left\| \frac{d^i({}^{m1}\phi_h)}{dx^i} \right\|_{L^2}$ and $\left\| \frac{d^i({}^{m2}\phi_h)}{dx^i} \right\|_{L^2}$; $i = 1, 2$, to be in relatively good agreement.

(b) However, when ${}^{m1}\phi_h$ is not weakly converged, jump discontinuities at the inter-element boundaries are significant. In such case, mapping the solution to rediscretizations is not a preferred strategy.

(c) Based on (a) and (b), it is rather straight-forward to see that when

$$\left\|\phi^{m1} - \phi_h\right\|_{L_2} \to 0 \tag{2.15}$$

the map of ${}^{m1}\phi_h$ to ${}^{m2}\phi_h$ is unique and so are their corresponding L_2-norms. Likewise, when

$$\left\|\frac{d({}^{m1}\phi_h)}{dx} - \frac{d\phi}{dx}\right\|_{L_2} \to 0 \tag{2.16}$$

the maps of $\frac{d({}^{m1}\phi_h)}{dx}$ to $\frac{d({}^{m2}\phi_h)}{dx}$ are unique and so are their corresponding L_2-norms.

(d) It is rather clear from (b) and (c) that before attempting to map the solution ${}^{m1}\phi_h$ on $\bar{\Omega}^T_{m2}$, it is preferable to achieve weak convergence of ${}^{m1}\phi_h$ to ϕ. This eliminates the mapping errors due to the fact that ${}^{m1}\phi_h \cong \phi$. Weakly converged solutions for higher p-level Lagrange elements (with function values as nodal dofs) shall permit good maps onto $\bar{\Omega}^T_{m2}$ in which higher order global differentiability is possible to preserve in the weak sense.

2.2 p-version Hierarchical Local Approximations of Class C^0: 1D case

Consider discretization $m1$ of Figure 2.1 in which the elements are three node p-version C^0 hierarchical elements with p-level of p_ξ. In this case ${}^{m1}\phi_h(\bar{\Omega}^T_{m1})$ is of class p_ξ over $\Omega^T_{m1} = int(\bigcup_e \bar{\Omega}^e_{m1})$ but is of class C^0 at the inter-element boundaries. Mapping of $\bar{\Omega}^T_{m2}$ onto $\bar{\Omega}^T_{m1}$ follows in the same procedure described in Section 2.1.1. However, mapping of ${}^{m1}\phi_h(\bar{\Omega}^T_{m1})$ onto $\bar{\Omega}^T_{m2}$ to obtain ${}^{m2}\phi_h(\bar{\Omega}^T_{m2})$ is somewhat different than the procedure discussed in section 2.1.2. We note that the dofs at the end nodes are function values whereas at the mid-side node of each element the dofs are $\frac{d^i\phi}{d\xi^i}$; $i = 2, \ldots, p_\xi$. Thus, at each mid-side node of elements $\bar{\Omega}^e_{m2}$ numerical values of $\frac{d^i\phi}{d\xi^i}$ needs to be obtained from the elements of discretization $\bar{\Omega}^T_{m1}$. This cannot be done accurately due to the fact that ${}^{m1}\phi_h$ is of class C^0globally.

This situation is not as hopeless as it might appear. A careful examination of the derivation

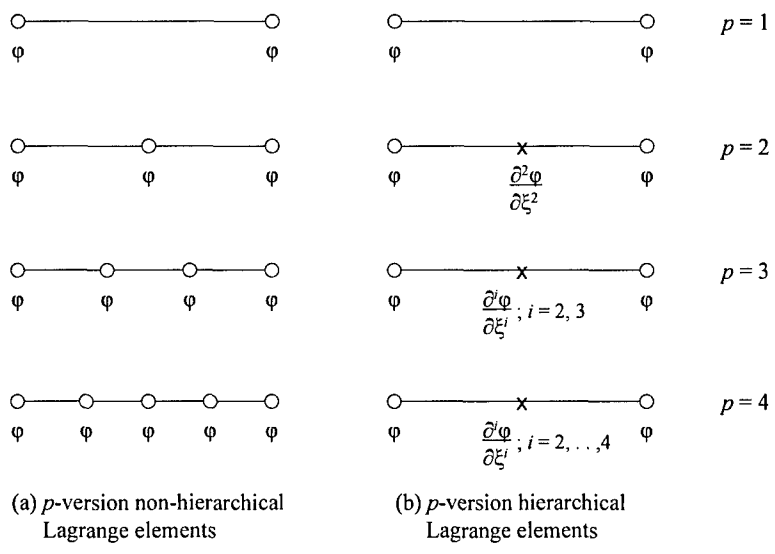

Figure 2.3: C^0 p-version (a) non-hierarchical and (b) hierarchical Lagrange elements

of C^0 p-version hierarchical basis functions leads to a resolution. Figure 2.3 shows C^0 p-version non-hierarchical Lagrange elements and the corresponding p-version hierarchical Lagrange elements derived from them for various p-levels. Let us assume that ${}^{m1}\phi_h(\bar{\Omega}^T_{m1})$ is a converged C^0 solution for discretization $m1$ at p-levels of p_ξ. It is desired to map this solution onto rediscretization $m2$. This obviously requires nodal values of ϕ at the non-hierarchical nodes and $\frac{d^i\phi}{d\xi^i}$; $i = 2, \ldots, p_\xi$ at each of the hierarchical nodes. Since the C^0 p-version hierarchical approximation functions are derived from the corresponding non-hierarchical Lagrange element with $(p_\xi + 1)$ equally spaced nodes between $-1 \leq \xi < 1$, we can proceed as follows.

(a) Consider $\bar{\Omega}^e_{m2}$ of $\bar{\Omega}^T_{m2}$ with the end nodes located at ${}^{m2}\chi^e_1$ and ${}^{m2}\chi^e_3$.

(b) Determine elements p and q of $\bar{\Omega}^T_{m1}$ containing these nodes with the corresponding values of ξ, i.e. $({}^{m2}\xi^p_1)^e$ and $({}^{m2}\xi^q_3)^e$.

(c) Consider $(p_\xi + 1)$ equally spaced points between ${}^{m2}\chi^e_1$ and ${}^{m2}\chi^e_3$ and determine their ξ coor-

dinates in elements p and q of $\bar{\Omega}^T_{m1}$

(d) Use the local approximations of elements p and q of $\bar{\Omega}^T_{m1}$ and the ξ coordinates determined in (c) to obtain function values at $(p_\xi + 1)$ equally spaced points.

(e) Convert these $(p_\xi + 1)$ function values to $\frac{d^i\phi}{d\xi^i}$; $i = 2, \ldots, p_\xi$, at the ${}^{m2}\chi^e_2$ coordinate location. This completes the map of ${}^{m1}\phi(\bar{\Omega}^T_{m1})$ over $\bar{\Omega}^e_{m2}$ of $\bar{\Omega}^T_{m2}$. This procedure is repeated for each element of $\bar{\Omega}^T_{m2}$ to obtain ${}^{m2}\phi_h(\bar{\Omega}^T_{m2})$.

Remarks

(1) When ${}^{m1}\phi_h(\bar{\Omega}^T_{m1})$ of class C^0 is weakly converged to good accuracy, $\left\|\phi - {}^{m1}\phi_h\right\|_{L_2} \to 0$ and the proximity of ${}^{m1}\phi_h$ to the theoretical solution ϕ is established.

(2) Based on (1), computations of $\frac{d^i\phi}{d\xi^i}$ for the hierarchical nodes of $\bar{\Omega}^T_{m2}$ using function values at $(p_\xi + 1)$ equally spaced points between the end nodes of each element of $\bar{\Omega}^T_{m2}$ appear to be a reasonable proposition.

(3) In this procedure, accuracy of the function is the best in the map and it deteriorates for progressively higher order derivative hierarchical dofs.

(4) This procedure is expected to yield better accuracy of the map ${}^{m2}\phi_h$ as compared to the procedure in which $\frac{d^i\phi}{d\xi^i}$ for the hierarchical nodes are directly computed using ${}^{m1}\phi_h(\bar{\Omega}^T_{m1})$.

(5) Numerical studies related to this procedure are not presented in this thesis and will be a subject of future study.

2.3 p-version Approximations of Higher Classes (C^j; $j = 1, \ldots$): 1D case

Consider discretizations $m1$ and $m2$ shown in Figure 2.1 in which the local approximations for each element can be of higher class. Consider ${}^{m1}\phi_h(\bar{\Omega}^T_{m1})$ of classes $C^J(\bar{\Omega}^T_{m1})$; $j = 1, 2, \ldots$ in scalar product spaces $H^{k,p}(\bar{\Omega}^e_{m1})$ in which $p = 2k - 1$ and $j = k - 1$. p-levels $p = 2j - 1$ are the minimum p-levels for $j = 1, 2, \ldots$. At these p-levels the hierarchical center node has no degrees of freedom.

Let m_2 be a rediscretization (Figure 2.1 (b)) in which the locations of the interior nodes of the mesh are not coincident with those in discretization m_1.

Mapping of discretization m_2 onto m_1 follows the same procedure as described in Section 2.1.1. For mapping of the known solution ${}^{m1}\phi_h(\bar{\Omega}^T_{m1})$ onto $\bar{\Omega}^T_{m2}$ to obtain ${}^{m2}\phi_h(\bar{\Omega}^T_{m2})$, we consider the following two cases.

(a) Let the p-level be $p = 2j - 1$ where j is the order of continuity. In this case, only the end nodes have dofs. We note that since ${}^{m1}\phi_h(\bar{\Omega}^T_{m1})$ is of class c^j in $\bar{\Omega}^T_{m1}$ but of class p in Ω^T_{m1}, i.e. at the inter-element boundaries the solution class is c^j but in the interiors of the element the solution class is c^p. When ${}^{m1}\phi_h$ is mapped onto $\bar{\Omega}^T_{m2}$ using the procedure described in section 2.1.2 we expect c^j global differentiability features to be preserved. Consider the following two cases.

(i) Discretization $m1$ (i.e. h and p) is such that ${}^{m1}\phi_h$ is not a converged solution

(ii) Discretization $m1$ is refined sufficiently with adequate p-levels to obtain a converged solution ${}^{m1}\phi_h$ before mapping it onto $\bar{\Omega}^T_{m2}$.

The convergence is assumed to be in the appropriate norms in the corresponding approximation spaces. Consequences of (i) or (ii) are discussed and illustrated numerically in Chapter 3.

(b) Consider p-levels $p_\xi > 2j + 1$ where j is the order of continuity of ${}^{m1}\phi_h(\bar{\Omega}^T_{m1})$. In the case the hierarchical center node of each element in both discretizations has dofs that are $\frac{d^i\phi}{d\xi^i}$; $i = 2j - 1, \ldots, p_\xi$. We consider the following two approaches for mapping ${}^{m1}\phi_h(\bar{\Omega}^T_{m1})$ onto $\bar{\Omega}^T_{m2}$.

(i) Obtain numerical values of $\frac{d^i\phi}{d\xi^i}$ for the hierarchical nodes of $\bar{\Omega}^T_{m2}$ directly using local approximations for the elements of discretization $\bar{\Omega}^T_{m1}$. In this case we expect the same type of contamination in ${}^{m2}\phi_h$ as described for C^0 p-version hierarchical approximations even when the solution ${}^{m1}\phi_h$ is converged. This obviously is due to the fact that global differentiability of ${}^{m1}\phi_h$ is lower than what is required for obtaining numerically accurate values of hierarchical dofs.

(ii) Use the alternate procedure described in Section 2.1.2 which employs corresponding C^0 Lagrange configuration to obtain $\frac{d^i\phi}{d\xi^i}$. In this approach higher accuracy of ${}^{m2}\phi_h$ is expected due to the fact that only converged function values are utilized in the computations of hierarchical dofs.

2.4 Two-dimensional Case: Rediscretization

Consider discretizations $m1$ and $m2$ of Fig. 2.4. Let m_1 be the original discretization for which the solution ${}^{m1}\phi_h(\bar{\Omega}^T_{m1})$ is known and $m2$ be a rediscretization for which ${}^{m2}\phi_h(\bar{\Omega}^T_{m2})$, a map of ${}^{m1}\phi_h(\bar{\Omega}^T_{m1})$, is desired. Regardless of whether the local approximation of type C^0 Lagrange, C^0 p-version hierarchical or that of higher order global differentiability, the mapping of the geometry of rediscretization $m2$ onto $m1$ remain the same. Hence, we consider this first.

2.4.1 Mapping of Rediscretization $m2$ onto discretization m_1

Let each element of the discretizations $m1$ and $m2$ be mapped onto a two-unit square natural coordinate space ξ-η with the origin of the coordinate system located at the center of the square. For simplicity, we assume the shape functions in the mapping to be quadratic. For a typical element e of $\bar{\Omega}^T_{m1}$, we can write

$$\begin{aligned} {}^{m1}x^e(\xi,\eta) &= \sum_{i=1}^{n} \bar{N}_i(\xi,\eta)\ {}^{m1}x^e_i \\ {}^{m1}y^e(\xi,\eta) &= \sum_{i=1}^{n} \bar{N}_i(\xi,\eta)\ {}^{m1}y^e_i \end{aligned} \tag{2.17}$$

To determine the map of $\bar{\Omega}^T_{m2}$ onto $\bar{\Omega}^T_{m1}$, we follow the procedure described in Section 2.1.1 for the 1D case. The basic steps are described in the following.

(a) Consider an element e of $\bar{\Omega}^T_{m2}$ with domain $\bar{\Omega}^e_{m2}$ and nodal coordinates $({}^{m2}x^e,\ {}^{m2}x^e)$; $i = 1,\ldots,n$, n being the number of nodes.

(b) Determine the elements in the discretization $\bar{\Omega}^T_{m1}$ containing these nodes. Let $p, q, r, \ldots$ be such elements.

(c) It is sufficient to consider a typical node of element $\bar{\Omega}^e_{m2}$. The procedure described for this node can be repeated for the remaining node. Consider node 1 with coordinates $({}^{m2}x^e_1, {}^{m2}y^e_1)$. Let these this node be located in element p of $\bar{\Omega}^T_{m1}$. Determine the ξ, η coordinates in element p for the location $({}^{m2}x^e_1, {}^{m2}y^e_1)$. Using the geometry mapping (2.17) for element p of $\bar{\Omega}^T_{m1}$, we have

$$\begin{aligned} {}^{m2}x^e_1 &= \sum_{n=1}^{n} \bar{N}_i(\xi,\eta)\ {}^{m1}x^p_i \\ {}^{m2}y^e_1 &= \sum_{n=1}^{n} \bar{N}_i(\xi,\eta)\ {}^{m1}y^p_i \end{aligned} \tag{2.18}$$

in which $({}^{m2}x^e, {}^{m2}y^e)$, $({}^{m1}x^p_i, {}^{m2}y^p_i)$; $i = 1, \ldots, n$ are known coordinates. Equations (2.18) are quadratic simultaneous equations in ξ and η. These are solved numerically using Newton's linear method. This yields two roots, i.e. two pairs are ξ and η. The values in the range $[\xi, \eta] = [-1, 1] \times [-1, 1]$ are retained while the others are discarded. Let $(({}^{m1}\xi^p_1)^e, ({}^{m1}\eta^p_1)^e)$ be the values of ξ and η for location $({}^{m2}x^e_1, {}^{m2}y^e_1)$ in element p of $\bar{\Omega}^T_{m1}$. Using this procedure the (ξ, η) locations for all nodes of $\bar{\Omega}^e_{m2}$ are determined in elements $p, q, r, \ldots$ of $\bar{\Omega}^T_{m1}$. Let $(({}^{m1}\xi^p_1)^e, ({}^{m1}\eta^p, 1)^e), (({}^{m1}\xi^q_2)^e, ({}^{m1}\eta^q_2)^e), \ldots$ be the desired ξ, η coordinates.

(d) This procedure described in (c) is repeated for each element of $\bar{\Omega}^T_{m2}$, thus establishing a map of $\bar{\Omega}^T_{m2}$ onto $\bar{\Omega}^T_{m1}$.

2.4.2 Mapping of ${}^{m1}\phi_h(\bar{\Omega}^T_{m1})$ onto $\bar{\Omega}^T_{m2}$, i.e. Determination of Solution Map ${}^{m2}\phi_h(\bar{\Omega}^T_{m2})$

It is sufficient to describe the solution mapping strategy for a typical element e of $\bar{\Omega}^T_{m2}$ with its domain $\bar{\Omega}^e_{m2}$ and the ξ, η coordinates of its map in elements $p, q, r, \ldots$ of $\bar{\Omega}^T_{m1}$ (determined in (c) of Section 2.4.1). For a typical element i of $\bar{\Omega}^T_{m1}$ the local approximation is given by

$${}^{m1}\phi^i_h(\xi,\eta) = \sum_{j=1}^{nd} \bar{N}_j(\xi,\eta)\ {}^{m1}\phi^i_j \tag{2.19}$$

in which ${}^{m1}\phi^i_h$ are the nd dofs for element i of $\bar{\Omega}^T_{m1}$. Consider the following types of local approximations for typical elements $\bar{\Omega}^e_{m1}$ and $\bar{\Omega}^e_{m2}$ of $\bar{\Omega}^T_{m1}$ and $\bar{\Omega}^T_{m2}$.

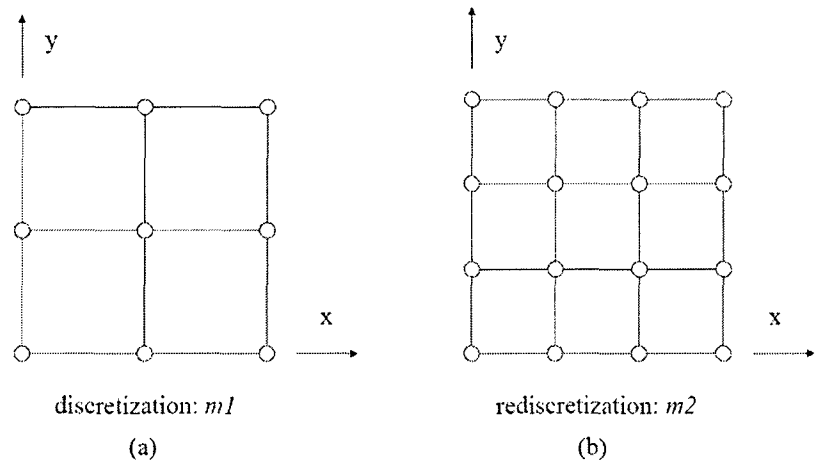

Figure 2.4: Discretization $m1$ (a): current mesh and rediscretization $m2$ (b): new mesh

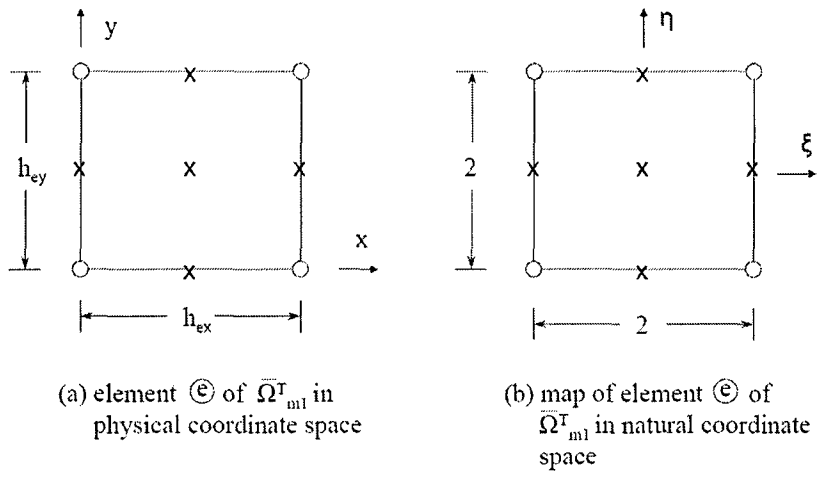

Figure 2.5: Element e and its map in natural coordinate space

(i) C^0 local approximations of Lagrange type:

Tensor product of 1D C^0 Lagrange functions can be used in ξ, η to generate the approximation functions for such elements. For such elements, each node of every element has only function values as a dof. Hence, using local approximations of the type (2.19) for the elements of $\bar{\Omega}^T_{m1}$ and the ξ, η coordinates of the nodes of the elements of $\bar{\Omega}^T_{m1}$, the function values can be easily determined. This procedure is exactly parallel to that described for 1D Lagrange C^0 elements in Section 2.1.2.

(ii) $C^{0,0}$ p-version hierarchical approximations:

These approximation functions can be derived using products of 1D p-version hierarchical basis functions in ξ and η. In this case the corner nodes are non-hierarchical nodes and have function values as dofs. Mid-side and center nodes on the other hand are hierarchical nodes and contain derivatives of the function with respect to ξ and η as dofs [9],[10]. We can proceed as follows and possibly develop two strategies.

(a) In the first case, dofs at the non-hierarchical nodes are determined using the approach described in (i). The hierarchical dofs are also determined using local approximations for the corresponding elements of $\bar{\Omega}^T_{m1}$. The problems in this approach are exactly the same as those in the 1D case in Section 2.2. It appears that in this approach, good maps of ${}^{m1}\phi_h(\bar{\Omega}^T_{m1})$ onto $\bar{\Omega}^T_{m2}$, i.e. ${}^{m2}\phi_h(\bar{\Omega}^T_{m2})$, are not possible. That is, ${}^{m2}\phi_h(\bar{\Omega}^T_{m2})$ is always contaminated due to inaccurate values of hierarchical dofs, which essentially is a consequence of limited global differentiability of ${}^{m1}\phi_h(\bar{\Omega}^T_{m1})$ (C^0 in this case).

(b) Non-hierarchical dofs, i.e. function values, are determined in the same way as in (a), but hierarchical dofs are determined using their corresponding C^0 Lagrange configurations as discussed for the 1D case in Section 2.2. This approach appears meritorious and will be investigated further in future work.

(iii) p-version Approximations of Higher Classes $C^{i,j}$; $i, j = 1, 2, \ldots$:

In this category we consider two different types of local approximations. In both cases, element nodal configuration is that of standard nine nodes.

(a) $C^{i,j}$ p-version higher order continuity approximations: rectangular elements

If the element shapes in the physical coordinate space are rectangular and if the coordinate axes x, y are parallel to ξ, η, then the approximation functions for these elements can be generated using tensor products of 1D C^i, C^j type p-version approximations in ξ and η natural coordinates [10].

(b) $C^{i,j}$ p-version higher order continuity approximations: distorted elements in the physical coordinate space

When the element shapes in the physical coordinate space are distorted, the tensor product cannot be utilized to determine approximation functions. In this case, an alternate procedure [11] is necessary.

Remarks

(1) The dofs at the corner nodes are function values as well as derivatives of the function with respect to ξ and η depending upon the order of continuity in x and y.

(2) The dofs at the corner nodes for elements of type (a) and (b) are not the same, the major difference being that all dofs at the corner nodes of type (a) cannot be transformed under pure rotation whereas those of type (b) cannot be.

(3) From (2), it is obvious that the dofs at the mid-side and center nodes of elements of type (a) and (b) are different as well.

(4) A comprehensive treatment of the mapping procedures for these elements are beyond the scope of this thesis and will be a subject of future study.

2.4.3 Present Study

In the present study we consider $C^{1,1}$ local approximations in which p-levels in the ξ and η directions are minimally conforming and the element shapes are rectangular with the ξ and η axes parallel to the x and y axes. In this case, p-levels in both ξ and η are three. There are nodal dofs at the hierarchical nodes. The dofs at each of the corner nodes are ϕ, $\frac{d\phi}{dx}$, $\frac{\partial\phi}{\partial y}$ and $\frac{\partial^2\phi}{\partial x \partial y}$. We also consider p-levels beyond minimally conforming in which case there are dofs at the mid-side and center nodes.

Remarks

(1) Computation of ϕ, $\frac{d\phi}{dx}$, and $\frac{\partial\phi}{\partial y}$ at the non-hierarchical nodes of $\bar{\Omega}^T_{m2}$ presents no problem due to global differentiability of ${}^{m1}\phi_h(\bar{\Omega}^T_{m1})$ of class C^1 in x and y. However, accurate determination of $\frac{\partial^2\phi}{\partial x\partial y}$ requires ${}^{m1}\phi_h$ to be of class C^2 in x and y. Hence, in this case when ${}^{m1}\phi_h$ is mapped onto $\bar{\Omega}^T_{m2}$, $\frac{\partial^2\phi}{\partial x\partial y}$ may be corrupted. Numerical studies presented in chapter 3 demonstrate the consequences of the inaccuracies in $\frac{\partial^2\phi}{\partial x\partial y}$ at the corner nodes of $\bar{\Omega}^T_{m2}$.

(2) Alternate methodology is needed to determine accurate maps of $\frac{\partial^2\phi}{\partial x\partial y}$. Use of Lagrange C^0 configurations is a possibility.

(3) Numerical studies for p-levels beyond minimally conforming are also presented in Chapter 3.

2.5 Rediscretization for Non-linear BVPs

The mapping procedure may result in inaccurate maps of the solution onto rediscretization due to either using non-weakly converged solutions or due to inaccurate maps of the hierarchical dofs. This is critical when the differential operators are self-adjoint or non-self adjoint due to the fact that in both cases the differential operators are linear and there are no straight-forward mechanisms to improve the accuracy of the mapped solution. When the differential operators are non-linear, the inaccurately mapped solution can be used as a starting or initial solution for the rediscretization and Newton's method with line search can be employed to obtain the improved solution for the rediscretization. This solution so obtained is expected to be identical to the solution that one would obtain if new computations were done for the rediscretization. This feature is powerful in the sense that it permits us to eliminate the mapping errors in the solution map onto the rediscretization. Numerical studies are presented using steady-state Burgers equation as a model problem to demonstrate this feature for non-linear BVPs.

2.6 Moving Meshes for 1D IVPs

In many IVPs, isolated high solution gradients (fronts) exist in relatively small portions of the total domain which propagate as evolution proceeds in time. In such cases, a highly refined discretization may be necessary in the portion of the domain containing these solution gradients, but a relatively coarser mesh may be employed elsewhere. However, due to the fact that the zone of high solution gradient advances in time during evolution, it becomes necessary to employ the same level of discretization ahead of the fronts if the fronts are to be resolved accurately. This gives rise to spatial discretization that may be computationally impractical. The Riemann shock tube is a classic example of these types of problems.

In such IVPs, an alternate strategy may be employed to overcome the problem of impractical discretizations. The moving mesh approach is one such option. In this work, we consider space-time integral forms of the IVPs over a single space-time strip in which the space-time integral forms are space-time variationally consistent and employ a space-time time marching process to compute the evolution state until the desired time is reached [1]. The space-time strip for the current increment of time is advanced in space for the subsequent increment of time with the same speed as that of the propagating front without rediscretization. This process is continued until the desired time is reached. Details are presented in the following.

Figure 2.6 shows a single space-time strip (1D IVP) for an increment of time Δt for $t_0 \leq t \leq t_0 + \Delta t$, t_0 being the initial time which can be conveniently assumed to be zero. Consider the first space-time strip discretization (Figure 2.6 (a)). There are four distinct zones A-D. Zone B contains the initial disturbance defined by initial conditions. The spatial discretization in this zone is such that the initial front is resolved accurately for a chosen Δt, p-levels in space and time as well as $k = (k_1, k_2)$ orders of the approximation spaces in space and time. Zone C has the same level of refinement as zone B, but its length in space is determined based upon the speed of propagation of the front in zone B at time $t = t_0$. A converged solution of desired accuracy is computed for the first space-time strip. During the evolution, the front moves from zone B to C with the desired resolution and accuracy. Hence, in zone B there is no need for the same level of refinement for the next increment of time. Thus, for the second increment of time the discretization for the first

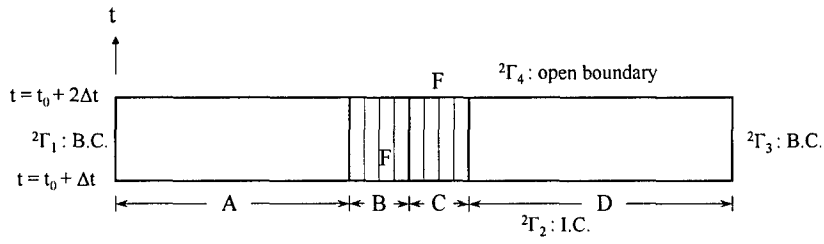

(b) Second space-time strip

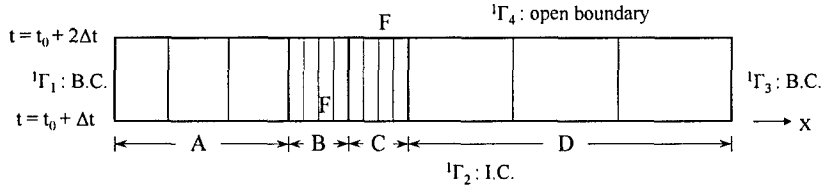

(b) First space-time strip

Figure 2.6: Moving mesh space-time strips for first and second increments of time: F indicate front location

increment of time is employed but is moved in space by a fixed distance determined by the speed of propagation of the front in the x-direction. Figure 2.6 (b) shows the space-time strip for the second increment of time ($t_0 + \Delta t \leq t \leq t_0 + 2\Delta t$).

Computation of the solution for the second space-time strip requires determination of initial conditions on boundary $^2\Gamma_2$ of the space-time strip from the solution on boundary $^1\Gamma_4$ of the first space-time strip, i.e. $^{1\Gamma_4}\phi_h$ from $^1\Gamma_4$ of the first space-time strip needs to be mapped onto $^2\Gamma_2$ of the second space-time strip ($^{2\Gamma_2}\phi_h$). This problem is similar to rediscretization except that in this method the map of the existing solution is only required from one boundary of the existing space-time strip onto another boundary of the next space-time strip as opposed to a complete map for the whole discretization of the space-time strip. Thus, all of the concepts and procedures presented for rediscretization for 2D BVPs are applicable here as well.

Remarks

(1) It is important to note that since the mapping of the solution and its accuracy depends upon the nature of the local approximations (C^0 Lagrange, C^0 p-version hierarchical, higher order continuity, etc), care must be taken to measure the accuracy of the solution map onto boundaries ${}^{i+1}\Gamma_2$ from boundaries ${}^{i}\Gamma_4$ (i being the space-time strip number) before time marching is commenced. Corrupted solution maps will obviously result in faulty evolution and may even cause the computations to cease.

(2) The thrust of the work presented here has been development of methodologies, concepts and their validity. Applications of these concepts to complex IVPs will be the subject of future work.

Chapter 3

Numerical Studies

In this chapter we present numerical studies for rediscretization for 1D and 2D BVPs (self-adjoint, non-self adjoint and non-linear differential operators) and moving meshes for 1D IVP. Numerical studies are organized as follows.

(a) One-dimensional BVP using steady-state 1D convection diffusion equation as a model problem.

  (a1) Local approximations of class C^0 Lagrange type.

  (a2) C^0 p-version hierarchical local approximations.

  (a3) Local approximations of type C^j; $j = 1, 2, \ldots$ with minimally conforming p-levels.

  (a4) Local approximations of type C^j; $j = 1, 2, \ldots$ with p-levels higher than minimally conforming.

(b) Two-dimensional BVP using Poisson's equation as a model problem.

  (b1) Local approximations of class $C^{0,0}$ Lagrange type.

  (b2) $C^{1,1}$ local approximations with minimally conforming p-level as well as p-levels higher than minimally conforming.

(c) One-dimensional non-linear BVP using 1D steady-state Burgers equation as a model problem.

(d) One-dimensional IVP using 1D transient convection diffusion equation.

3.1 One-dimensional BVP: Steady-state Convection Diffusion Equation, Local Approximations of Class C^0 Lagrange Type ($Pe = 10$)

Consider

$$\frac{d\phi}{dx} - \frac{1}{Pe}\frac{d^2\phi}{dx^2} = 0 \quad in \quad \Omega = (0,1) \tag{3.1}$$

with

$$\phi(0) = 1 \quad and \quad \phi(1) = 0.$$

A theoretical solution of (3.1) can be found in reference [9]. The differential operator in (3.1) is non-self adjoint. We consider a least squares formulation of (3.1) using auxiliary variable $\tau = \frac{d\phi}{dx}$ so that solutions of class C^0 can be considered. The integral for in this case is variationally consistent. We consider a low Pe, say 10, for which the solution is highly diffused and free of sharp fronts and hence has good smoothness. We consider a ten-element uniform discretization with p-level $p = 1$ (original discretization: m_1). The rediscretization considered here is a twelve-element uniform mesh ($m2$) with p-level $p = 1$. We consider the following.

(i) Computation of the solution for the original ten-element discretization: ${}^{m1}\phi_h$ (original solution).

(ii) A map ${}^{m1}\phi_h$ onto rediscretization $m2$: ${}^{m2}\phi_h$ (mapped solution).

(iii) Computation of a new solution for the rediscretization $m2$: $({}^{m2}\phi_h)_{new}$ (new solution).

Due to coarser discretization and low p-level, ${}^{m1}\phi_h$ has significant error. The least squares functional I, dofs, p-levels and L_2-norms of the errors are given in Table 3.1. The purpose of this study is to show how the solution errors map onto the rediscretization when the original solution is not weakly converged. Figures 3.1 and 3.2 show graphs of ϕ and $\frac{d\phi}{dx}$ versus x. Solution ϕ from all three cases (original, mapped and new) are in disagreement. We note that the locations of the $\frac{d\phi}{dx}$ jump discontinuities shift and their magnitudes change as well. The mapped solution is not in agreement with the new solution, which is the correct solution for the rediscretization $m2$. The study clearly

shows the problems associated with mapping unconverged solutions from the original discretization onto the rediscretization. The solution errors in $m1$ and $m2$ are not the same. The inter-element flux problems in $m1$ shift to different locations in $m2$ with different magnitudes. Mapping such ${}^{m1}\phi_h$ is of little value, if any.

We now consider a highly refined uniform discretization $m1$ of 1000 elements with $p = 1$ and obtain ${}^{m1}\phi_h$ and its map onto a rediscretization containing 1200 uniform elements ($m2$). We also compute a new solution for the rediscretization by revolving the BVP. Figures 3.3 and 3.4 show graphs of ϕ and $\frac{d\phi}{dx}$ versus x. In this case, the solution ${}^{m1}\phi_h$ is sufficiently converged (weakly) and thus all three solutions are their derivatives are in excellent agreement. No visible inter-element flux problems exist in any of the solutions. Table 3.2 shows details of least squares error functional I, dofs, error norms, etc.

This study shows the importance of the weak convergence of ${}^{m1}\phi_h$ before mapping it onto the rediscretization $m2$. Weakly converged solutions when mapped onto the rediscretization do not exhibit significant flux problems. In this study, $p = 1$ has been used. Similar findings also hold for higher p-levels when the local approximations are of C^0 Lagrange type.

Table 3.1: Convection diffusion equation (BVP): C^0 Lagrange local approximations.

Solution	Elements	p-level	I	$\|\phi_h - \phi\|_{L_2}$	$\left\|\frac{d(\phi_h)}{dx} - \frac{d\phi}{dx}\right\|_{L_2}$
${}^{m1}\phi_h$	10	1	0.278391e0	0.130565e0	0.800277e0
${}^{m2}\phi_h$	12	1	-	0.134777e0	0.799217e0
$({}^{m2}\phi_h)_{new}$	12	1	0.215044e0	0.100951e0	0.658679e0
${}^{m1}\phi_h$	1000	1	0.416684e-4	0.196047e-4	0.645575e-2
${}^{m2}\phi_h$	1200	1	-	0.202418e-4	0.552887e-2
$({}^{m2}\phi_h)_{new}$	1200	1	0.289365e-4	0.136146e-4	0.537967e-2

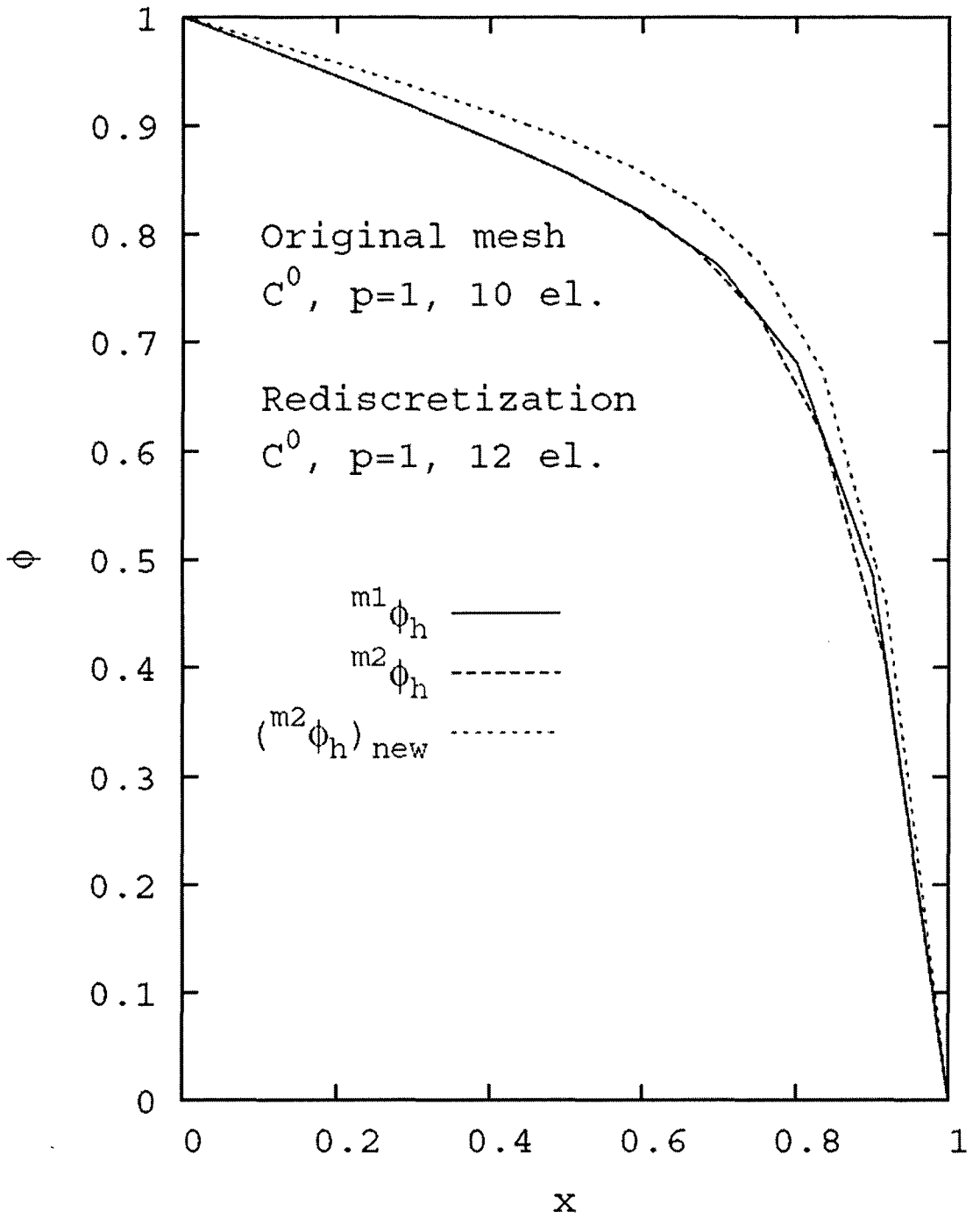

Figure 3.1: Convection diffusion equation (BVP): ϕ versus x for original, mapped and new solutions.

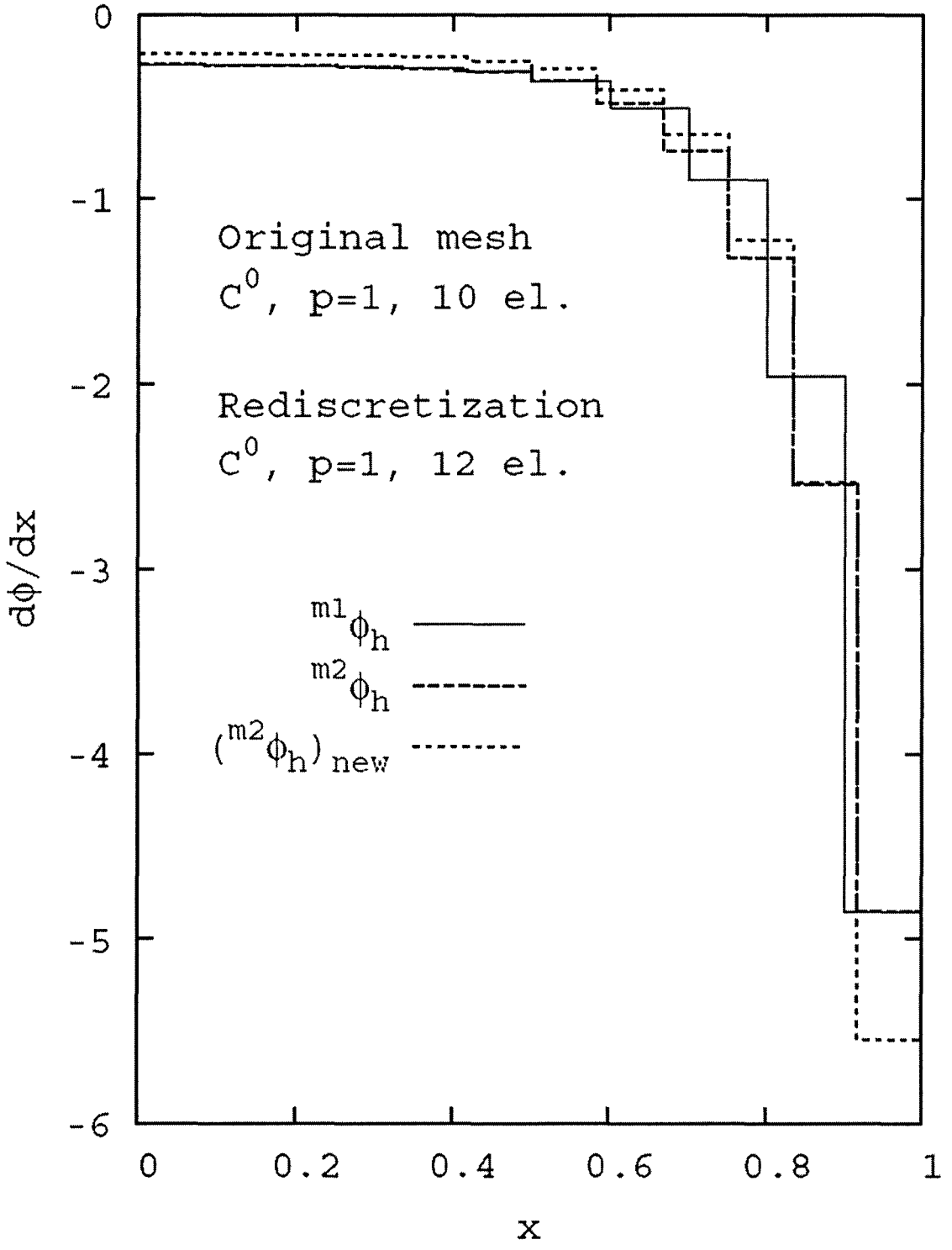

Figure 3.2: Convection diffusion equation (BVP): $\frac{d\phi}{dx}$ versus x for original, mapped and new solutions.

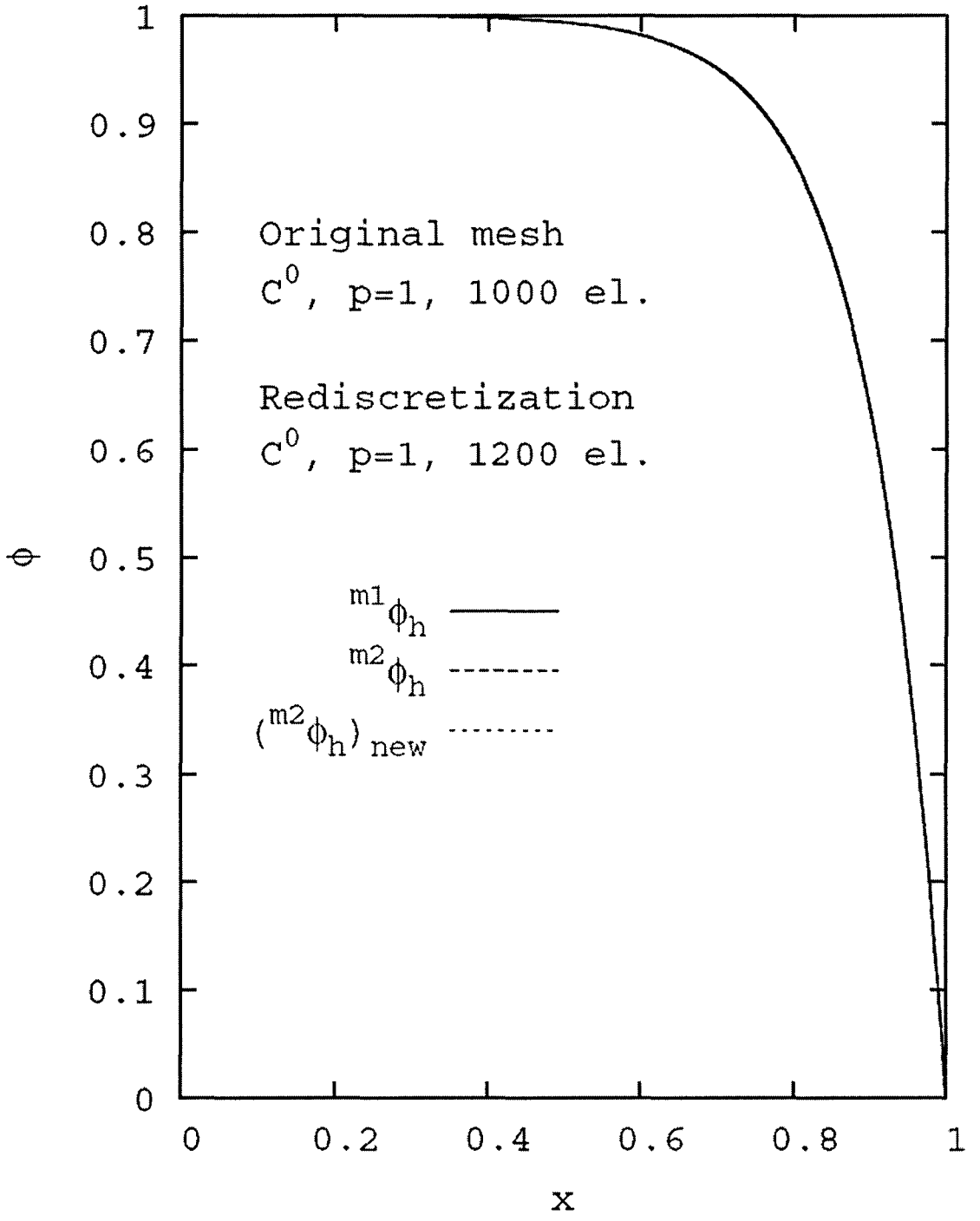

Figure 3.3: Convection diffusion equation (BVP): ϕ versus x for original, mapped and new solutions.

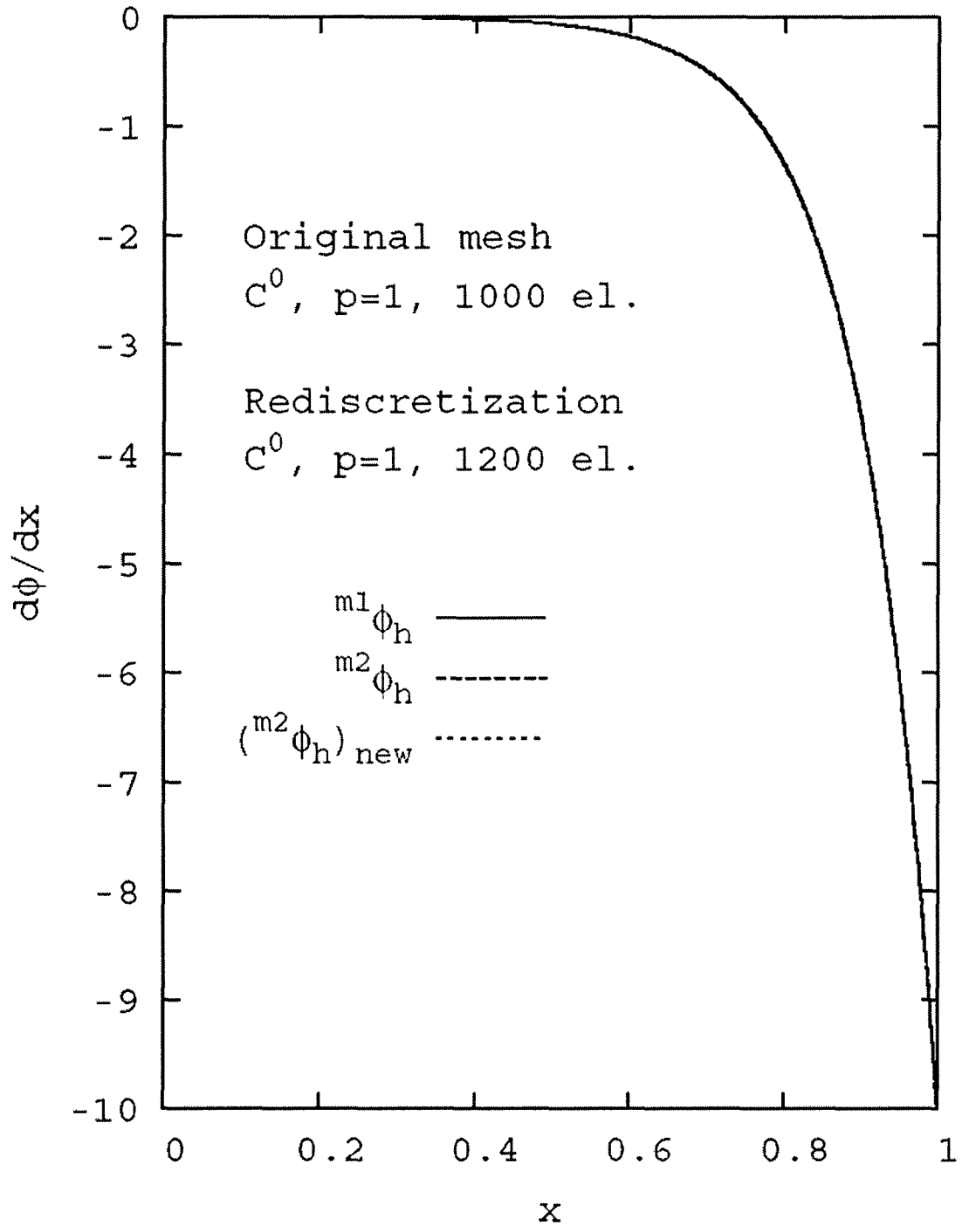

Figure 3.4: Convection diffusion equation (BVP): $\frac{d\phi}{dx}$ versus x for original, mapped and new solutions.

3.2 One-dimensional BVP: Steady-state Convection Diffusion Equation, Local Approximations of C^0 p-version Hierarchical Type ($Pe = 10$)

We consider the BVP (3.1). We consider two different original discretizations.

Case 1: A ten-element uniform original discretization and a twelve element uniform rediscretization both at p-levels of 5, 9, and 15.

Case 2: A 1000-element uniform original discretization and a 1200 element uniform rediscretization both at p-levels of 5, 9, and 15.

For both original discretizations, solutions are computed at p-levels of 5,9 and 15 and then mapped onto the corresponding rediscretizations. Also, new solutions are computed for the rediscretizations by resolving the BVP. Figures 3.5 - 3.7 show graphs of ϕ versus x for $p = 5, 9$, and 15 for case 1. The graphs of $\frac{d\phi}{dx}$ versus x are shown in Fig.s 3.8 - 3.10 for case 1. Figures 3.5 - 3.7 show the original and new solutions in good agreement at all three p-levels, however the mapped solution differs (maybe not significantly). The graphs of $\frac{d\phi}{dx}$ versus x in Fig.s 3.8 - 3.10 clearly show excellent agreement between the original and new solutions but the mapped solution differs significantly and shows significant inter-element jumps in $\frac{d\phi}{dx}$ at all three p-levels. This is due to inaccurate maps of the hierarchical derivatives which progressively deteriorate as the p-levels and hence, the orders of the derivatives increase. At all three p-levels ${}^{m1}\phi_h$ is converged, but the inaccuracies in the maps are due to inaccurate mapping of the hierarchical dofs. Table 3.2 gives mesh details, I, and various L_2-norms.

The inaccuracies in the map shown above can be minimized with mesh refinement (as in case 2). Figures 3.11 - 3.13 show graphs of ϕ versus x and Fig.s 3.14 - 3.16 show graphs of $\frac{d\phi}{dx}$ versus x for all three p-levels. The results show excellent agreement between all three solutions and their derivatives at all three p-levels. Even though the L_2-norms differ for ϕ and $\frac{d\phi}{dx}$ for the mapped solution, for all practical purposes (as shown in the figures) the maps are generally good. In this case, we have purposely used an exceptionally refined mesh to demonstrate that the inaccuracies

in the maps of the hierarchical dofs can indeed be minimized by mesh refinement.

Table 3.2: Convection diffusion equation (BVP): C^0 p-version hicrarchical local approximations.

Solution	Elements	p-level	I	$\|\phi_h - \phi\|_{L_2}$	$\left\|\frac{d(\phi_h)}{dx} - \frac{d\phi}{dx}\right\|_{L_2}$
${}^{m1}\phi_h$	10	5	0.432714e-9	0.104665e-6	0.207345e-4
${}^{m2}\phi_h$	12	5	-	0.615416e-2	0.2360702e0
$({}^{m2}\phi_h)_{new}$	12	5	0.728349e-10	0.357703e-7	0.851514e-5
${}^{m1}\phi_h$	10	9	0.728966e-21	0.752119e-13	0.269668e10
${}^{m2}\phi_h$	12	9	-	0.615716e-2	0.236839e0
$({}^{m2}\phi_h)_{new}$	12	9	0.286326e-22	0.125148e-13	0.534643e-11
${}^{m1}\phi_h$	10	15	0.944106e-22	0.252814e-13	0.914020e-11
${}^{m2}\phi_h$	12	15	-	0.615718e-2	0.409828e-2
$({}^{m2}\phi_h)_{new}$	12	15	0.205984e-21	0.299340e-13	0.132347e-14
${}^{m1}\phi_h$	1000	5	0.296098e-23	0.400021e-12	0.367759e-11
${}^{m2}\phi_h$	1200	5	-	0.623740e-6	0.236693e-2
$({}^{m2}\phi_h)_{new}$	1200	5	0.551350e-21	0.109110e-10	0.443337e-10
${}^{m1}\phi_h$	1000	9	0.6334062e21	0.106185e-10	0.463778e-10
${}^{m2}\phi_h$	1200	9	-	0.623748e-6	0.236693e-2
$({}^{m2}\phi_h)_{new}$	1200	9	0.926781e-21	0.139454e-10	0.584280e-10
${}^{m1}\phi_h$	1000	15	0.247810e-17	0.147141e-10	0.156245e-8
${}^{m2}\phi_h$	1200	15	-	0.789122e-6	0.409828e-2
$({}^{m2}\phi_h)_{new}$	1200	15	0.141826e-17	0.297155e-11	0.116684e-8

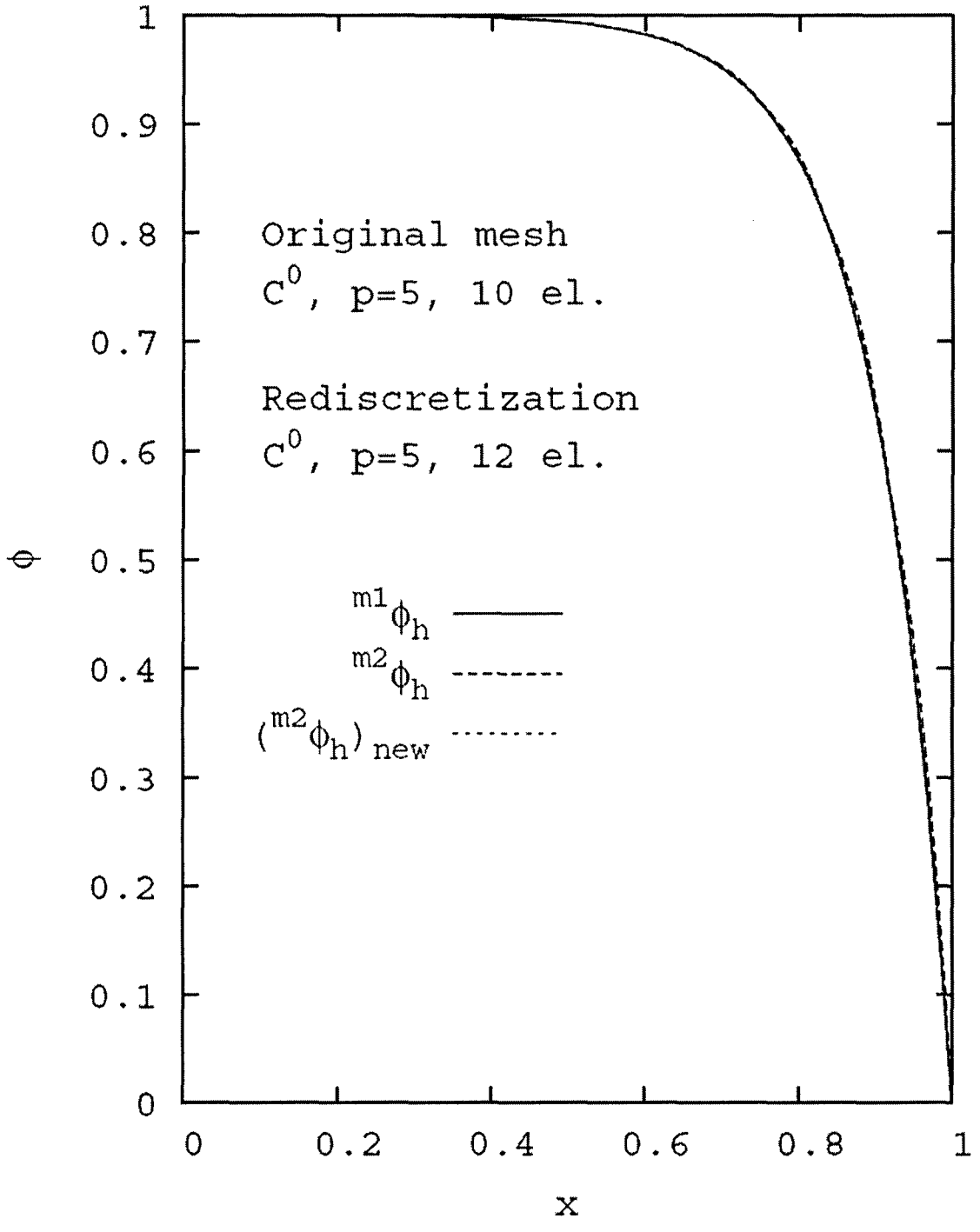

Figure 3.5: Convection diffusion equation (BVP): ϕ versus x for original, mapped and new solutions.

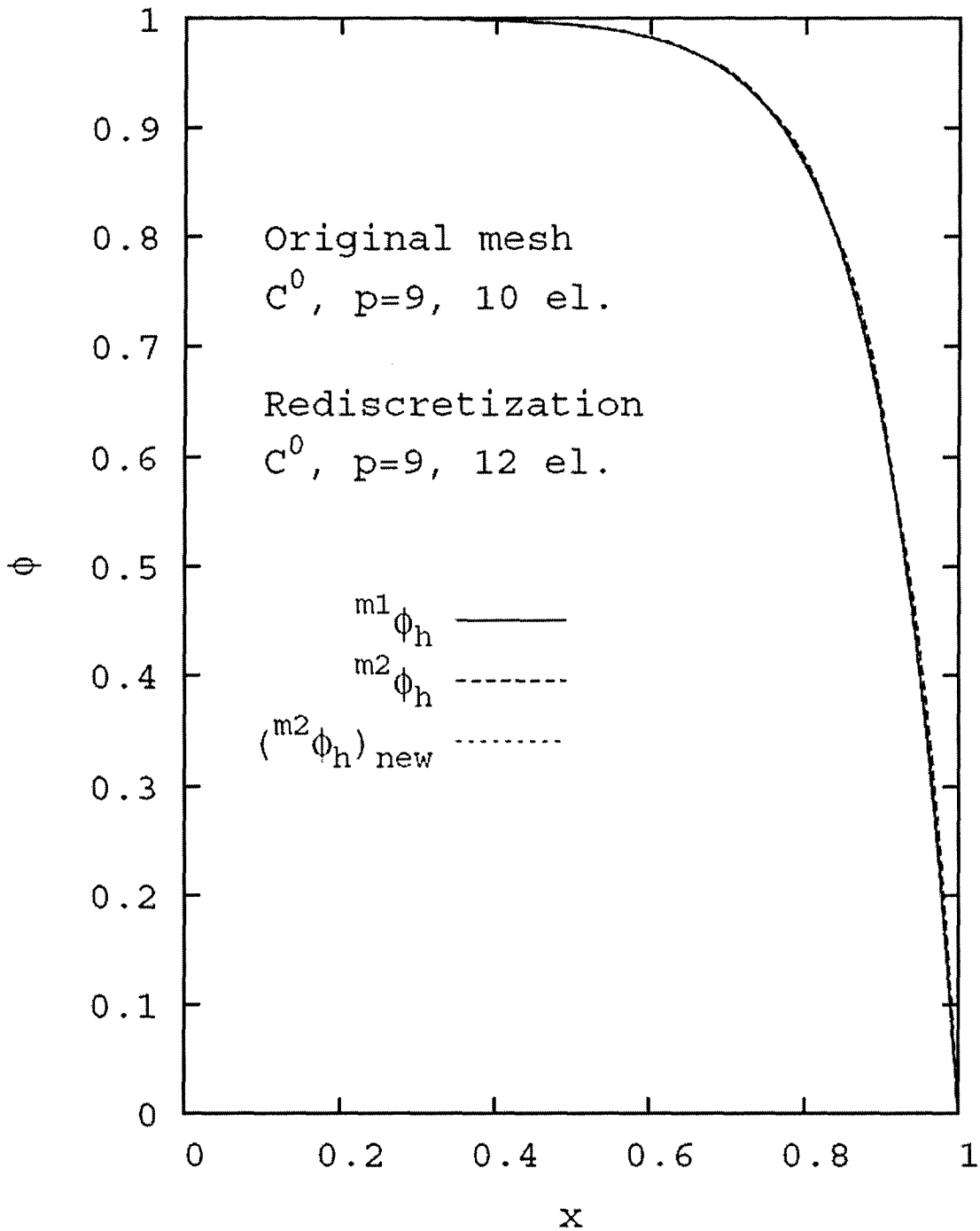

Figure 3.6: Convection diffusion equation (BVP): ϕ versus x for original, mapped and new solutions.

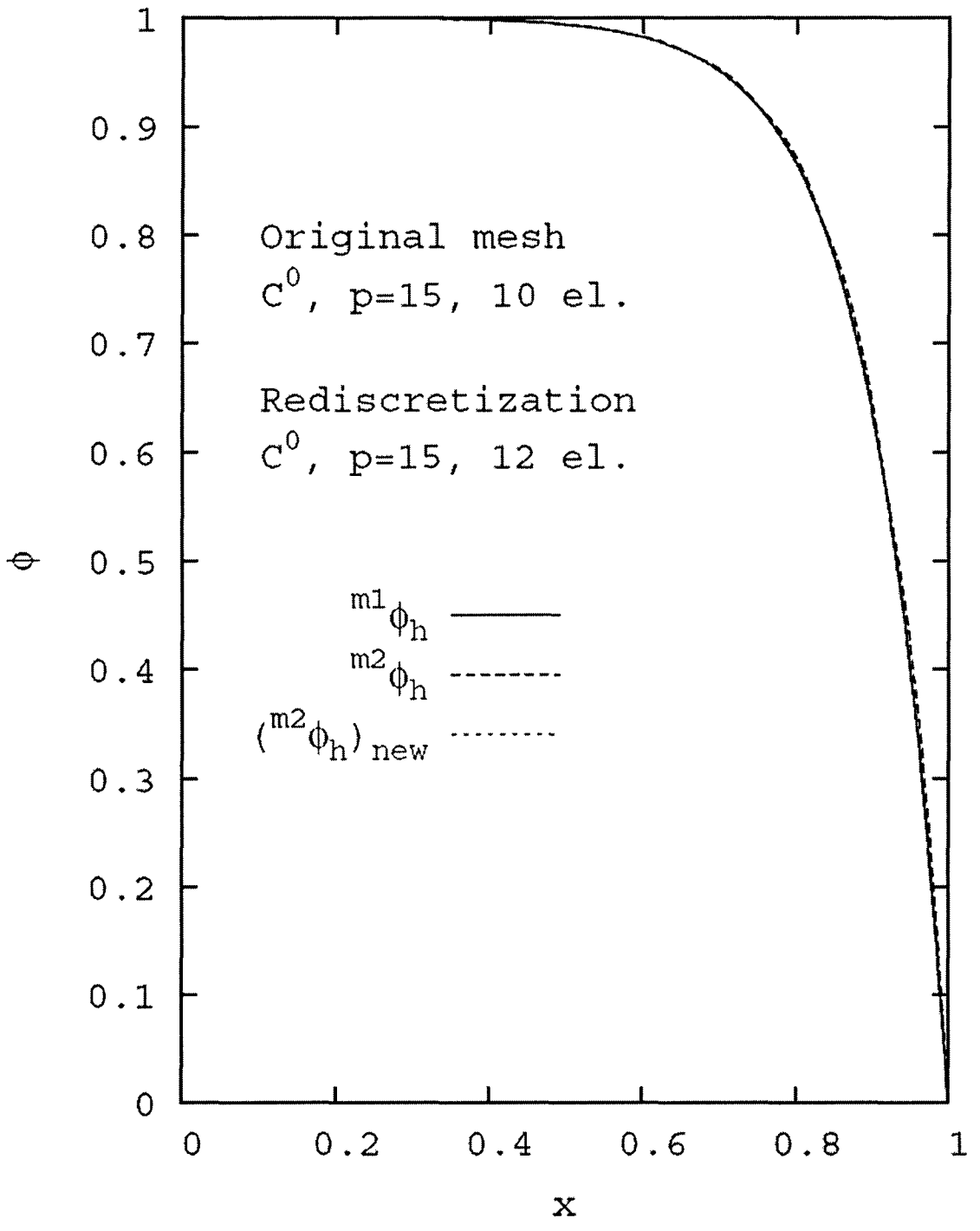

Figure 3.7: Convection diffusion equation (BVP): ϕ versus x for original, mapped and new solutions.

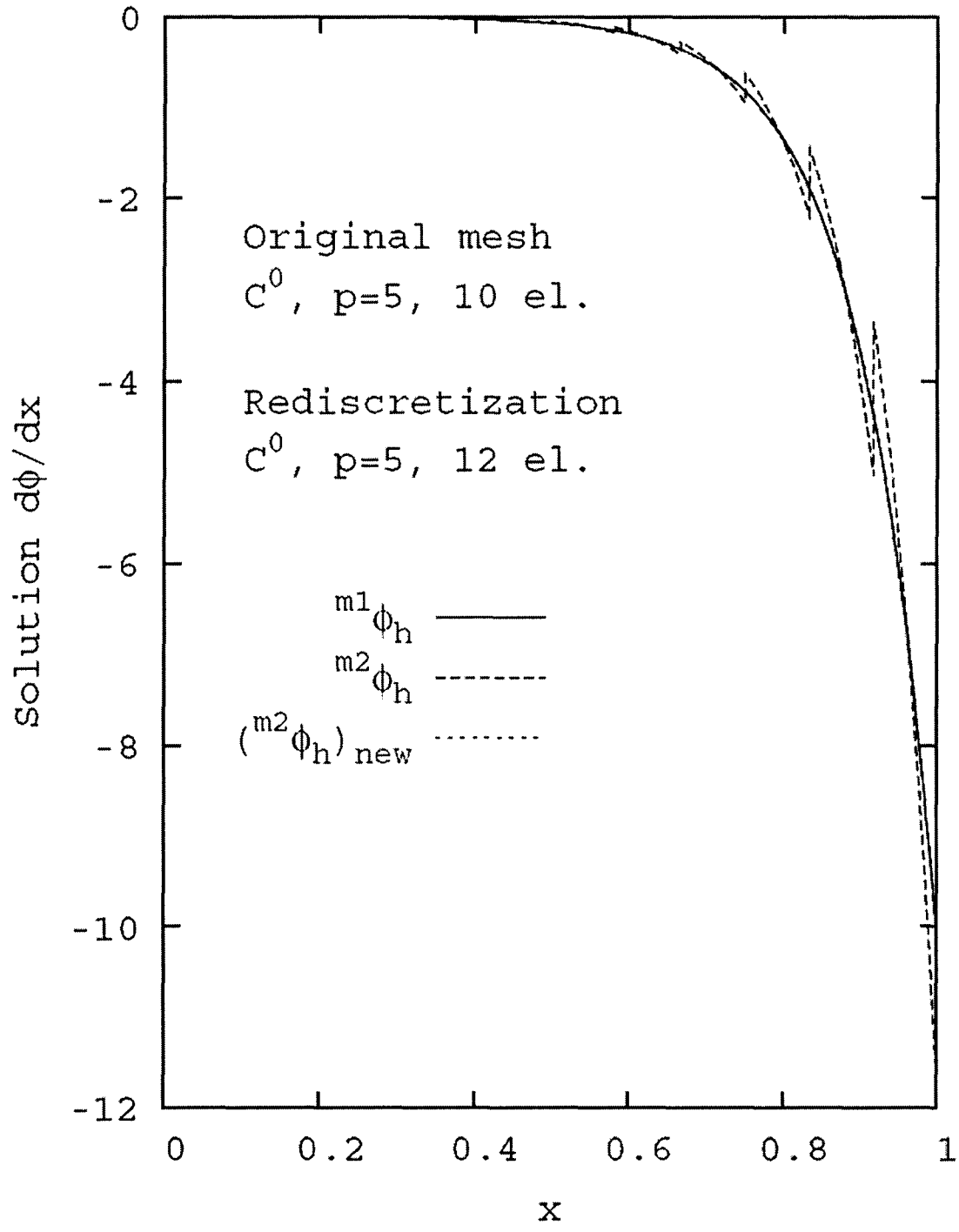

Figure 3.8: Convection diffusion equation (BVP): $\frac{d\phi}{dx}$ versus x for original, mapped and new solutions.

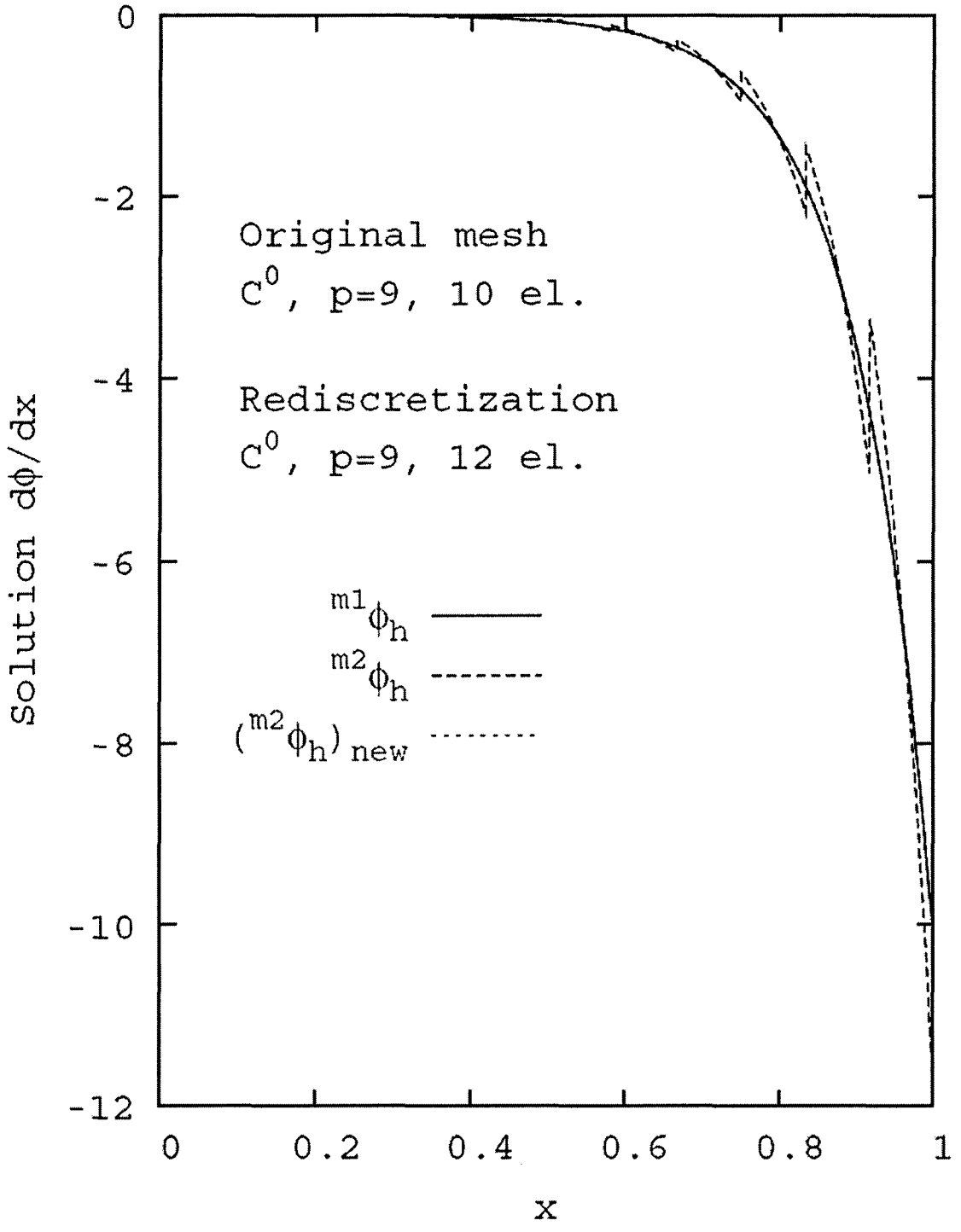

Figure 3.9: Convection diffusion equation (BVP): $\frac{d\phi}{dx}$ versus x for original, mapped and new solutions.

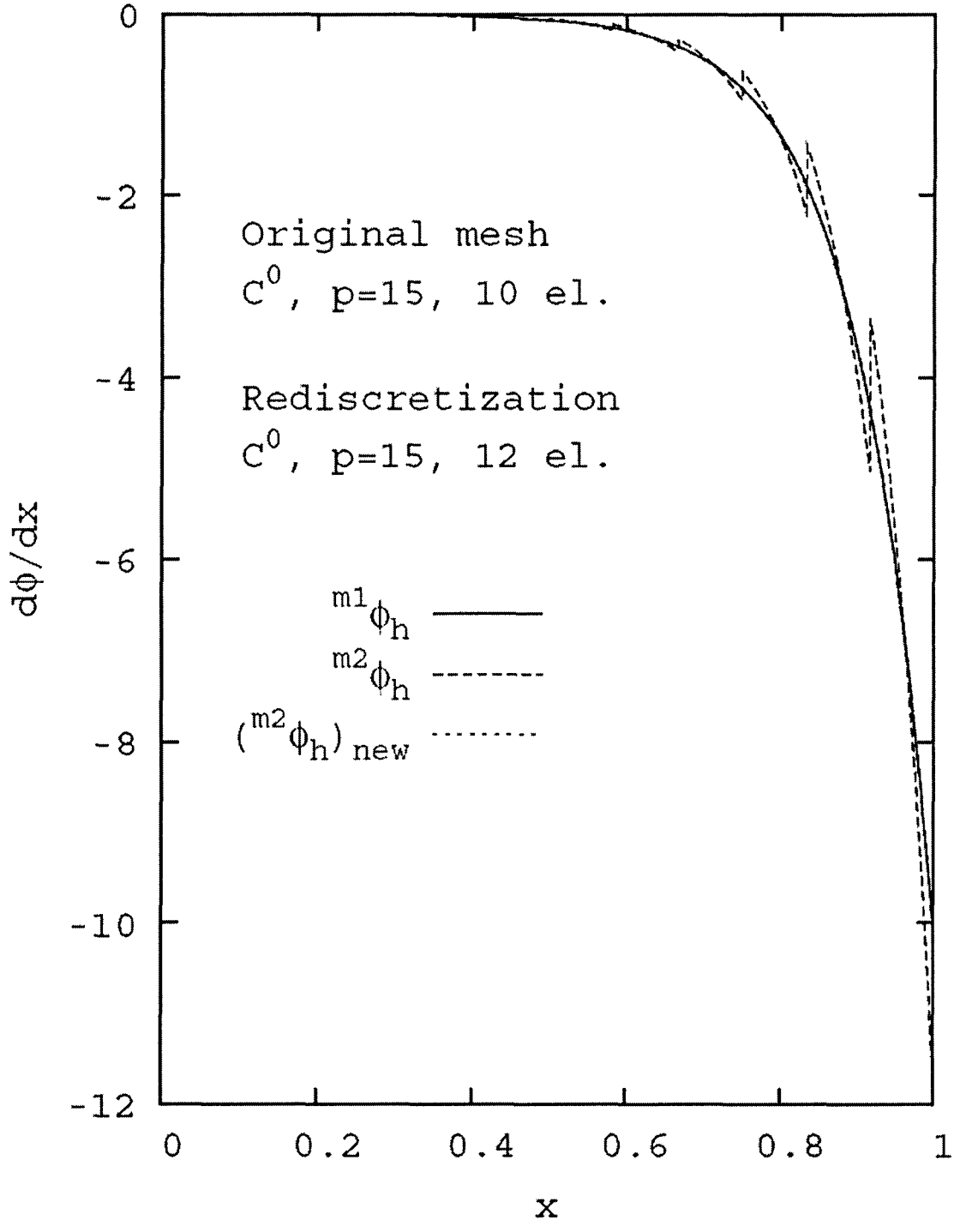

Figure 3.10: Convection diffusion equation (BVP): $\frac{d\phi}{dx}$ versus x for original, mapped and new solutions.

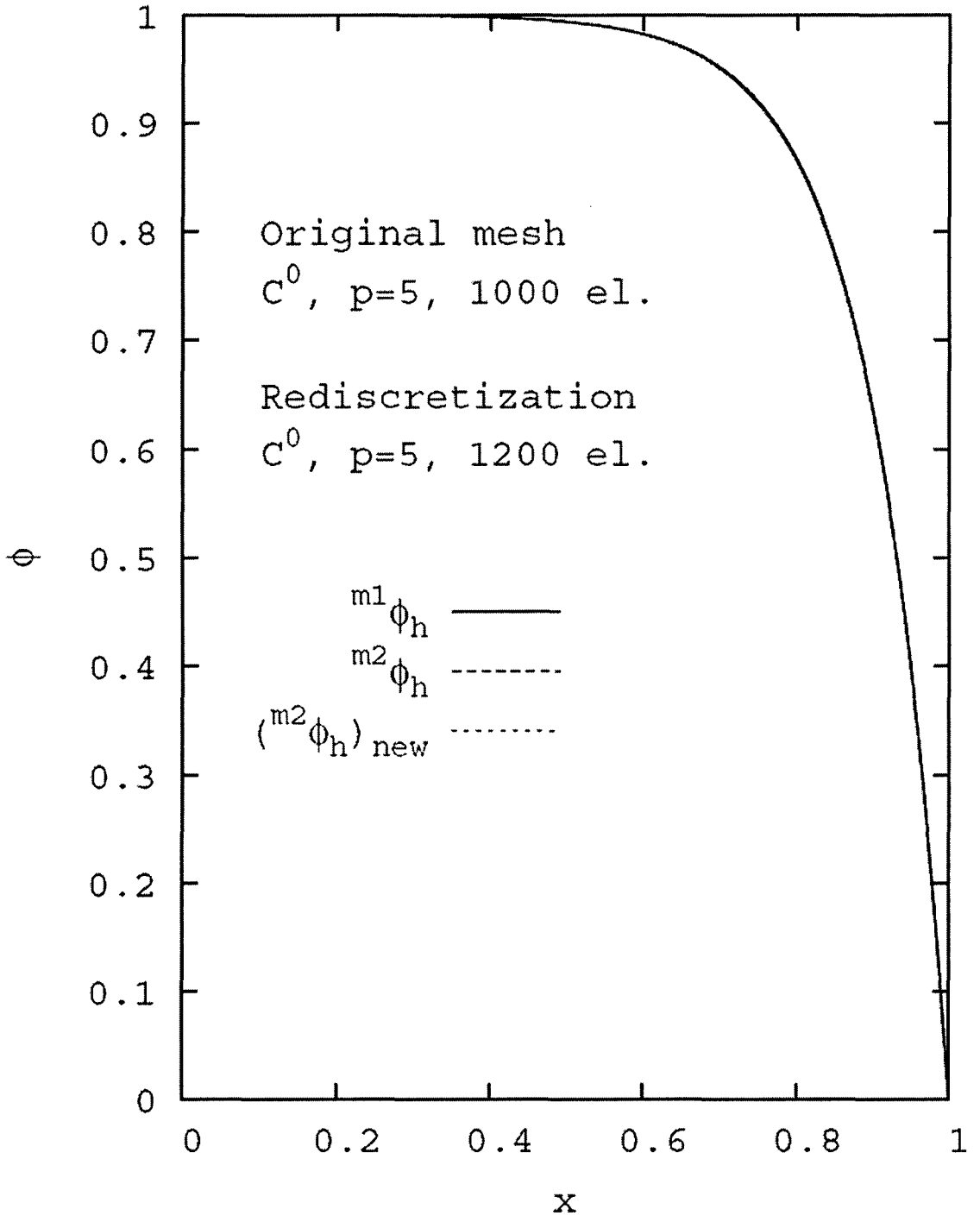

Figure 3.11: Convection diffusion equation (BVP): ϕ versus x for original, mapped and new solutions.

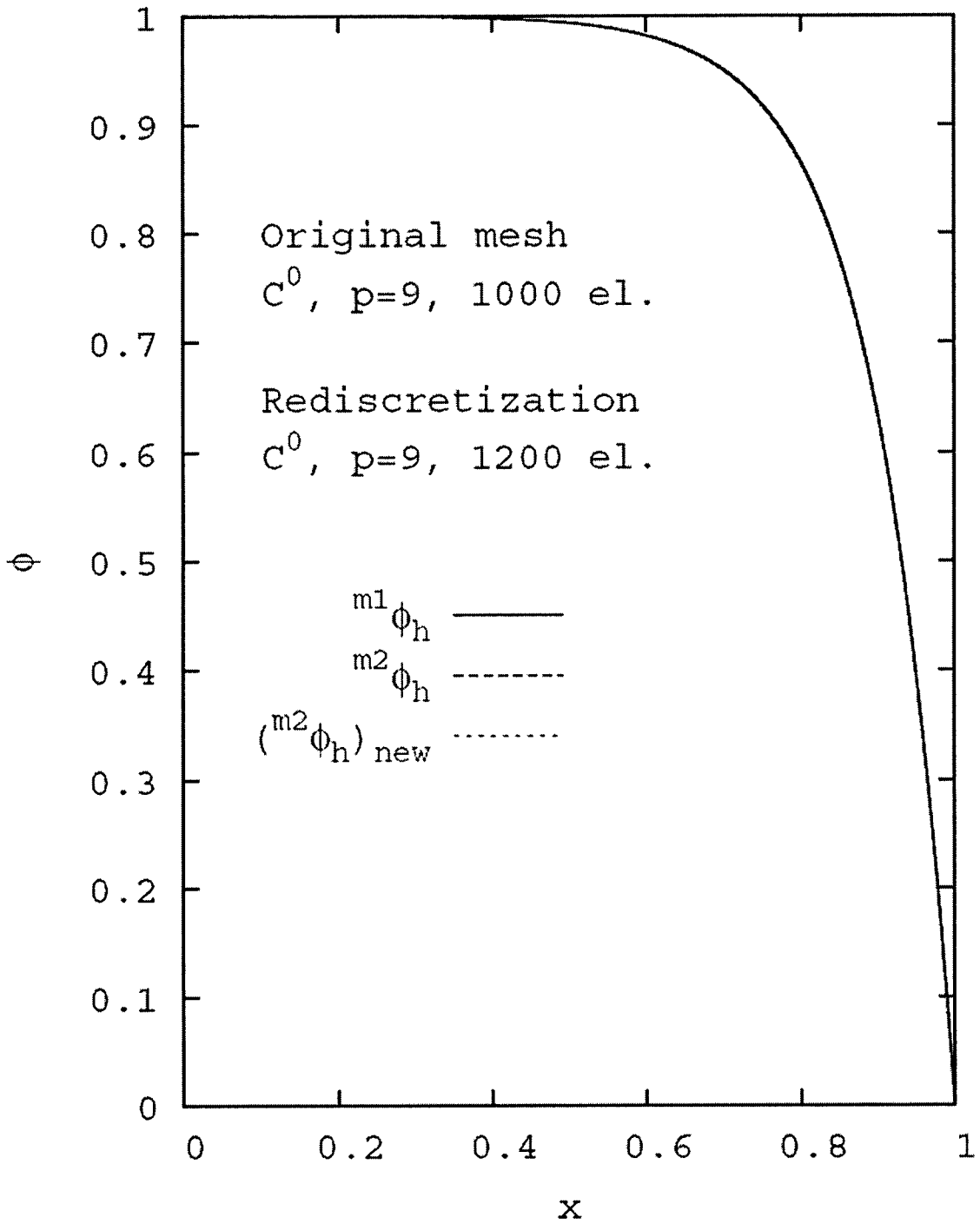

Figure 3.12: Convection diffusion equation (BVP): ϕ versus x for original, mapped and new solutions.

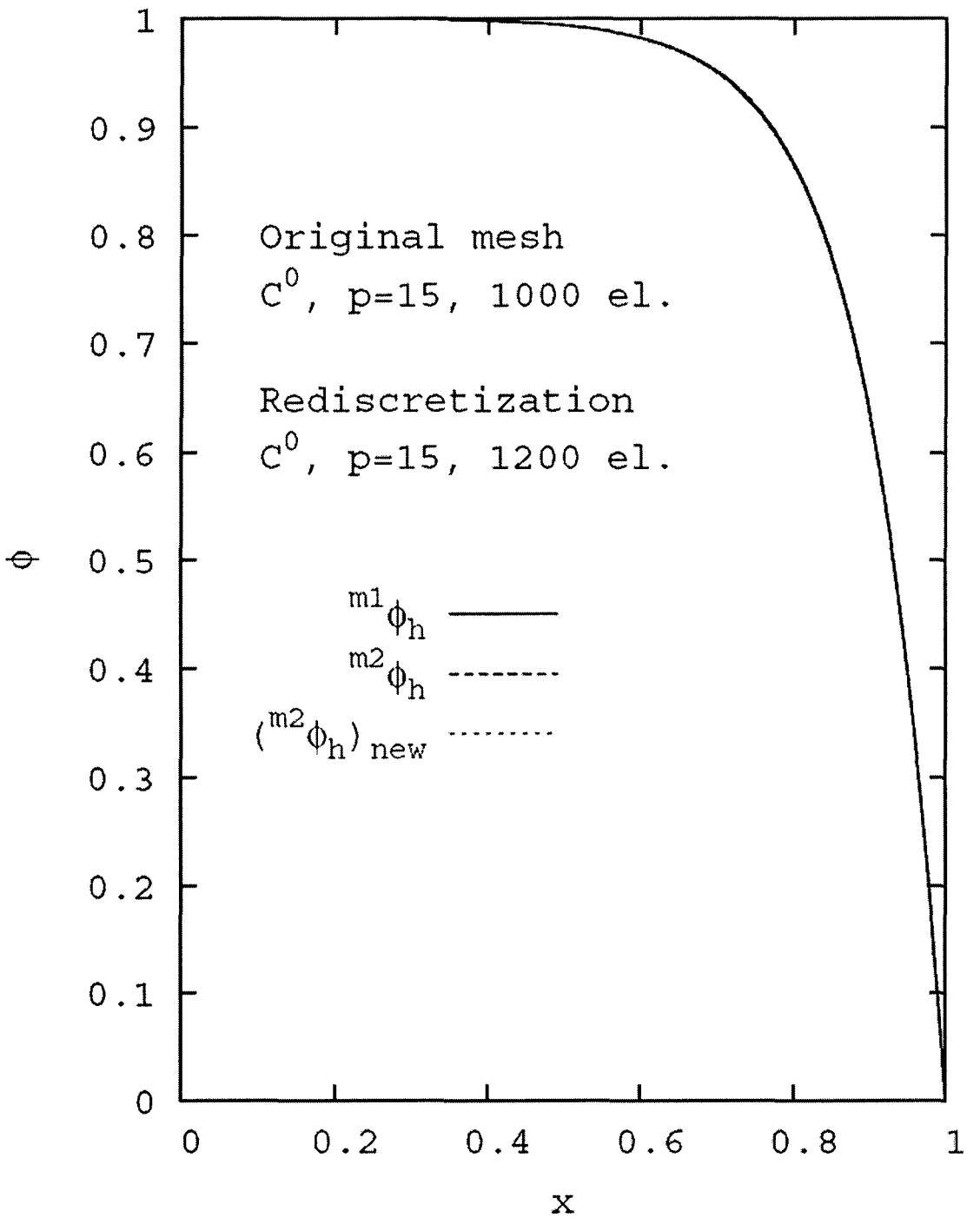

Figure 3.13: Convection diffusion equation (BVP): ϕ versus x for original, mapped and new solutions.

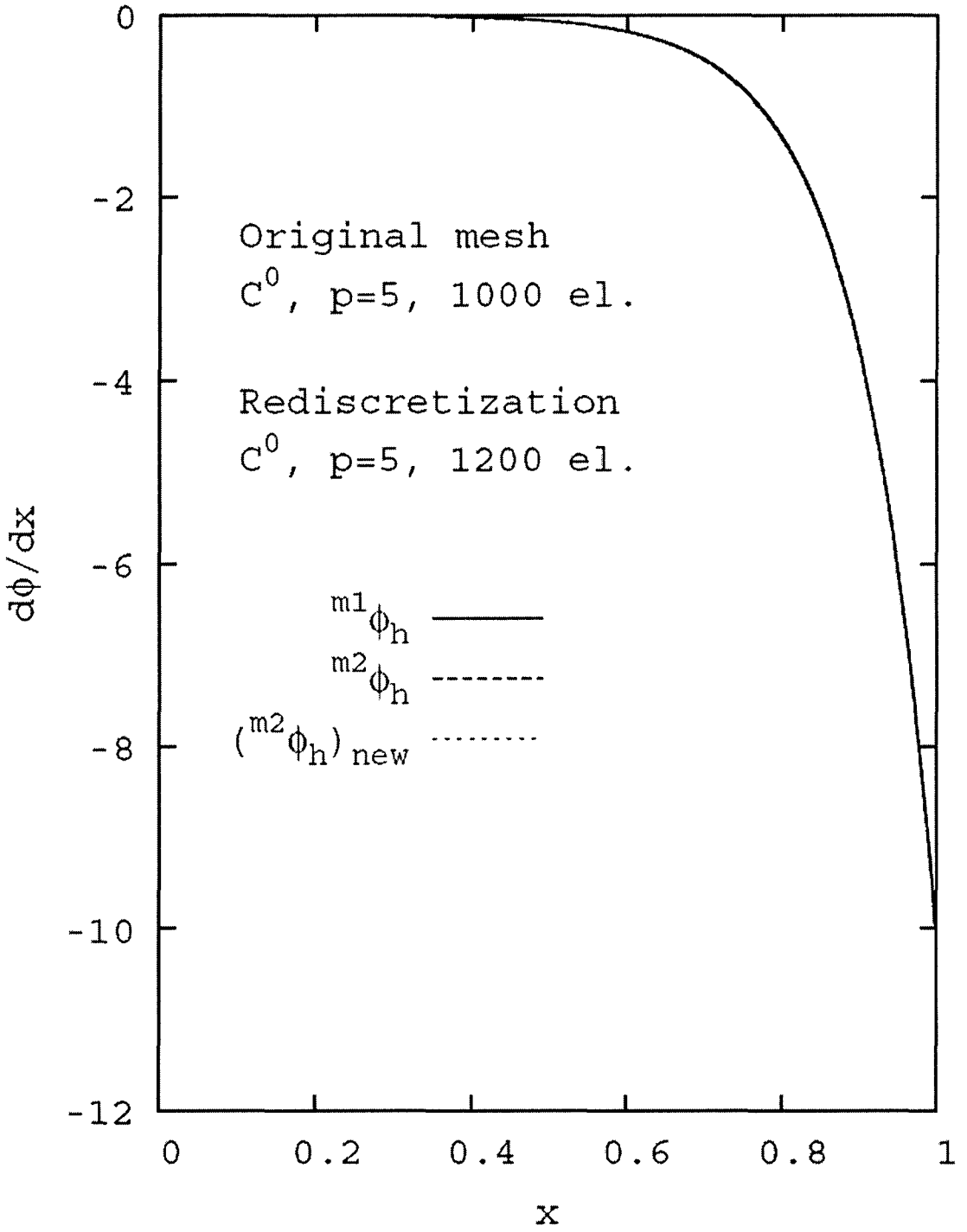

Figure 3.14: Convection diffusion equation (BVP): $\frac{d\phi}{dx}$ versus x for original, mapped and new solutions.

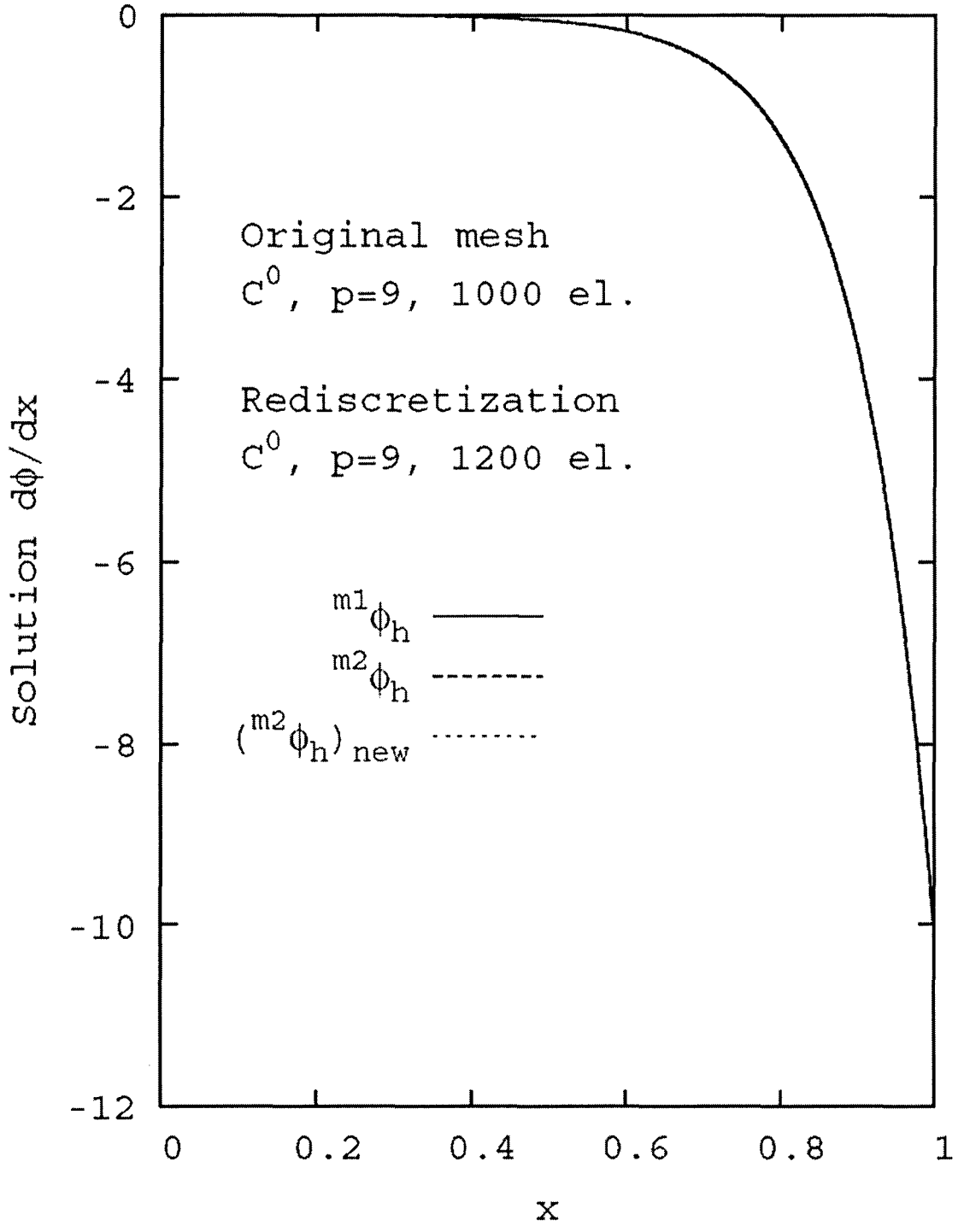

Figure 3.15: Convection diffusion equation (BVP): $\frac{d\phi}{dx}$ versus x for original, mapped and new solutions.

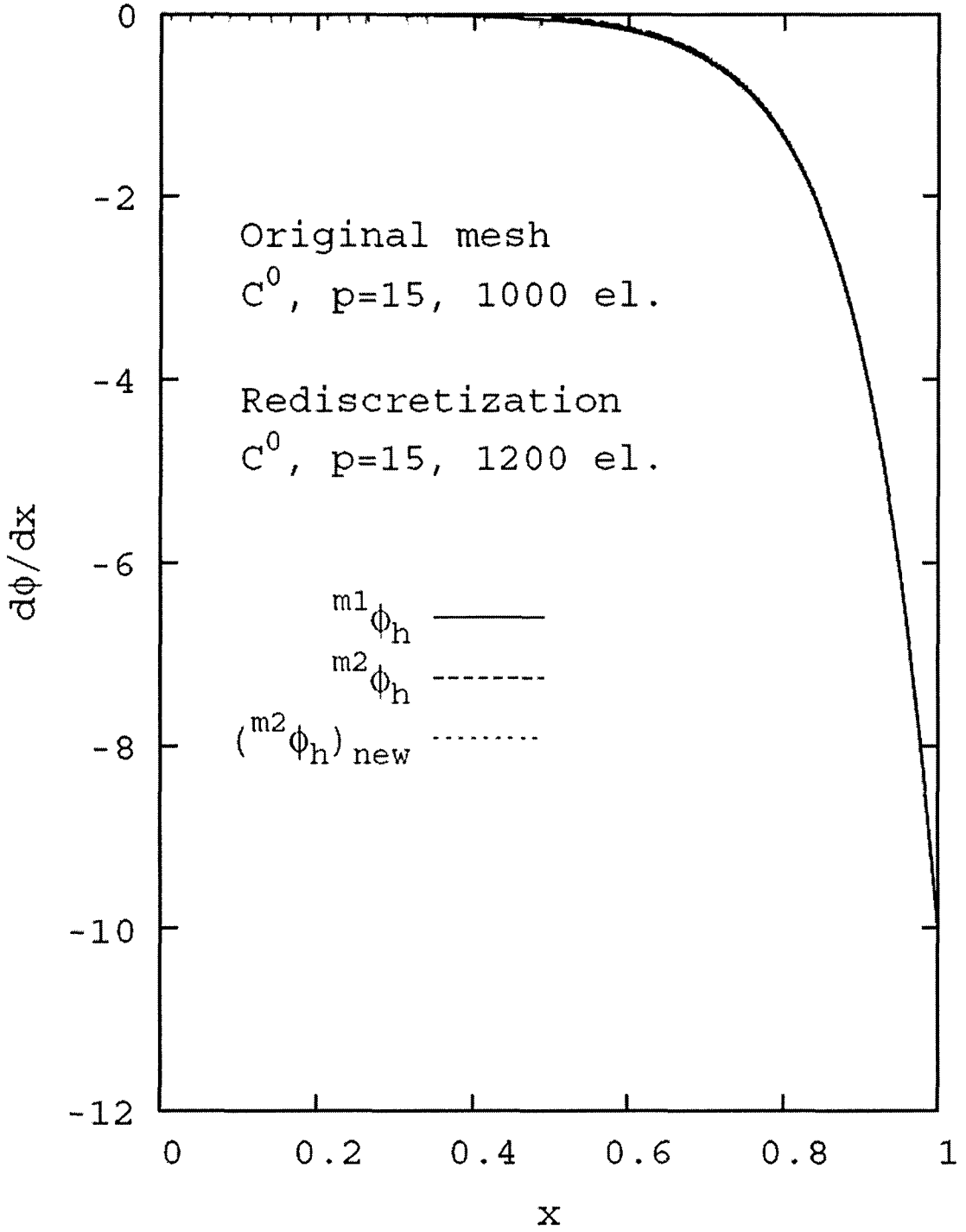

Figure 3.16: Convection diffusion equation (BVP): $\frac{d\phi}{dx}$ versus x for original, mapped and new solutions.

3.3 One-dimensional BVP: Steady-state Convection Diffusion Equation, Local Approximations of C^j; $j = 1, 2, 3, 4$ $(Pe = 10)$

In this case we consider the original discretization to be a five-element uniform mesh ($m1$). The re-discretization consists of s seven-element uniform mesh ($m2$). In the studies, we consider minimally conforming p-levels for each class as well as p-levels higher than minimally conforming. Results are presented in the following figures and tables.

(a) C^1, $p = 3$: Figures 3.17 - 3.19, Table 3.3

(b) C^1, $p = 15$: Figures 3.20 - 3.22, Table 3.3

(c) C^2, $p = 5$: Figures 3.23 - 3.26, Table 3.4

(d) C^2, $p = 15$: Figures 3.27 - 3.30, Table 3.4

(e) C^3, $p = 7$: Figure 3.31, Table 3.5

(f) C^3, $p = 15$: Figure 3.32, Table 3.5

(g) C^4, $p = 9$: Figure 3.33, Table 3.6

(h) C^4, $p = 15$: Figure 3.34, Table 3.6

First, we discuss results for with minimally conforming p-levels. The solution of progressively higher classes exhibit progressively better maps of the solution as well as the derivatives of up to order C^j. When the solutions are of class C^j, the maps of the derivatives of order $j + 1$ improve with progressively increasing order of the approximation space when the p-levels are minimally conforming. This is due to increasing p-levels progressively by increasing the order of the space but with the absence of hierarchical dofs which may not map accurately. When p-levels are increased beyond minimally conforming, the map of the derivatives of order C^{j+1} become inaccurate (Fig.s 3.22, 3.30) for classes C^1 and C^2 but remain good for classes C^3 and C^4. This is due to the fact that minimally conforming p-levels for classes C^3 and C^4 are 7 and 9, respectively, at which the original solution is relatively well converged and there are still no hierarchical dofs. Hence, the

maps onto the rediscretization should be good. At p-level 15, $\frac{d^4\phi}{dx^4}$ and $\frac{d^5\phi}{dx^5}$ show very good maps for solutions of classes C^3 and C^4 (Fig.s 3.32, 3.34).

Table 3.3: Convection diffusion equation (BVP): C^1 p-version hierarchical local approximations.

Solution	Elements	p-level	I	$\|\phi_h - \phi\|_{L_2}$	$\left\|\frac{d(\phi_h)}{dx} - \frac{d\phi}{dx}\right\|_{L_2}$	$\left\|\frac{d^2(\phi_h)}{dx^2} - \frac{d^2\phi}{dx^2}\right\|_{L_2}$
${}^{m1}\phi_h$	5	3	0.730018e-1	0.295100e-1	0.132388e0	0.321291e1
${}^{m2}\phi_h$	7	3	-	0.290958e-1	0.126901e0	0.307579e1
$({}^{m2}\phi_h)_{new}$	7	3	0.234047e-1	0.951054e-2	0.465439e-1	0.131715e1
${}^{m1}\phi_h$	5	15	0.847645e-23	0.175931e-14	0.180028e-1	0.290602e-10
${}^{m2}\phi_h$	7	15	-	0.406817e-2	0.988658e-1	0.538991e1
$({}^{m2}\phi_h)_{new}$	7	15	0.382862e-23	0.323930e-14	0.892078e-13	0.195499e-10

Table 3.4: Convection diffusion equation (BVP): C^2 p-version hierarchical local approximations.

Solution	Elements	p-level	I	$\|\phi_h - \phi\|_{L_2}$	$\left\|\frac{d(\phi_h)}{dx} - \frac{d\phi}{dx}\right\|_{L_2}$	$\left\|\frac{d^2(\phi_h)}{dx^2} - \frac{d^2\phi}{dx^2}\right\|_{L_2}$	$\left\|\frac{d^3(\phi_h)}{dx^3} - \frac{d^3\phi}{dx^3}\right\|_{L_2}$
${}^{m1}\phi_h$	5	5	0.364287e-4	0.258286e-4	0.995085e-3	0.595288e-1	0.538991e1
${}^{m2}\phi_h$	7	5	-	0.258998e-4	0.961396e-3	0.552387e-1	0.482149e1
$({}^{m2}\phi_h)_{new}$	7	5	0.444796e-7	0.126933e-6	0.144157e-4	0.210407e-2	0.467172e0
${}^{m1}\phi_h$	5	15	0.293984e-22	0.378121e-14	0.311355e-12	0.541314e-10	0.201389e-7
${}^{m2}\phi_h$	7	15	-	0.142223e-3	0.393234e-2	0.182809e0	0.122291e2
$({}^{m2}\phi_h)_{new}$	7	15	0.277480e-22	0.773083e-14	0.209901e-12	0.526357e-10	0.262811e-7

Table 3.5: Convection diffusion equation (BVP): C^3 p-version hierarchical local approximations.

Solution	Elements	p-level	I	$\left\| \frac{d^4(\phi_h)}{dx^4} - \frac{d^4\phi}{dx^4} \right\|_{L_2}$
${}^{m1}\phi_h$	5	7	0.448956e-8	0.976222e1
${}^{m2}\phi_h$	7	7	-	0.937789e1
$({}^{m2}\phi_h)_{new}$	7	7	0.115551e-9	0.281397e1
${}^{m1}\phi_h$	5	15	0.129770e-22	0.606670e-5
${}^{m2}\phi_h$	7	15	-	0.228179e2
$({}^{m2}\phi_h)_{new}$	7	15	0.821314e-22	0.261075e-4

Table 3.6: Convection diffusion equation (BVP): C^4 p-version hierarchical local approximations.

Solution	Elements	p-level	I	$\left\| \frac{d^5(\phi_h)}{dx^5} - \frac{d^5\phi}{dx^5} \right\|_{L_2}$
${}^{m1}\phi_h$	5	9	0.105628e-12	0.153421e2
${}^{m2}\phi_h$	7	9	-	0.148577e2
$({}^{m2}\phi_h)_{new}$	7	9	0.608197e-18	0.310044e1
${}^{m1}\phi_h$	5	15	0.107051e-22	0.176433e-2
${}^{m2}\phi_h$	7	15	-	0.228179e2
$({}^{m2}\phi_h)_{new}$	7	15	0.260707e-23	0.161274e-2

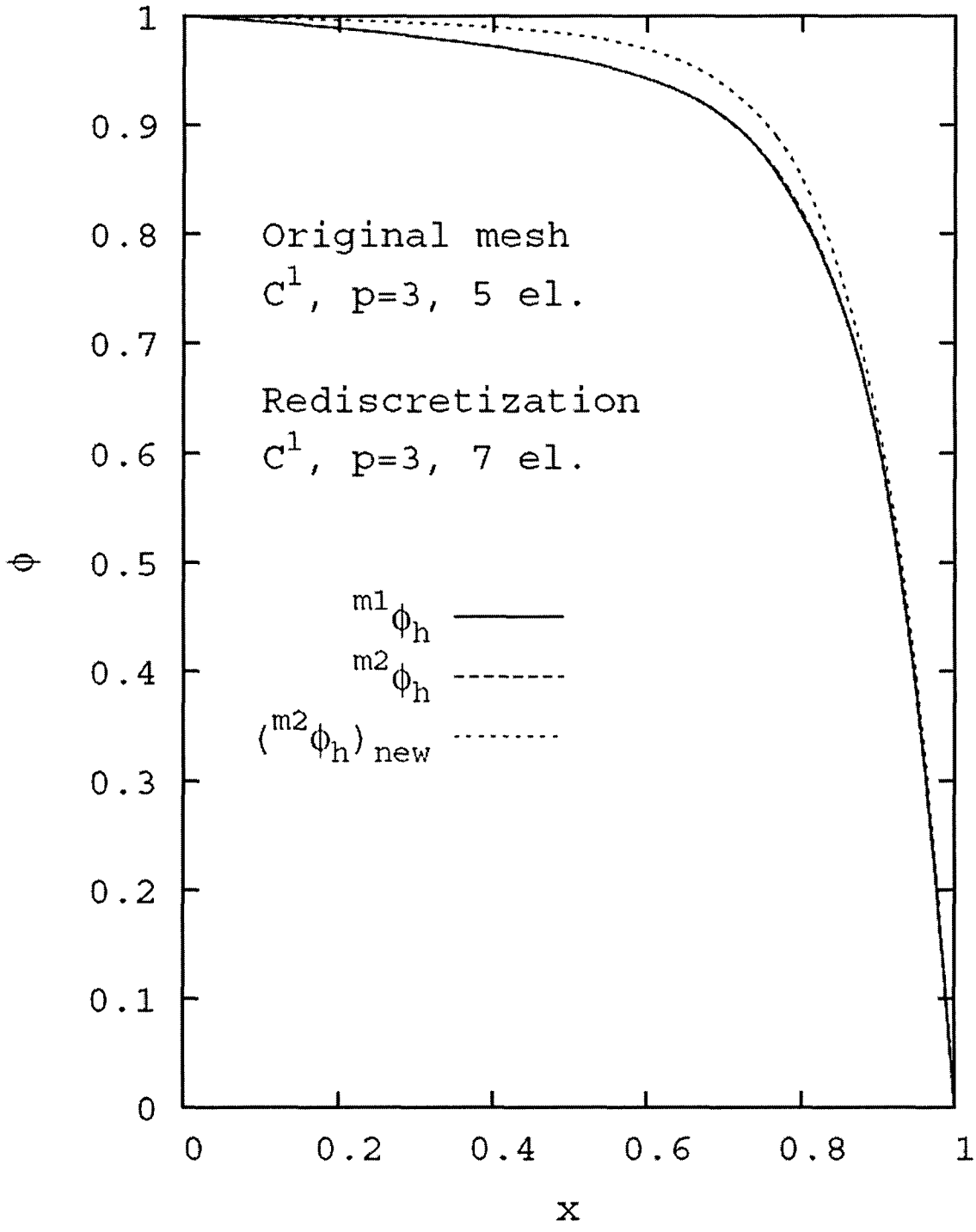

Figure 3.17: Convection diffusion equation (BVP): ϕ versus x for original, mapped and new solutions.

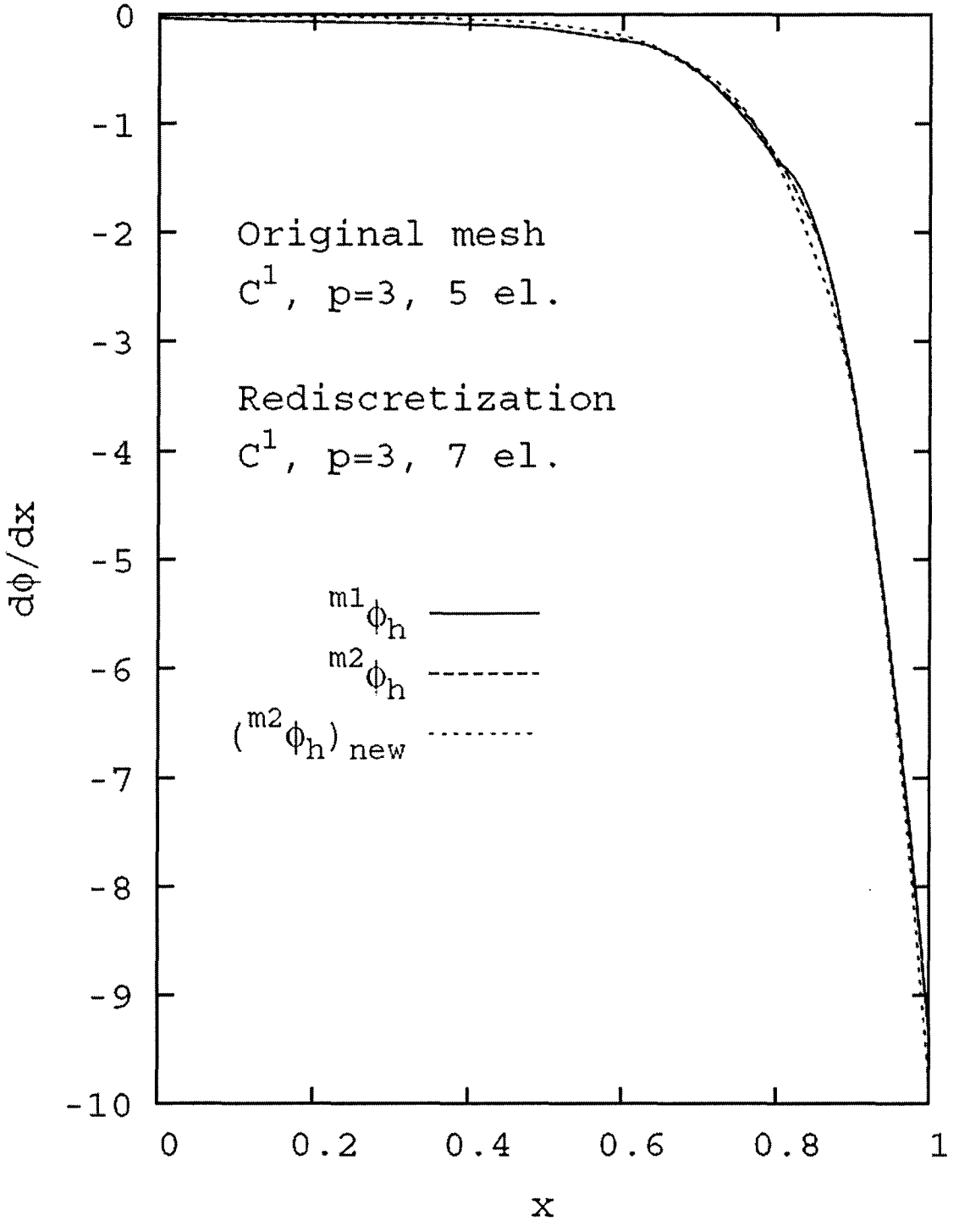

Figure 3.18: Convection diffusion equation (BVP): $\frac{d\phi}{dx}$ versus x for original, mapped and new solutions.

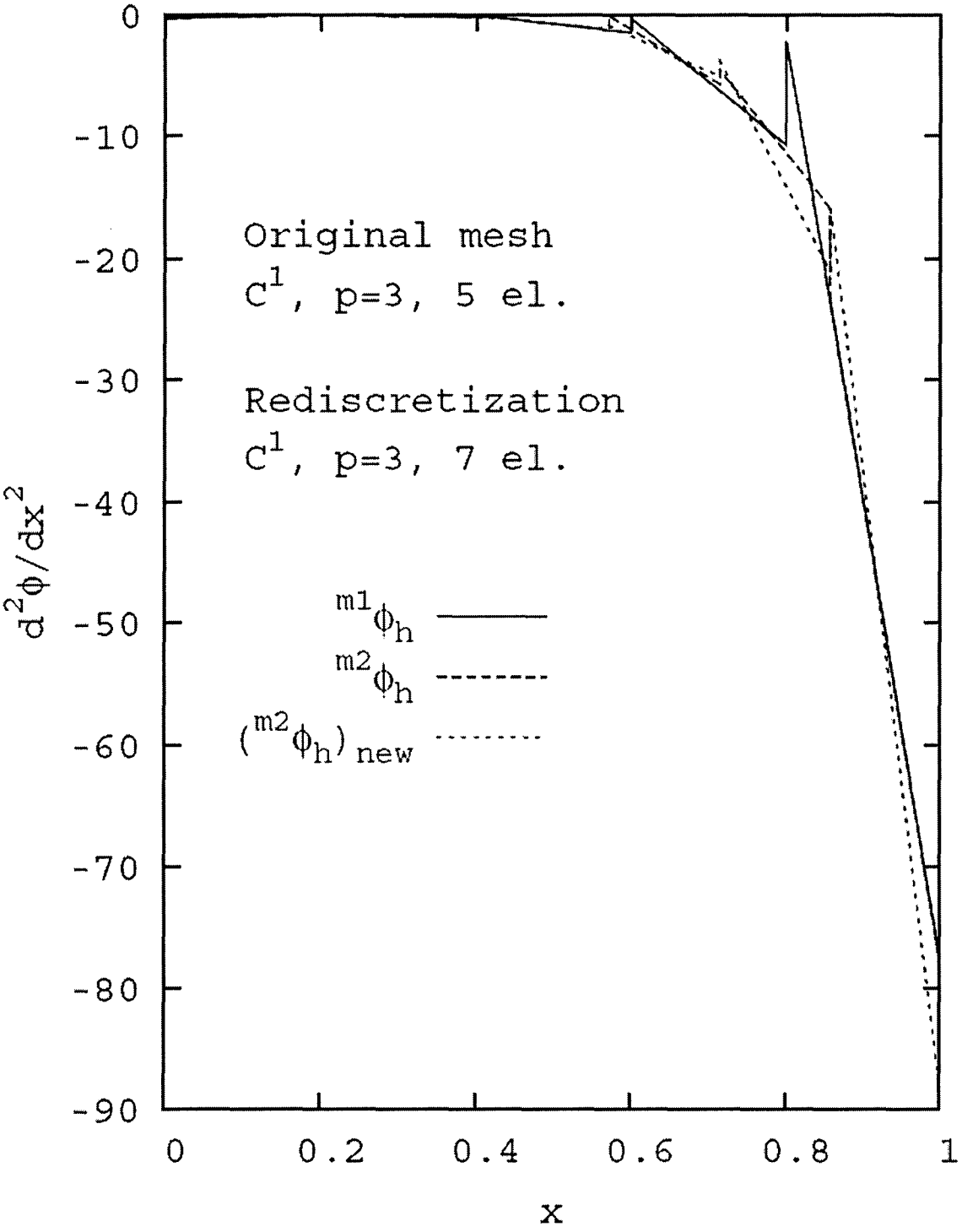

Figure 3.19: Convection diffusion equation (BVP): $\frac{d^2\phi}{dx^2}$ versus x for original, mapped and new solutions.

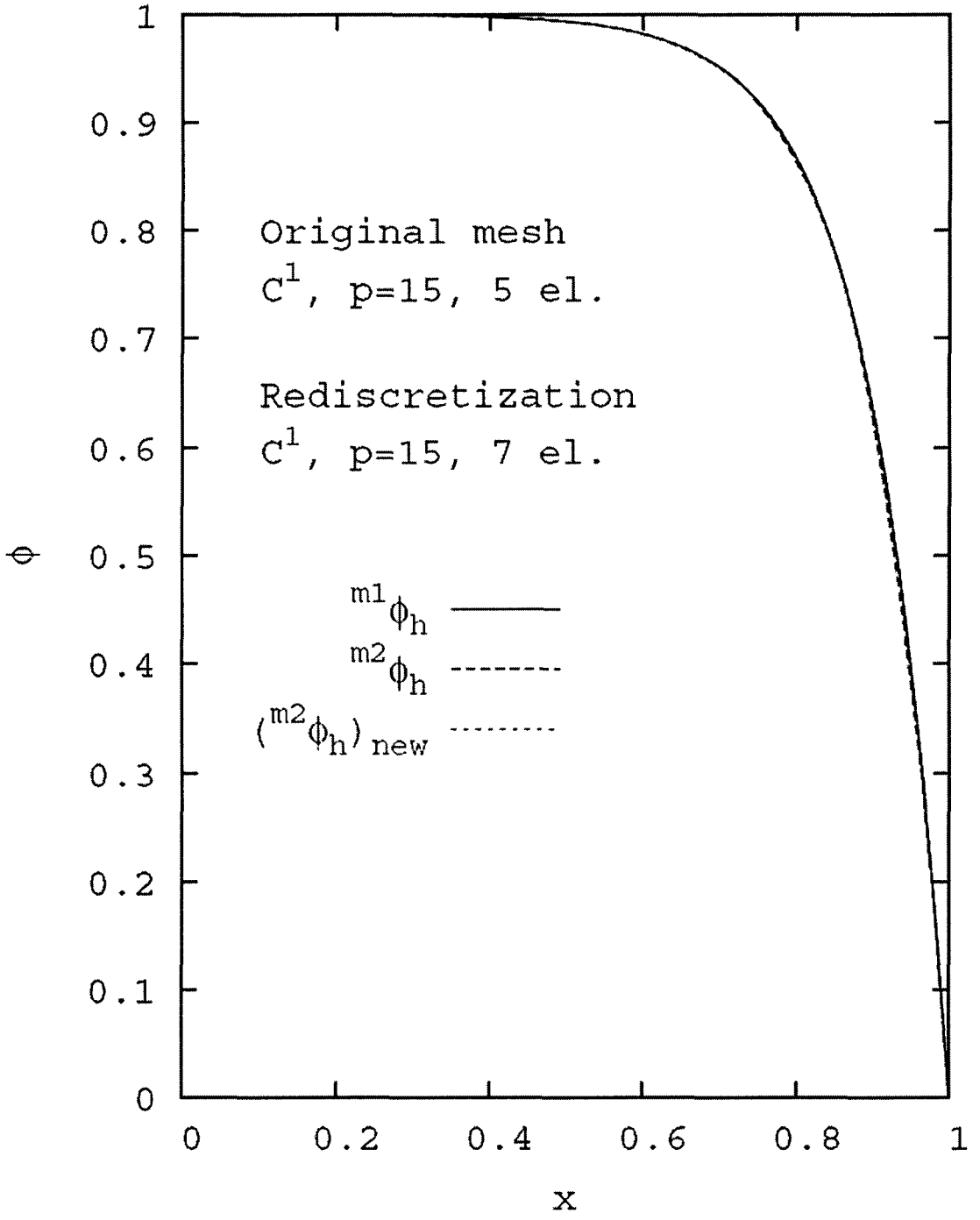

Figure 3.20: Convection diffusion equation (BVP): ϕ versus x for original, mapped and new solutions.

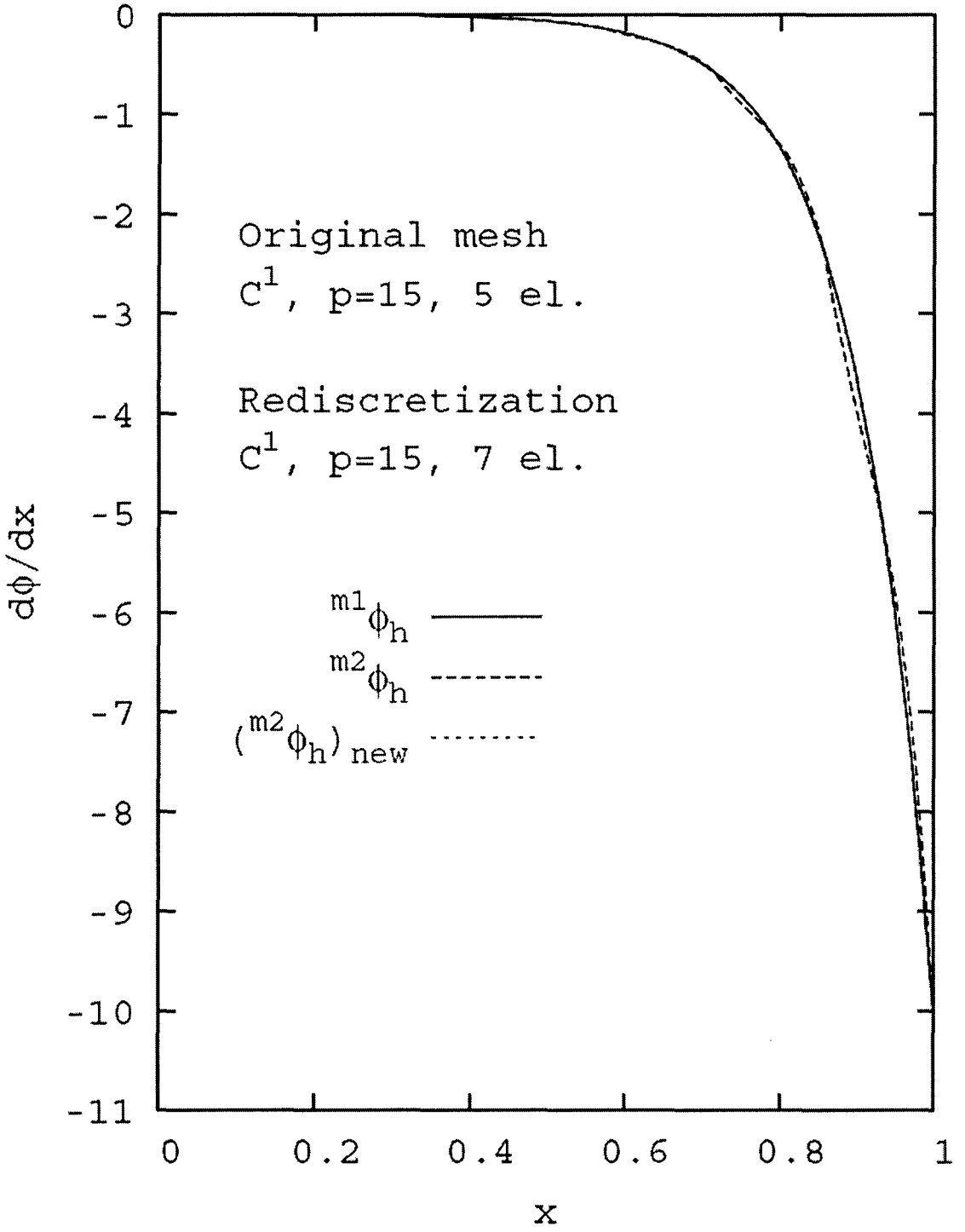

Figure 3.21: Convection diffusion equation (BVP): $\frac{d\phi}{dx}$ versus x for original, mapped and new solutions.

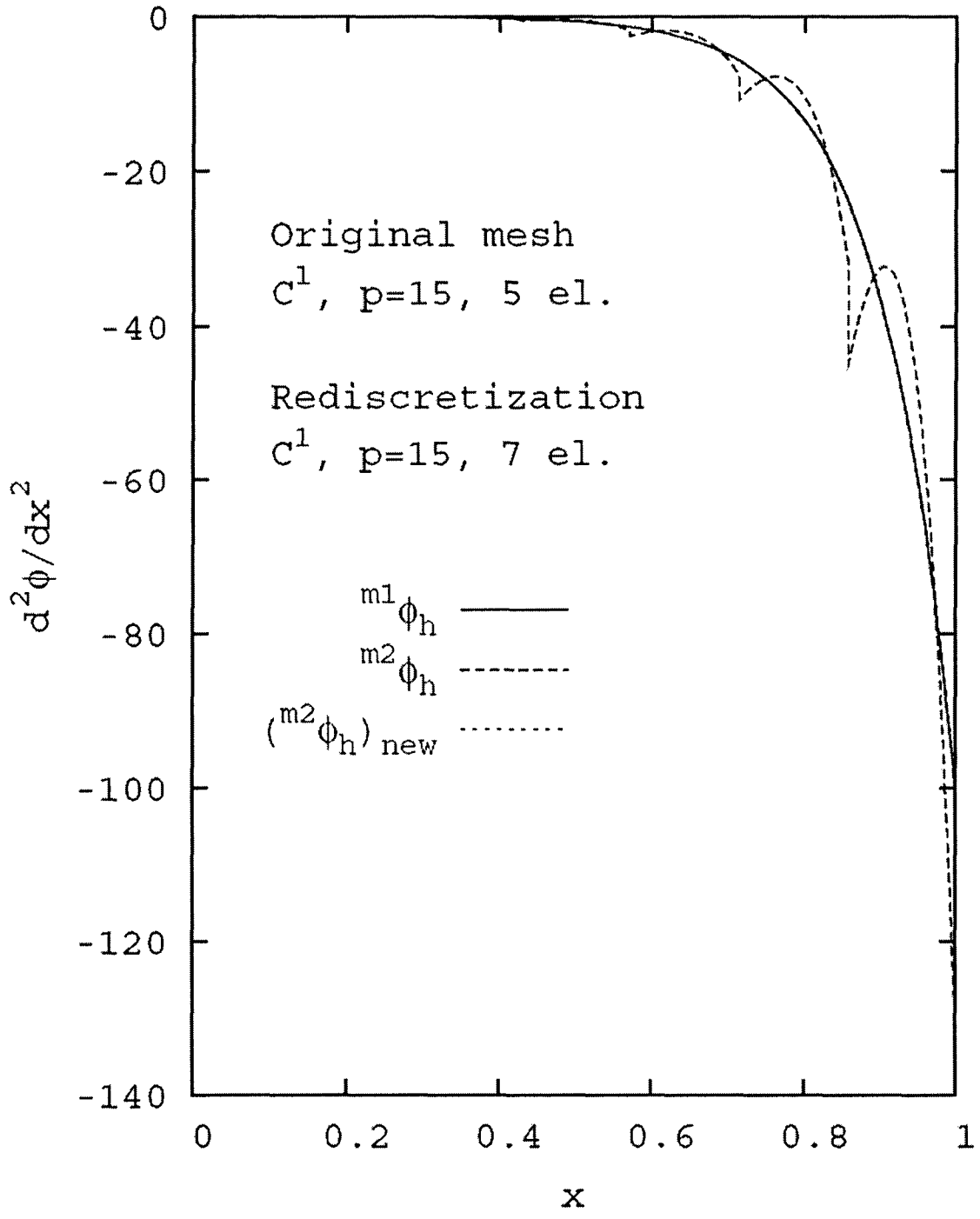

Figure 3.22: Convection diffusion equation (BVP): $\frac{d^2\phi}{dx^2}$ versus x for original, mapped and new solutions.

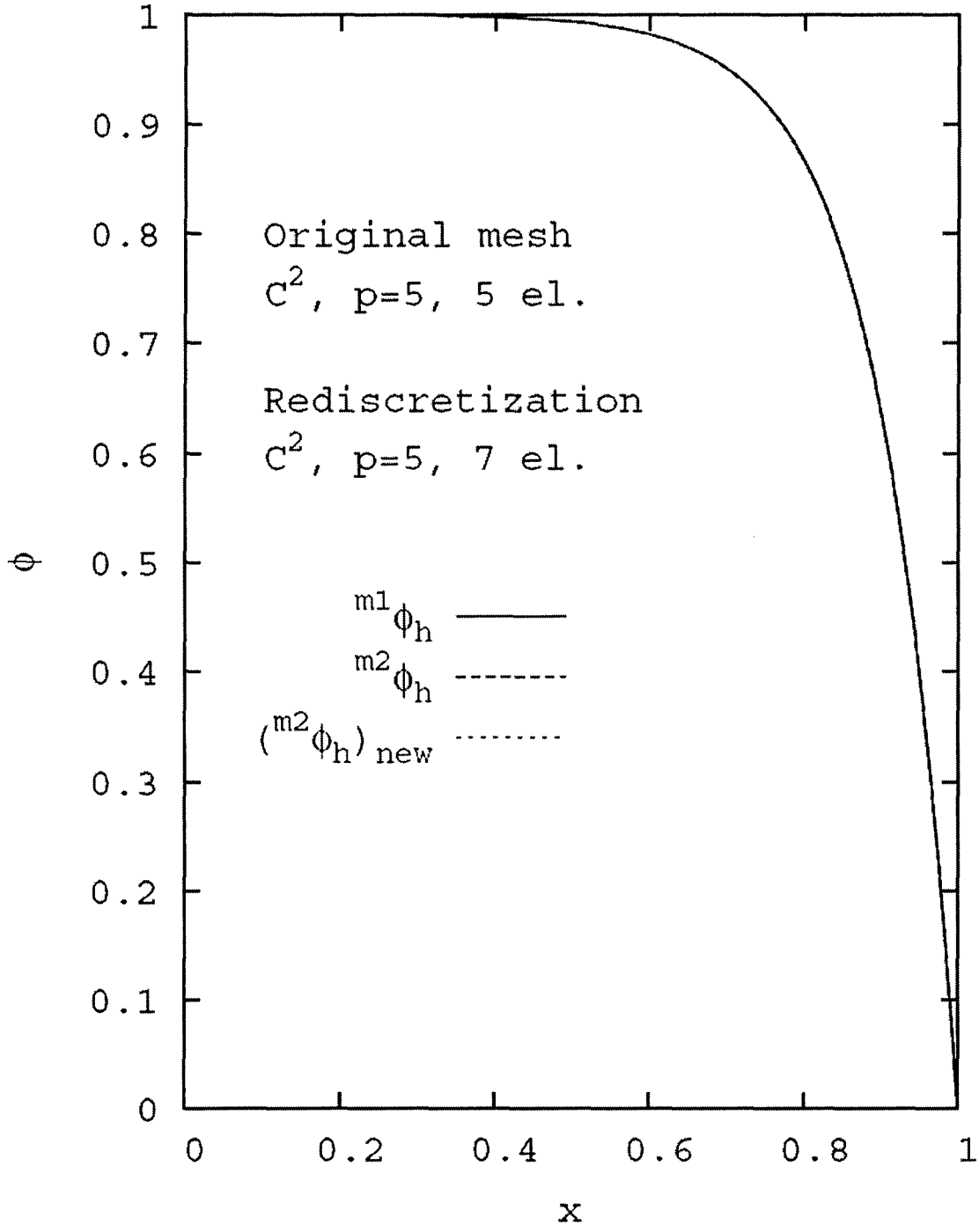

Figure 3.23: Convection diffusion equation (BVP): ϕ versus x for original, mapped and new solutions.

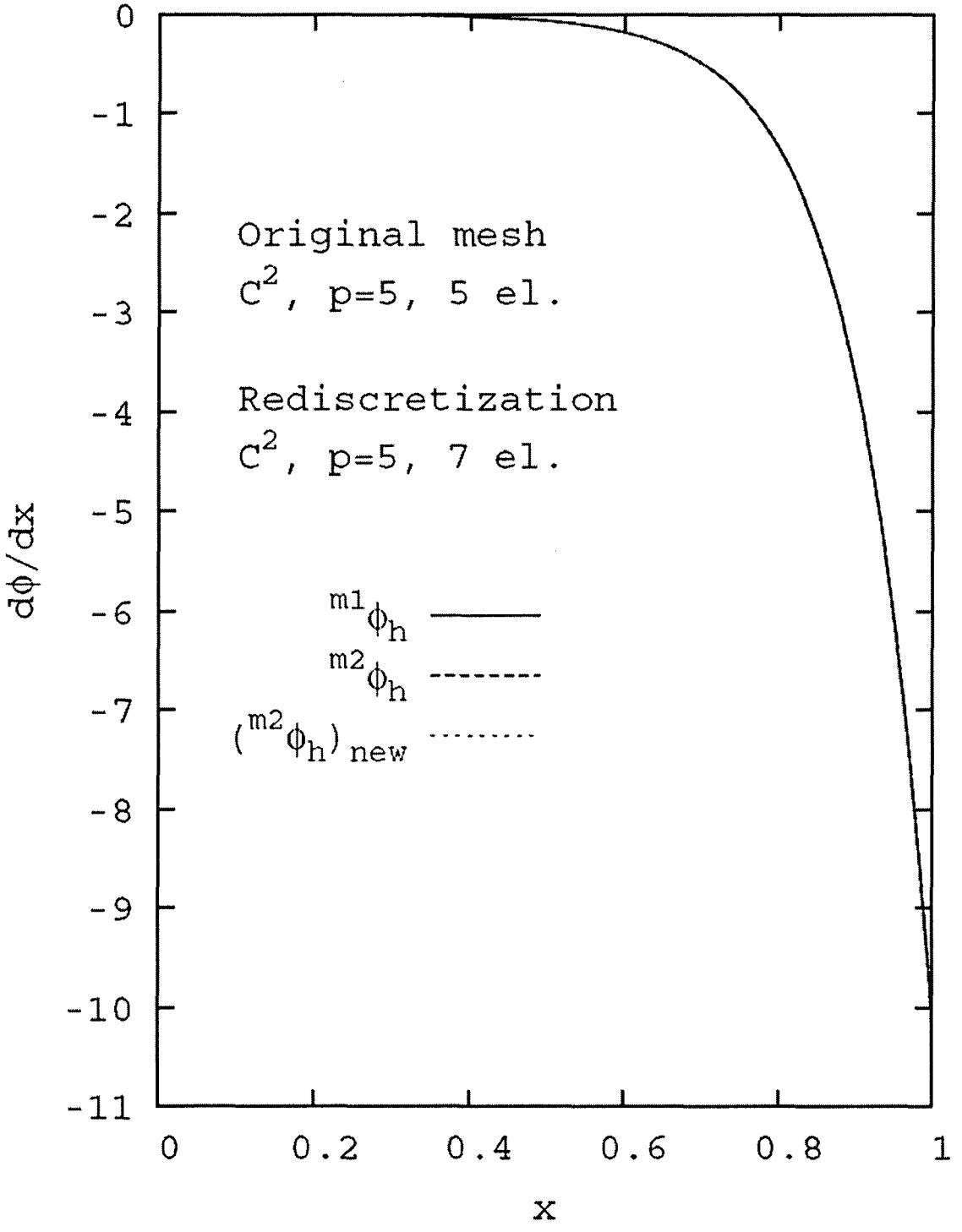

Figure 3.24: Convection diffusion equation (BVP): $\frac{d\phi}{dx}$ versus x for original, mapped and new solutions.

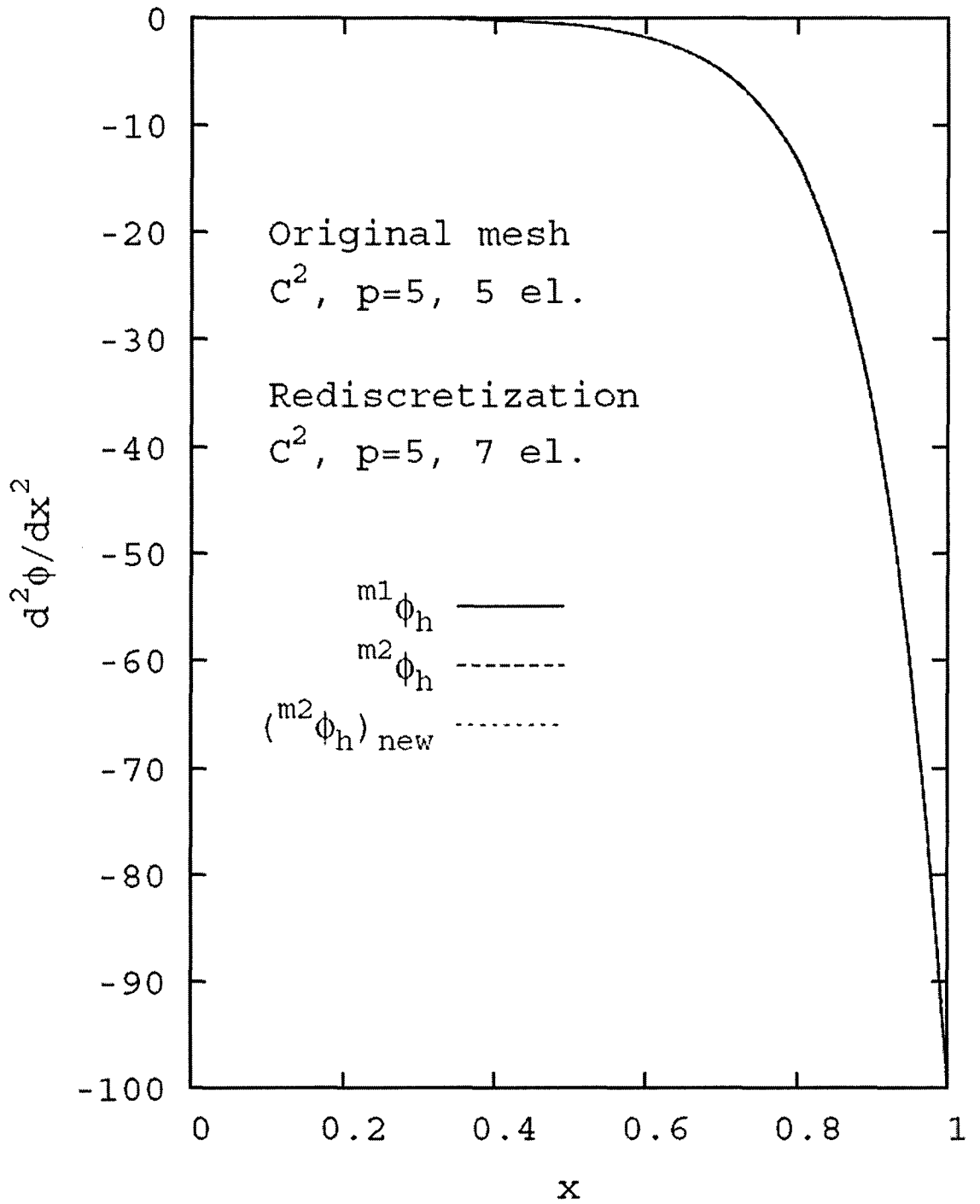

Figure 3.25: Convection diffusion equation (BVP): $\frac{d^2\phi}{dx^2}$ versus x for original, mapped and new solutions.

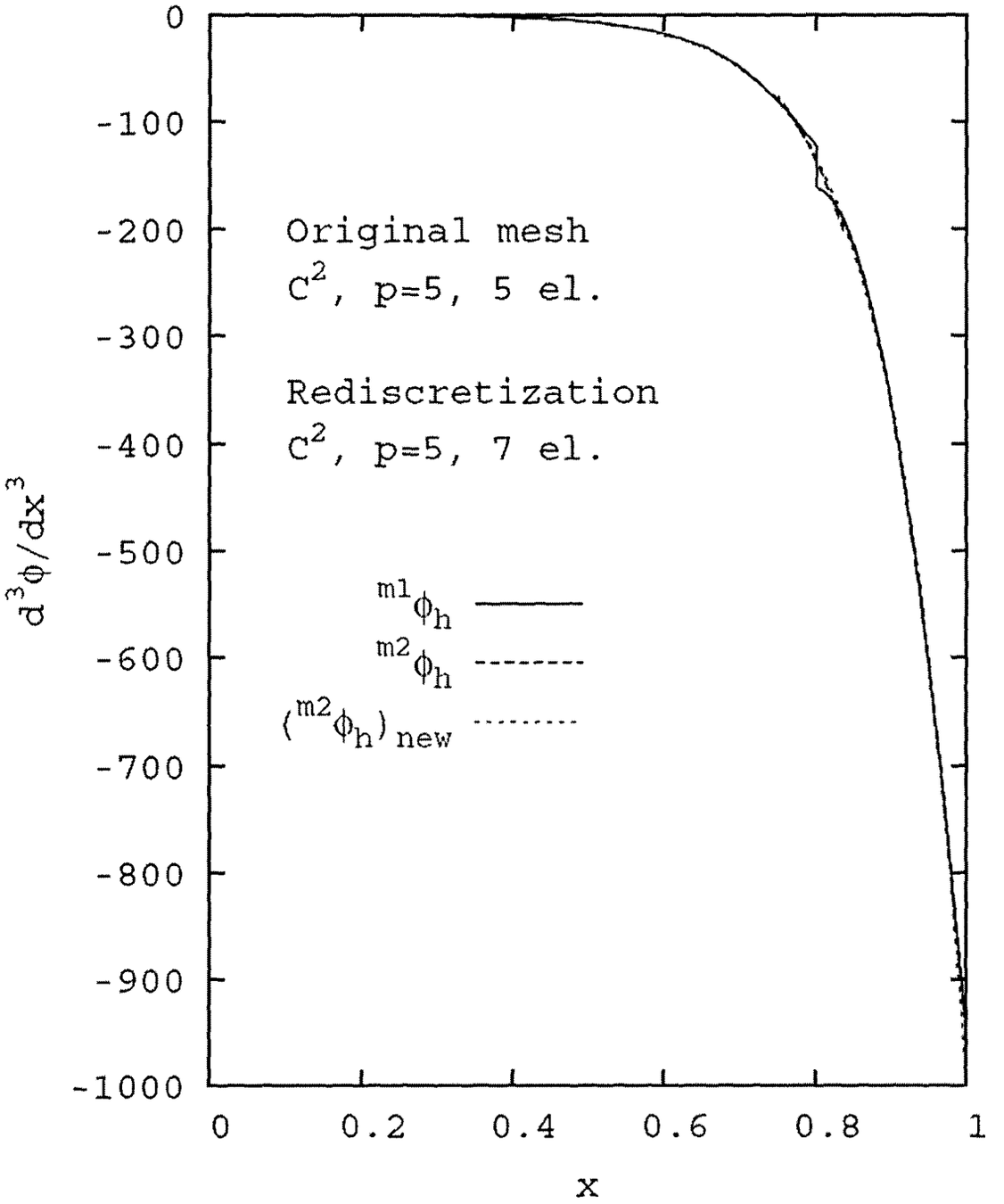

Figure 3.26: Convection diffusion equation (BVP): $\frac{d^3\phi}{dx^3}$ versus x for original, mapped and new solutions.

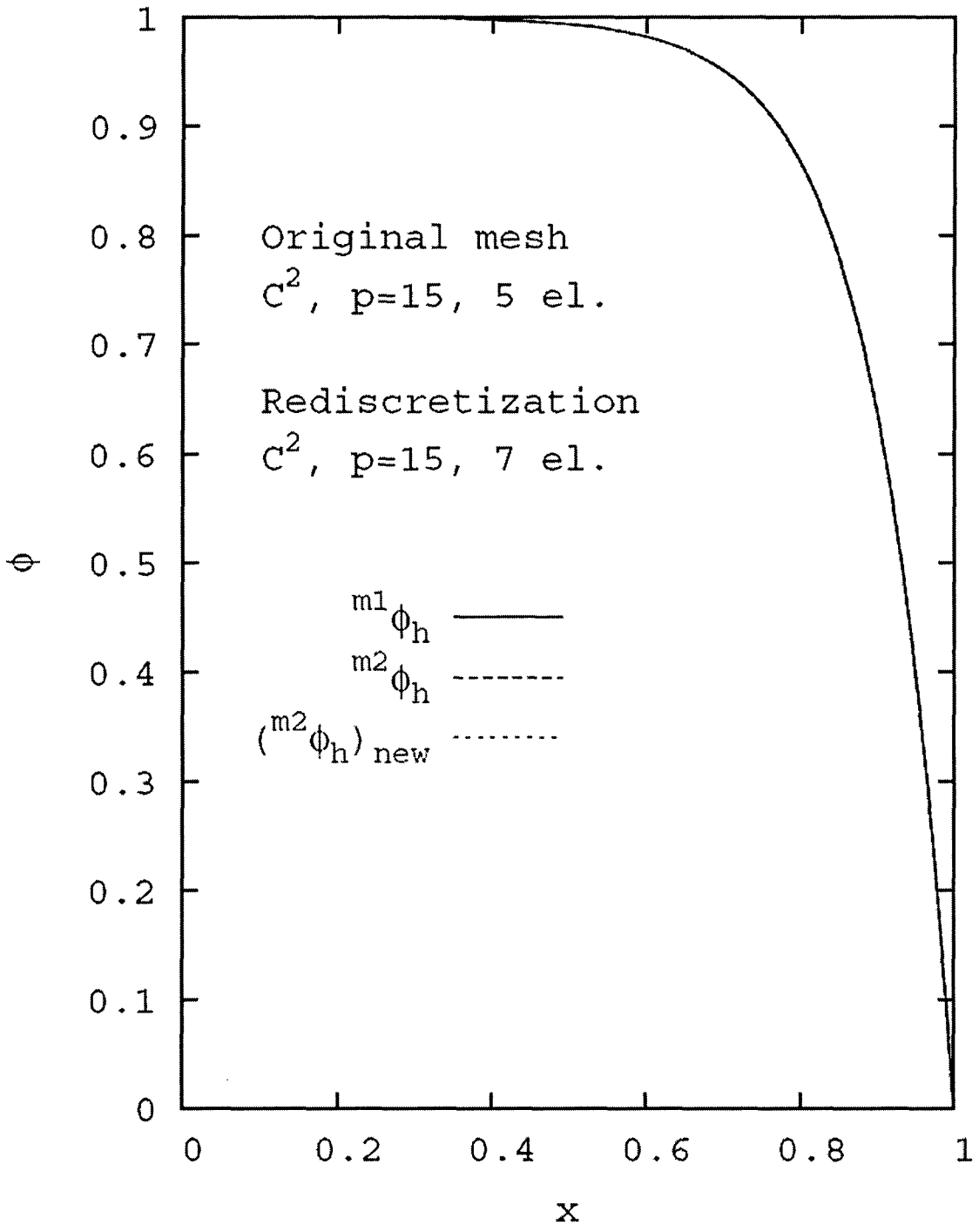

Figure 3.27: Convection diffusion equation (BVP): ϕ versus x for original, mapped and new solutions.

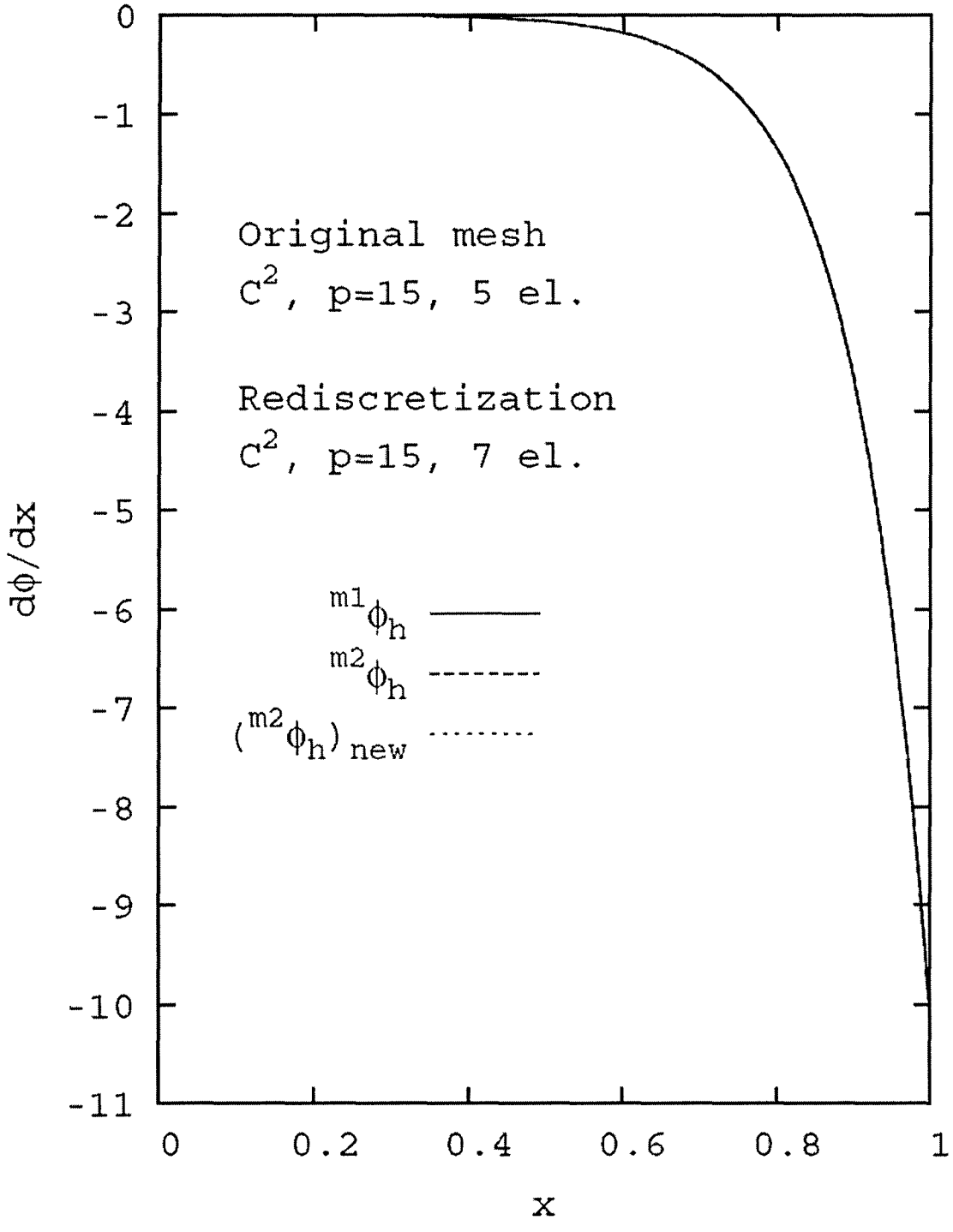

Figure 3.28: Convection diffusion equation (BVP): $\frac{d\phi}{dx}$ versus x for original, mapped and new solutions.

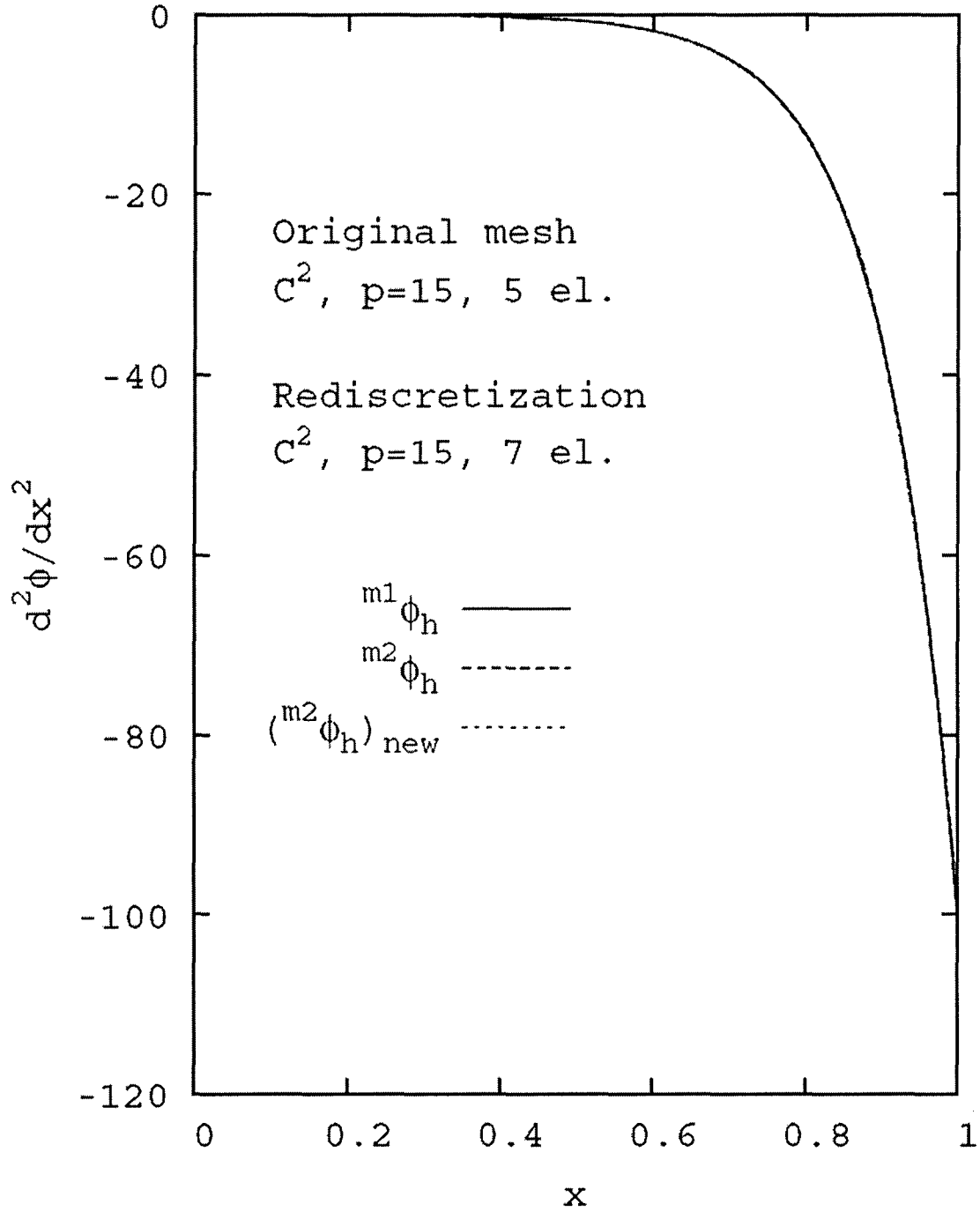

Figure 3.29: Convection diffusion equation (BVP): $\frac{d^2\phi}{dx^2}$ versus x for original, mapped and new solutions.

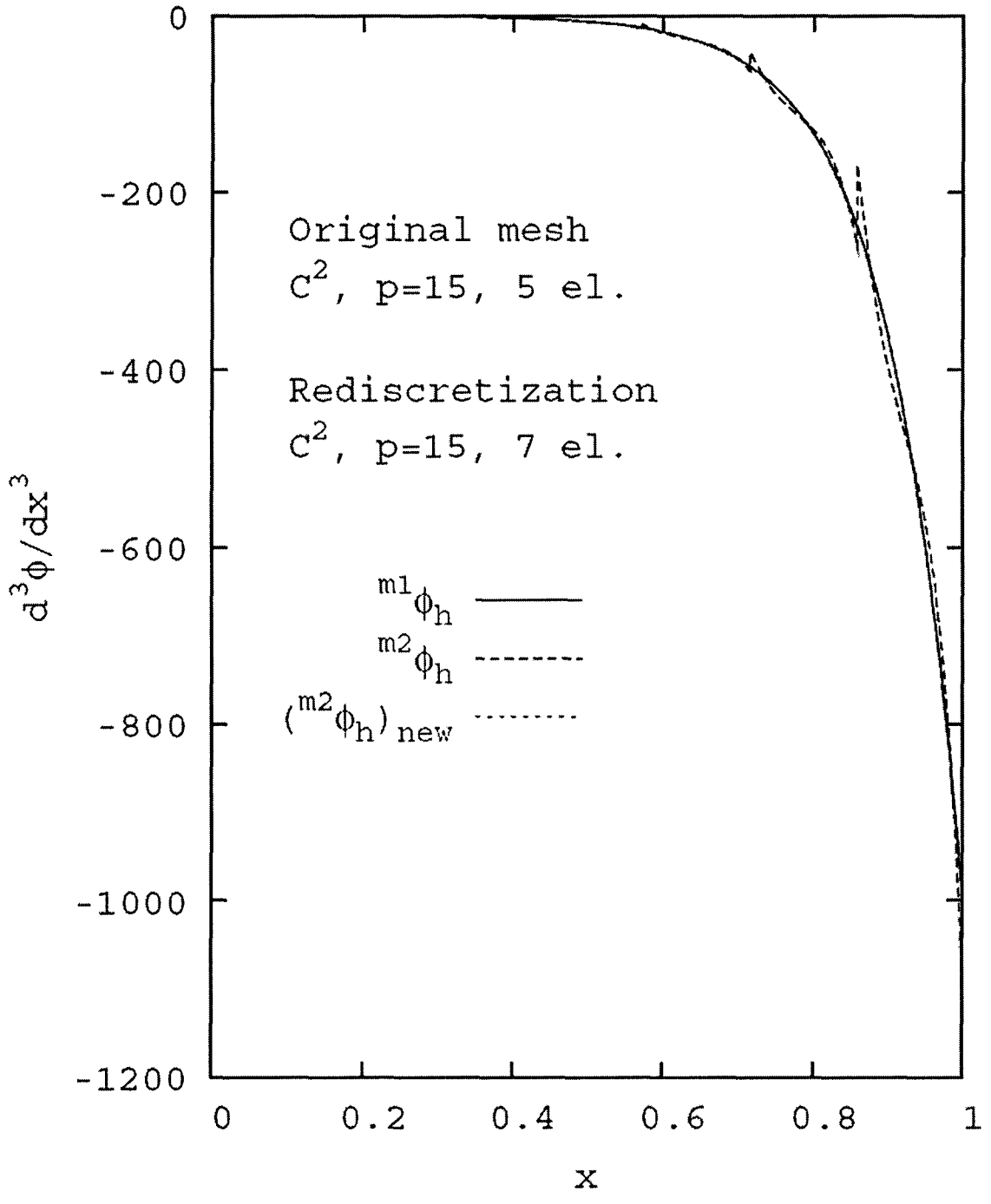

Figure 3.30: Convection diffusion equation (BVP): $\frac{d^3\phi}{dx^3}$ versus x for original, mapped and new solutions.

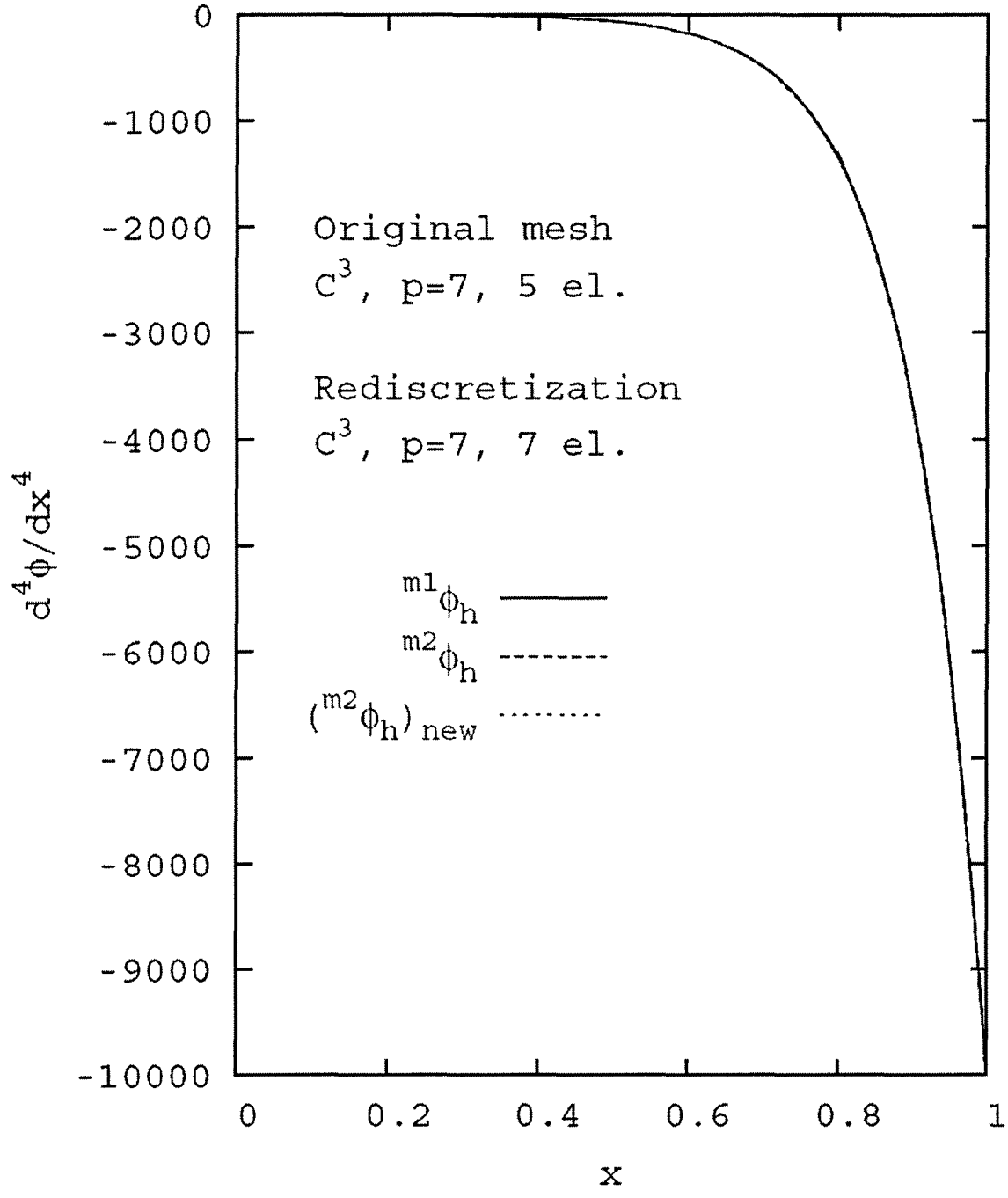

Figure 3.31: Convection diffusion equation (BVP): $\frac{d^4\phi}{dx^4}$ versus x for original, mapped and new solutions.

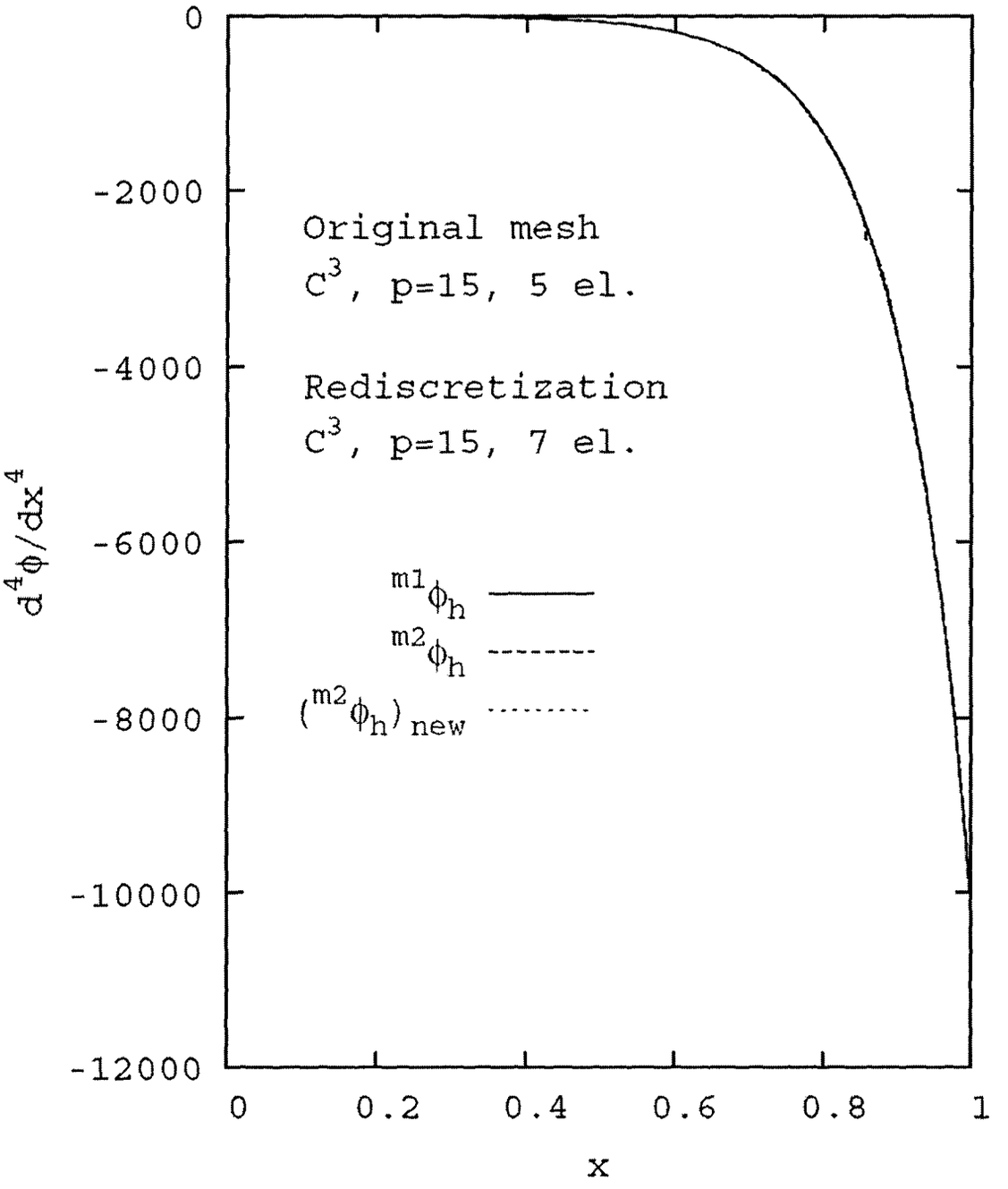

Figure 3.32: Convection diffusion equation (BVP): $\frac{d^4\phi}{dx^4}$ versus x for original, mapped and new solutions.

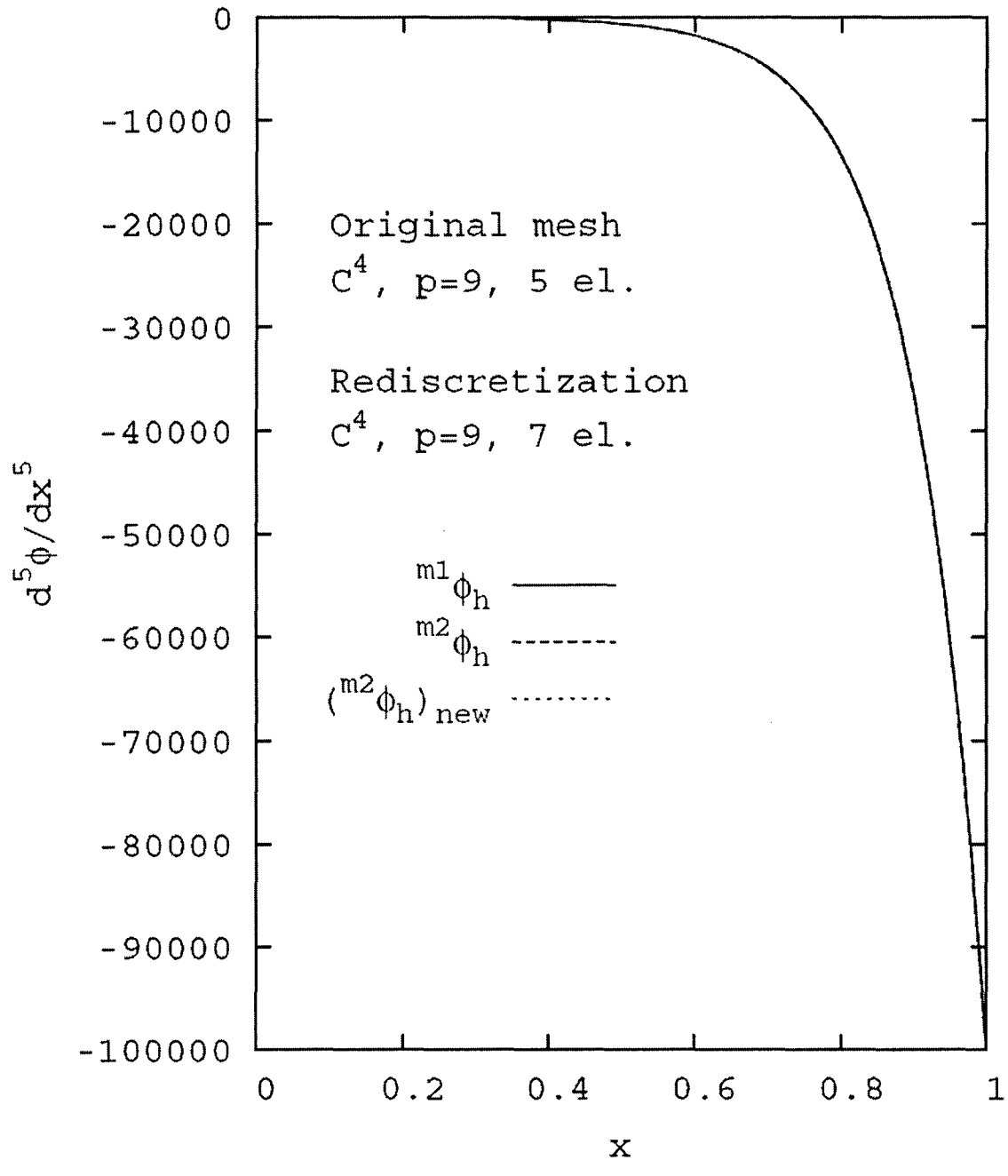

Figure 3.33: Convection diffusion equation (BVP): $\frac{d^5\phi}{dx^5}$ versus x for original, mapped and new solutions.

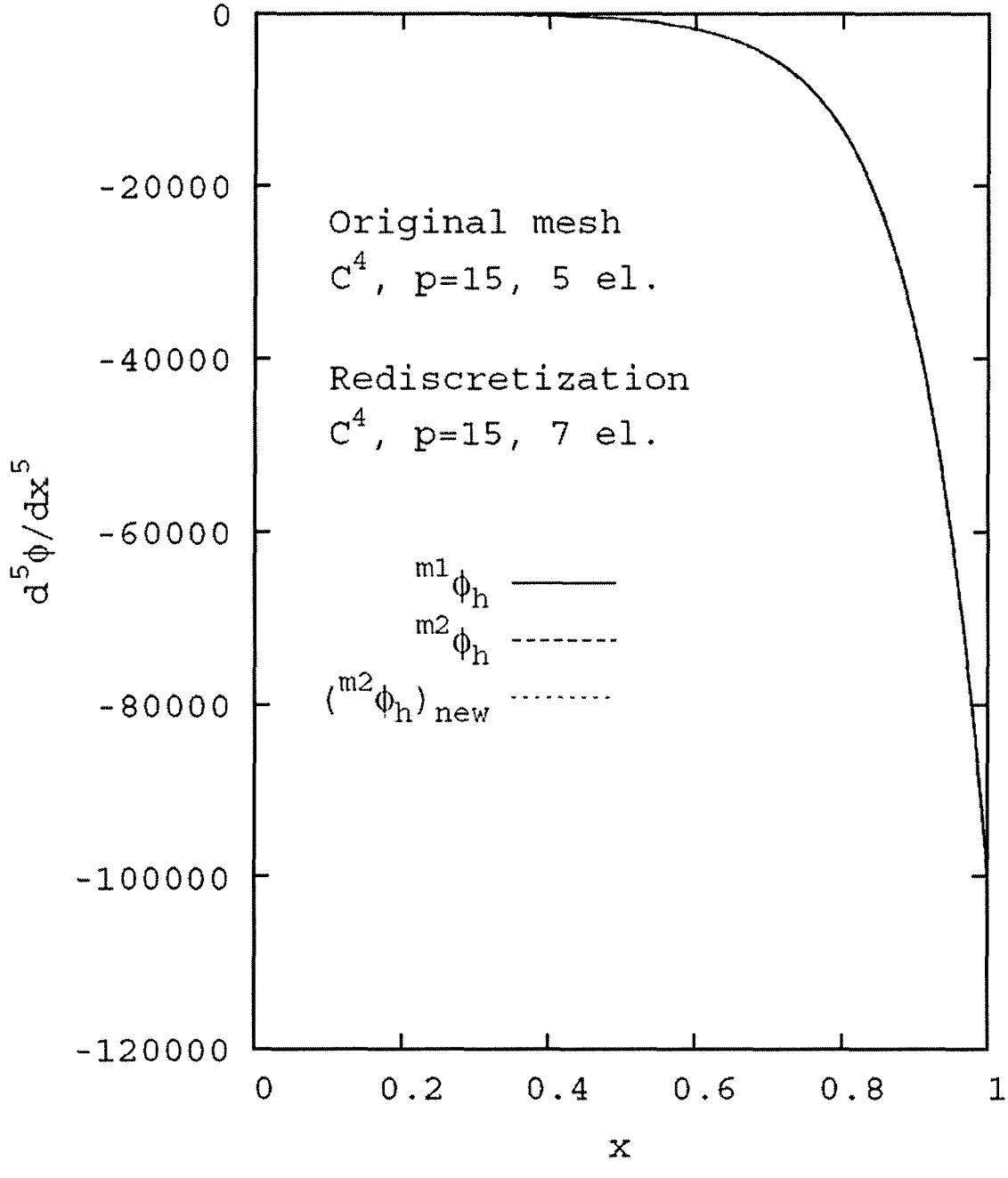

Figure 3.34: Convection diffusion equation (BVP): $\frac{d^5\phi}{dx^5}$ versus x for original, mapped and new solutions.

3.4 Two-dimensional BVP: Poisson's Equation, Local Approximations of Classes $C^{0,0}$ Lagrange Type with $p_\xi = p_\eta = 1, 15$ and $C^{1,1}$ with $p_\xi = p_\eta = 3, 15$

We consider steady-state Poisson's equation

$$\frac{\partial^2 \phi}{\partial x^2} + \frac{\partial^2 \phi}{\partial y^2} = -f(x,y) \quad over \quad \Omega = (-1,1)x(-1,1) \tag{3.2}$$

with

$$\phi(-1,y) = \phi(1,y) = \phi(x,-1) = \phi(x,1)$$

where $f(x,y)$ is such that the theoretical solution is given by

$$\phi(x,y) = e^{(1-x^2)(1-y^2)}.$$

The differential operator is self-adjoint and hence the integral form from Galerkin method with weak form is variationally consistent. Figure 3.35 (a) shows a schematic of the domain Ω as the original 5×5 uniform discretization (Figure 3.35 (b)) as well as a 7×7 uniform rediscretization (Figure 3.35 (c)). We consider the following studies.

(1) Local approximations of class $C^{0,0}$ Lagrange type with $p_\xi = p_\eta = 1$ and of class $C^{0,0}$ p-version hierarchical with p-level of $p_\xi = p_\eta = 15$. We consider the integral form based on Galerkin method with weak form.

(2) Local approximations of class $C^{1,1}$ p-version hierarchical with p-levels of $p_\xi = p_\eta = 3, 15$. The integral form is based on least squares method without auxiliary variables (i.e. strong form of the GDE).

In all cases ${}^{m1}\phi_h$ is computed for $m1$ and mapped onto $m2$ to obtain ${}^{m2}\phi_h$. A new solution is also computed for $m2$ to obtain $({}^{m2}\phi_h)_{new}$ for the rediscretization $m2$ by resolving the BVP. Results are summarized in the following figures and tables.

(a) $C^{0,0}$, $p_\xi = p_\eta = 1$; Figures 3.36, 3.37 (a), (b) and (c), Table 3.7

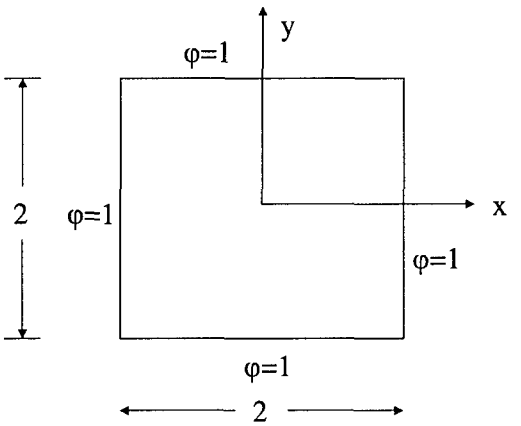

(a) Schematic of Ω for Poisson's equation

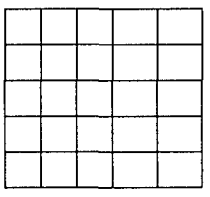

(b) 5x5 uniform discretization m1

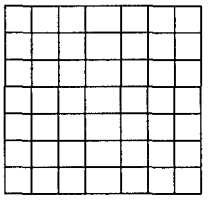

(c) 7x7 uniform rediscretization m2

Figure 3.35: Schematic, discretization and rediscretization for Poisson's equation.

(b) $C^{0,0}$, $p_\xi = p_\eta = 15$; Figures 3.37 (d), (e) and (f), Table 3.7

(c) $C^{1,1}$, $p_\xi = p_\eta = 3$; Figures 3.38, 3.39 and 3.40, Table 3.8

(d) $C^{1,1}$, $p_\xi = p_\eta = 15$; Figures 3.41, 3.42 and 3.43, Table 3.8

The ${}^{m1}\phi_h$ solution of class $C^{0,0}$ with $p_\xi = p_\eta = 1$ for discretization $m1$ is unconverged and hence has errors (Table 3.7). Graphs of $\frac{\partial \phi}{\partial x}$ and $\frac{\partial \phi}{\partial y}$ clearly demonstrate inter-element jumps in the first partial derivatives at different locations for ${}^{m1}\phi_h$ and ${}^{m2}\phi_h$ with different magnitudes as well. ${}^{m2}\phi_h$ is not in agreement with $({}^{m1}\phi_h)_{new}$, which is the correct solution for $m2$. This demonstrates the inter-element flux problems caused in the mapped solution due to inter-element flux problems in the original solution ${}^{m1}\phi_h$. Due to $p_\xi = p_\eta = 1$ only function values are dofs at the nodes. Just as in the case of the 1D convection diffusion equation, here also, mesh refinement will minimize the flux problems in ${}^{m1}\phi_h$ as well as ${}^{m2}\phi_h$. Higher p-level Lagrange elements behave in a similar fashion similar to the 1D case.

Next, we consider C^0 p-version hierarchical approximations for $m1$ and $m2$ (Figures 3.37 (d)-(f)). Even though the mesh is relatively coarse, due to high p-level ${}^{m1}\phi_h$ and $({}^{m2}\phi_h)_{new}$ are sufficiently converged and are in good agreement with each other (Figures 3.37 (d) and (f)). Due to the C^0 nature of the local approximations, maps of the hierarchical dofs at the mid-side and center nodes of the elements require maps of second and higher order derivatives of ϕ with respect to ξ and η. As a result, ${}^{m2}\phi_h$ is spurious (Figure 3.37 (e)). Similar behavior is also observed for the maps of the derivatives $\frac{\partial \phi}{\partial x}$ and $\frac{\partial \phi}{\partial y}$ onto rediscretization $m2$ (not shown). This problem can be minimized or possibly corrected by first mapping the solution ${}^{m1}\phi_h$ onto the corresponding Lagrange configurations (requiring only function values) and then obtaining the hierarchical dofs from these configuration.

The solutions of class $C^{1,1}$ at $p_\xi = p_\eta = 3$ (Figures 3.38-3.40) show good maps and are in good agreement with ${}^{m1}\phi_h$ and $({}^{m1}\phi_h)_{new}$, indicating no potential mapping problems for ϕ as well as its derivatives up to second order confirming weak convergence of the original solution ${}^{m1}\phi_h$ as well as $({}^{m1}\phi_h)_{new}$. Solutions of class $C^{1,1}$ at $p_\xi = p_\eta = 15$ (Figures 3.41-3.43) show good maps as well even though higher order hierarchical dofs are mapped in this case. This is due to the fact that

since $p_\xi = p_\eta = 3$ solutions (with no hierarchical dofs) are sufficiently converged, the hierarchical dofs beyond $p_\xi = p_\eta = 3$ are not contributing significantly to the improvement in the solution and hence the inaccuracies in their maps are of little or no consequence.

Table 3.7: Poisson's equation (BVP): $C^{0,0}$ Lagrange local approximations.

Solution	Mesh	p-level	I	$\|\phi_h\|_{L_2}$	$\left\|\frac{\partial(\phi_h)}{\partial x}\right\|_{L_2}$
${}^{m1}\phi_h$	5×5	1	-	0.336199e1	0.247853e1
${}^{m2}\phi_h$	7×7	1	-	0.331366e1	0.237681e1
$({}^{m2}\phi_h)_{new}$	7×7	1	-	0.338225e1	0.250033e1
${}^{m1}\phi_h$	5×5	15	-	0.3403821e1	0.252413e1
${}^{m2}\phi_h$	7×7	15	-	0.375170e1	0.105981e2
$({}^{m2}\phi_h)_{new}$	7×7	15	-	0.340557e1	0.252327e1

Table 3.8: Poisson's equation (BVP): $C^{1,1}$ p-version hierarchical local approximations.

Solution	Mesh	p-level	I	$\|\phi_h\|_{L_2}$	$\left\|\frac{\partial(\phi_h)}{\partial x}\right\|_{L_2}$	$\left\|\frac{\partial^2(\phi_h)}{\partial x^2}\right\|_{L_2}$	$\left\|\frac{\partial^2(\phi_h)}{\partial x \partial y}\right\|_{L_2}$
${}^{m1}\phi_h$	5×5	3	0.368110e-1	0.340376e1	0.252341e1	0.424995e1	0.401647e1
${}^{m2}\phi_h$	7×7	3	-	0.340365e1	0.252322e1	0.424924e1	0.401610e1
$({}^{m2}\phi_h)_{new}$	7×7	3	0.964658e-2	0.340380e1	0.252394e1	0.425025e1	0.401784e1
${}^{m1}\phi_h$	5×5	15	0.321561e-11	0.340382e1	0.252413e1	0.425034e1	0.401835e1
${}^{m2}\phi_h$	7×7	15	-	0.340363e1	0.252359e1	0.425034e1	0.401708e1
$({}^{m2}\phi_h)_{new}$	7×7	15	0.100513e-9	0.340384e1	0.252411e1	0.425035e1	0.401847e1

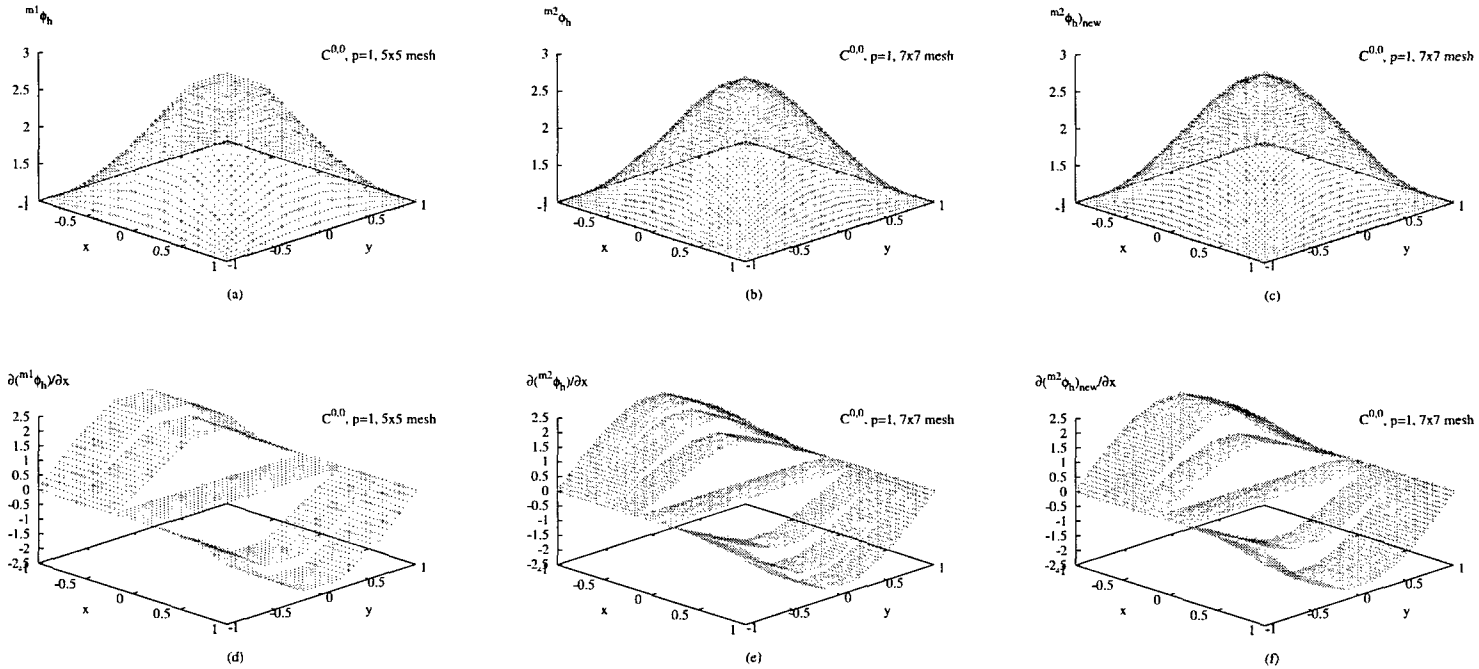

Figure 3.36: Poisson's equation (BVP): (a) - (c) ϕ and (d) - (f) $\frac{\partial(\phi_h)}{\partial x}$ versus x for original, mapped and new solutions.

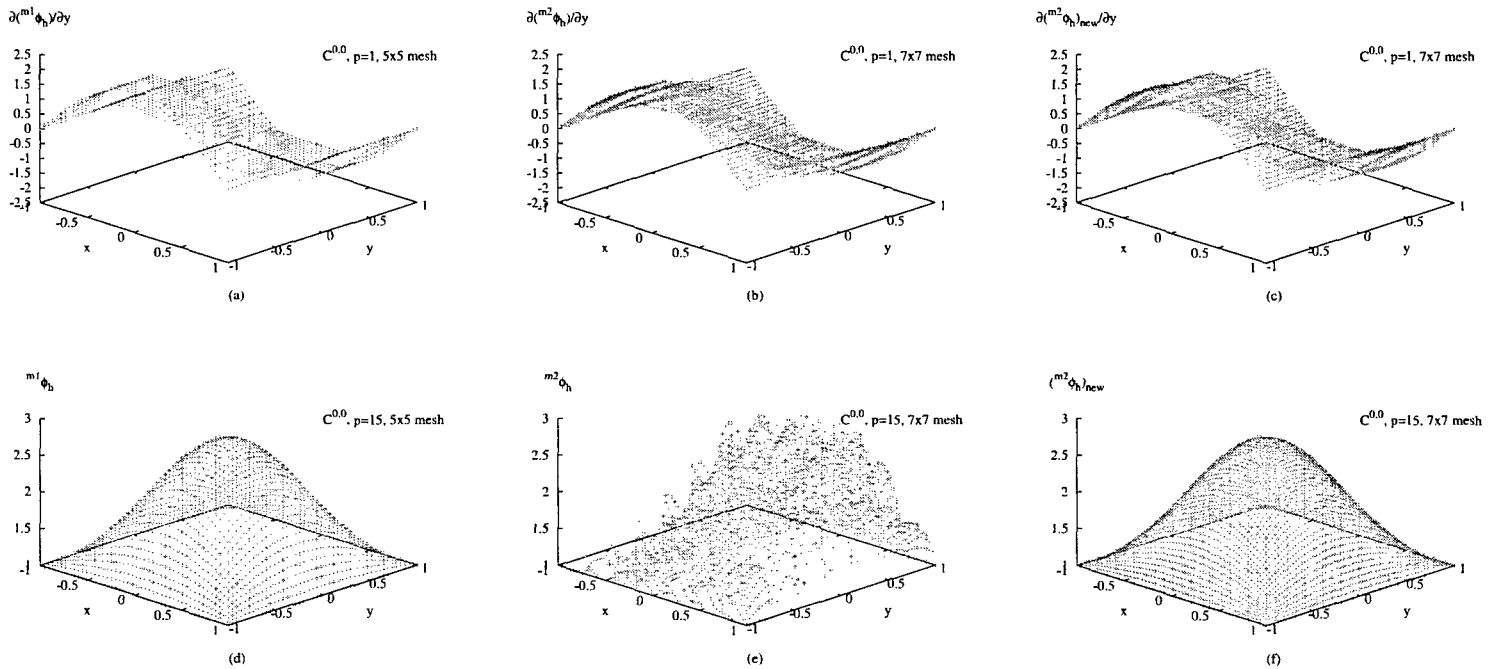

Figure 3.37: Poisson's equation (BVP): (a) - (c) $\frac{\partial(\phi_h)}{\partial y}$ and (d) - (f) ϕ versus x for original, mapped and new solutions.

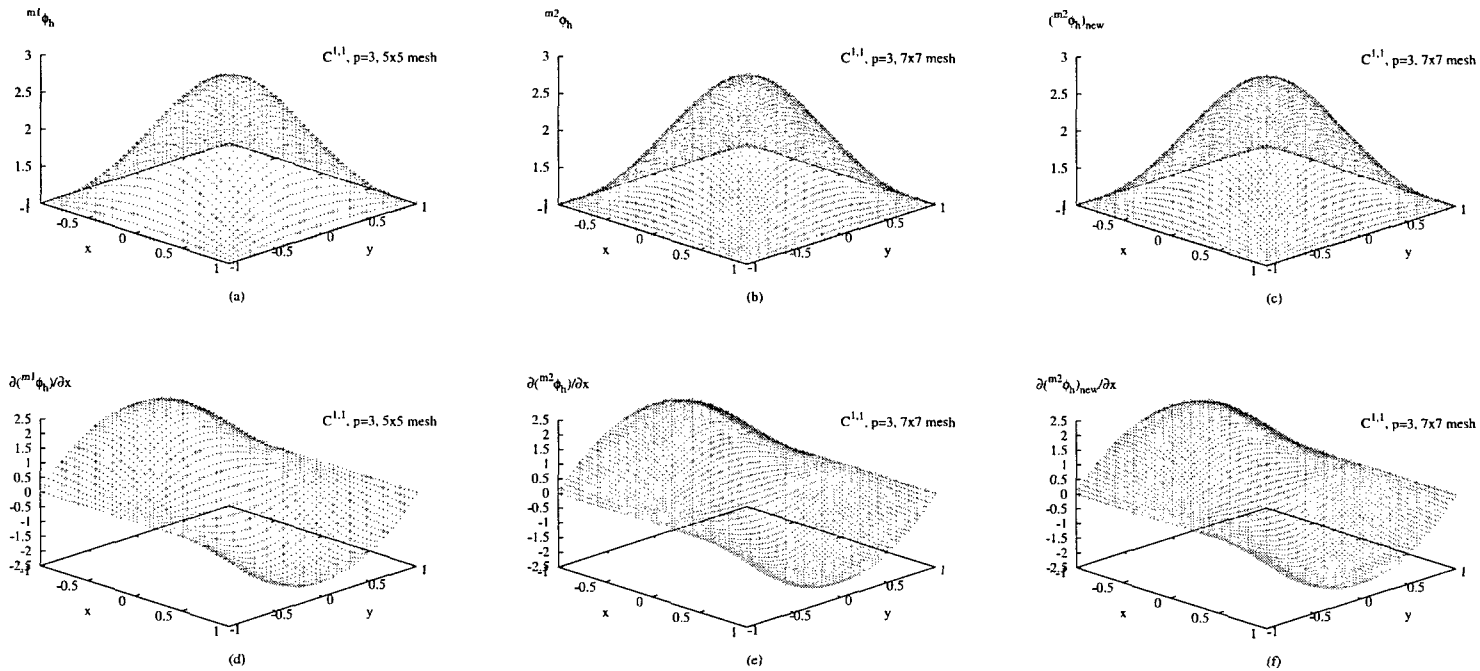

Figure 3.38: Poisson's equation (BVP): (a) - (c) ϕ and (d) - (f) $\frac{\partial(\phi_h)}{\partial x}$ versus x for original, mapped and new solutions.

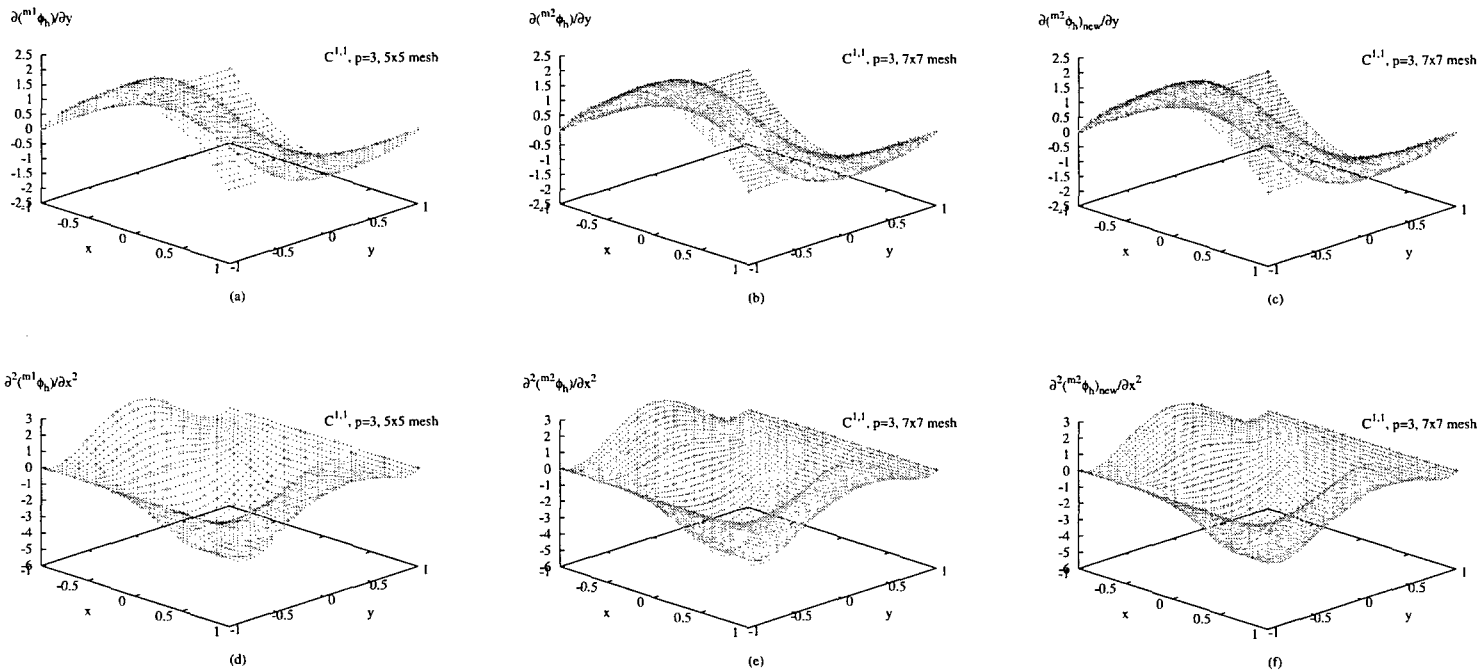

Figure 3.39: Poisson's equation (BVP): (a) - (c) $\frac{\partial(\phi_h)}{\partial y}$ and (d) - (f) $\frac{\partial^2(\phi_h)}{\partial x^2}$ versus x for original, mapped and new solutions.

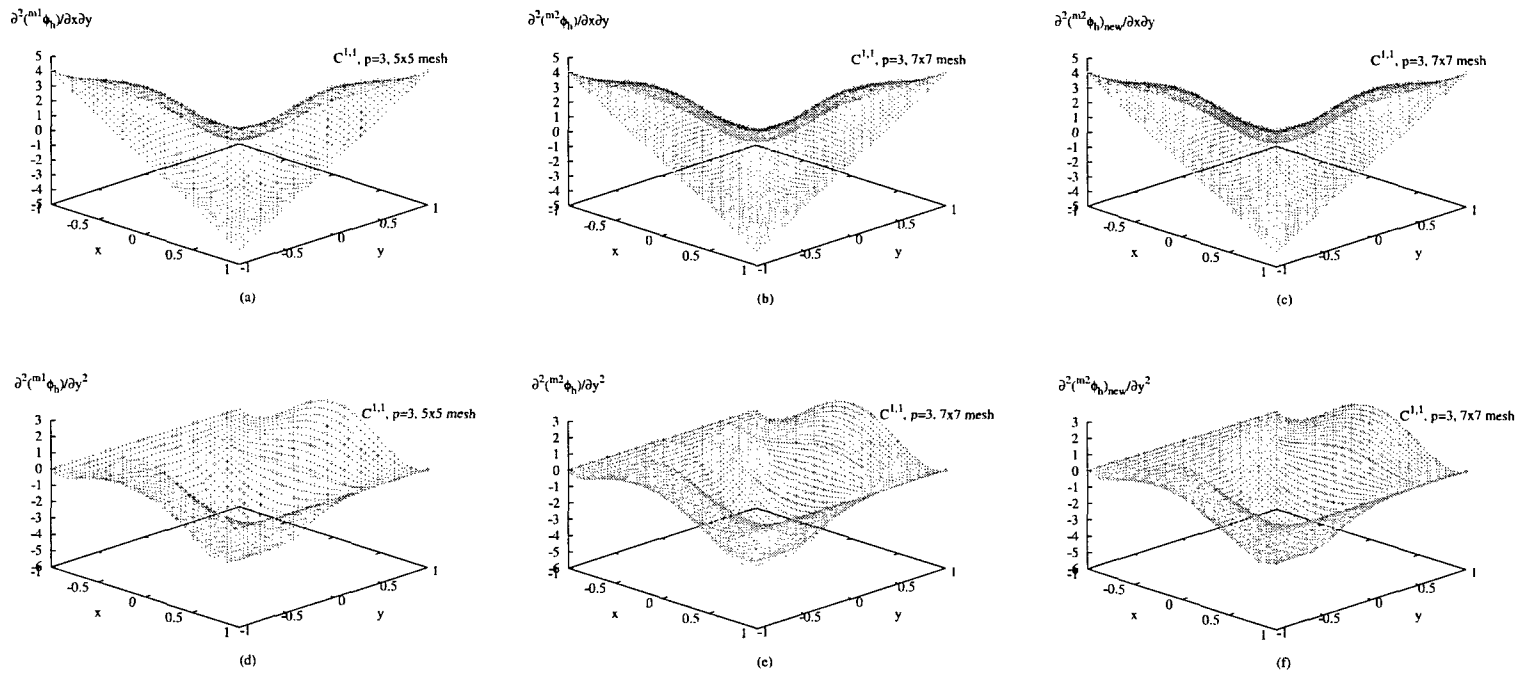

Figure 3.40: Poisson's equation (BVP): (a) - (c) $\frac{\partial^2(\phi_h)}{\partial x \partial y}$ and (d) - (f) $\frac{\partial^2(\phi_h)}{\partial y^2}$ versus x for original, mapped and new solutions.

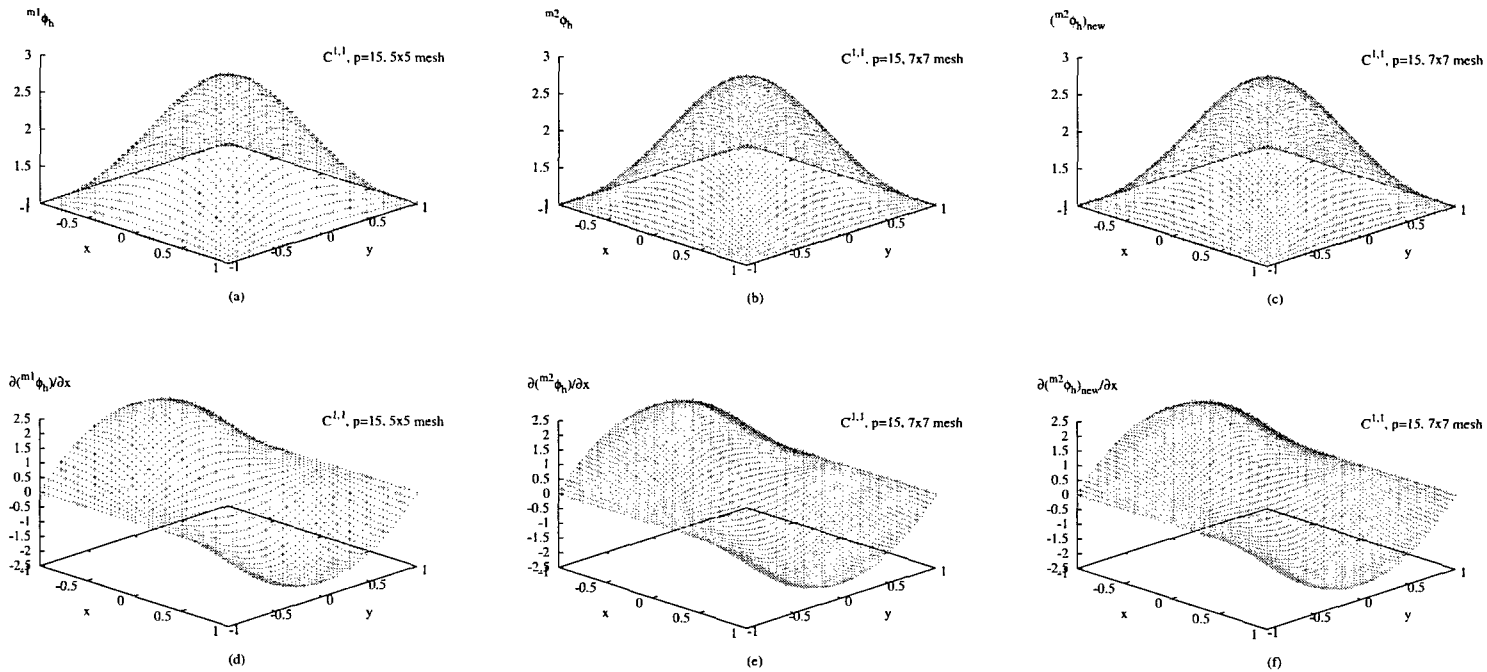

Figure 3.41: Poisson's equation (BVP): (a) - (c) ϕ and (d) - (f) $\frac{\partial(\phi_h)}{\partial x}$ versus x for original, mapped and new solutions.

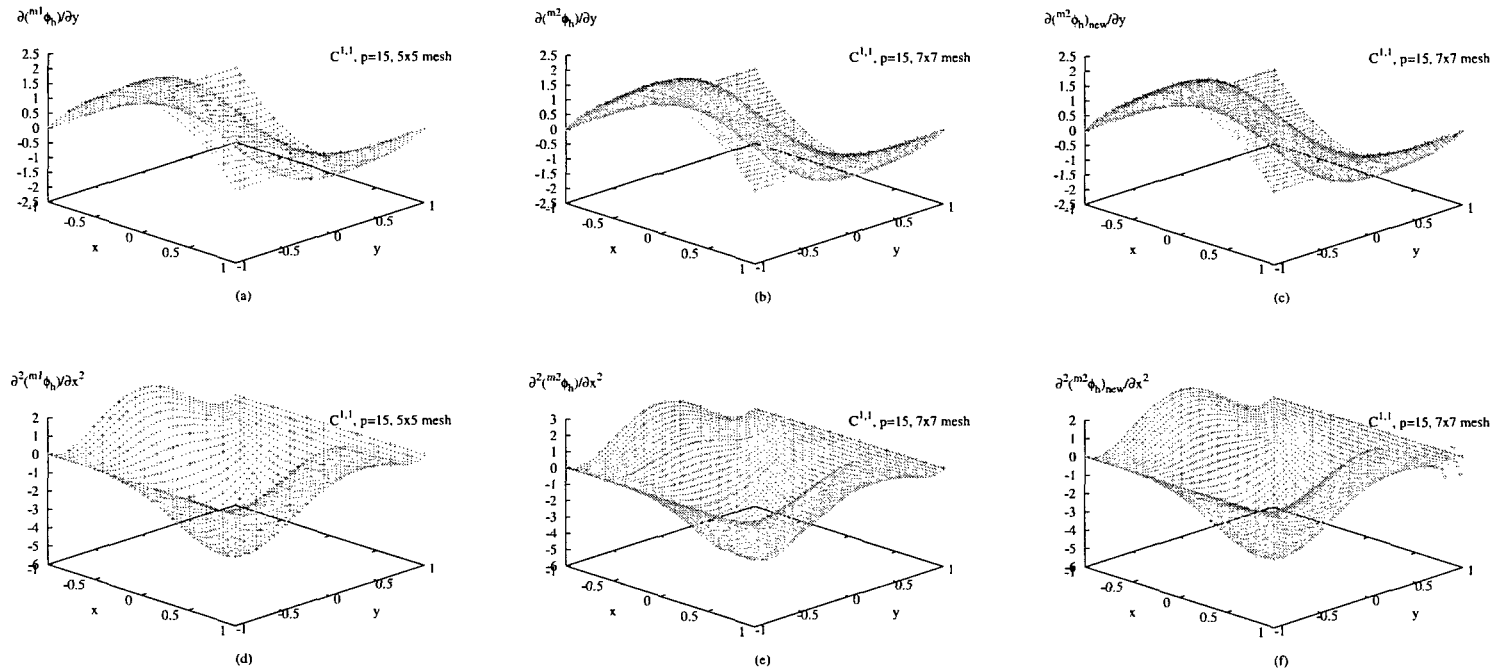

Figure 3.42: Poisson's equation (BVP): (a) - (c) $\frac{\partial(\phi_h)}{\partial y}$ and (d) - (f) $\frac{\partial^2(\phi_h)}{\partial x^2}$ versus x for original, mapped and new solutions.

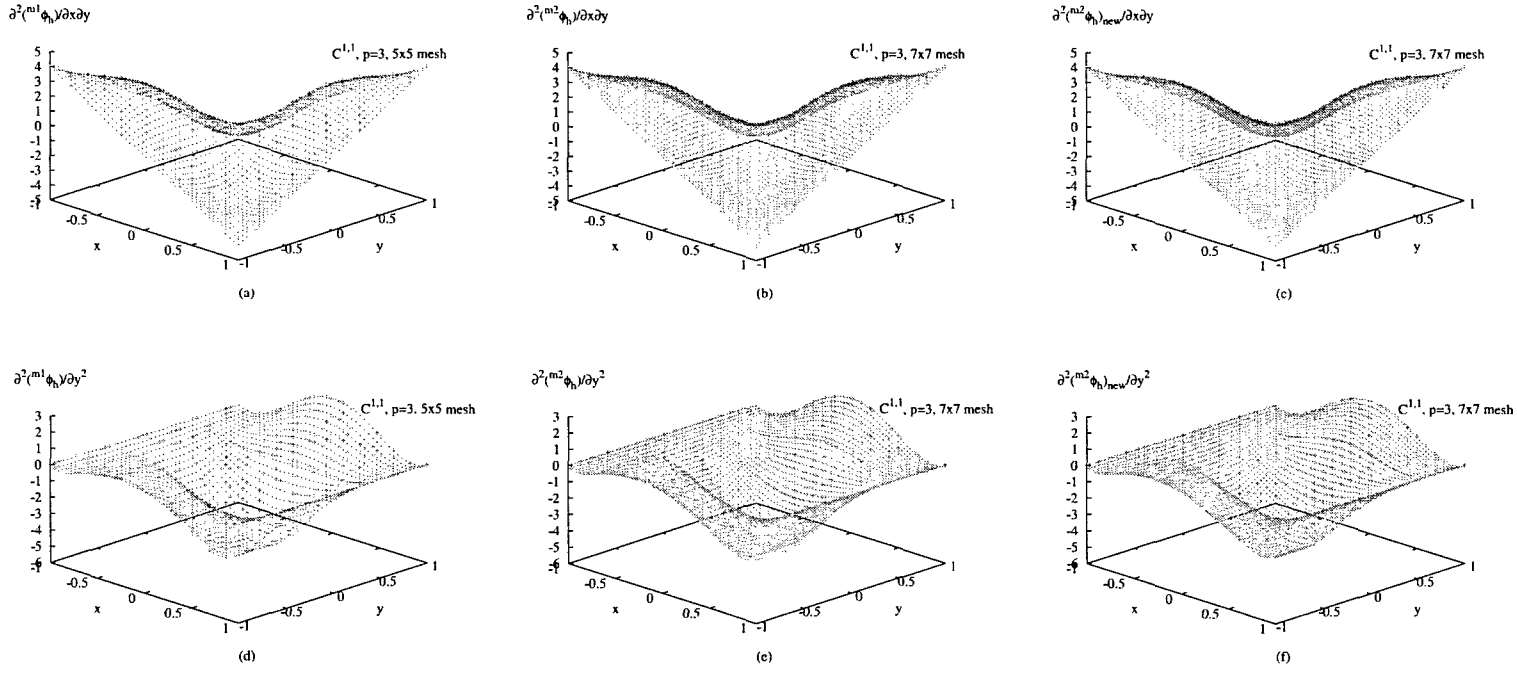

Figure 3.43: Poisson's equation (BVP): (a) - (c) $\frac{\partial^2(\phi_h)}{\partial x \partial y}$ and (d) - (f) $\frac{\partial^2(\phi_h)}{\partial y^2}$ versus x for original, mapped and new solutions.

3.5 One-dimensional Non-linear BVP: Steady-state Burgers Equation ($Re = 25$)

Here, we consider the steady-state Burgers equation as a model BVP.

$$\phi \frac{d\phi}{dx} - \frac{1}{Pe} \frac{d^2\phi}{dx^2} = 0 \quad in \quad \Omega = (0,1) \tag{3.3}$$

with

$$\phi(0) = 1 \quad , \quad \phi(1) = 0.$$

We consider $Re = 25$, for which the theoretical solution is smooth and there are no sharp fronts. We consider a uniform discretization of five p-version elements ($m1$) and a uniform rediscretization of seven p-version elements ($m2$). In (3.3), the differential operator is non-linear. We consider least squares formulation of (3.3) (strong form of GDE) for which C^1 is the minimally conforming approximation class if we permit weak convergence of the second derivative of ϕ. We consider the following two cases.

(a) p-level of 5, at which ${}^{m1}\phi_h$ is unconverged and hence has errors.

(b) p-level of 15, at which the solution ${}^{m1}\phi_h$ is weakly converged and hence is relatively free of errors.

For each of the above cases, we choose local approximations of class C^1 and perform the following computations.

(i) A solution is computed for discretization $m1$: ${}^{m1}\phi_h$.

(ii) ${}^{m1}\phi_h$ is mapped onto $\bar{\Omega}^T_{m2}$ to obtain ${}^{m2}\phi_h$.

(iii) A new solution is computed for the rediscretization $m2$ using boundary conditions in (3.2): $({}^{m2}\phi_h)_{new}$.

(iv) The mapped solution ${}^{m2}\phi_h$ is used as an initial solution for rediscretization $m2$ and Newton's method with line search is employed to obtain a converged solution: $({}^{m2}\phi_h)^{is}_{new}$ by resolving the BVP.

The results are summarized in the following figures and Table 3.9.

(a) C^1, $p_\xi = 3$; ${}^{m1}\phi_h$, ${}^{m2}\phi_h$, $({}^{m1}\phi_h)_{new}$ and their derivatives up to second order; Figures 3.44-3.46

(b) C^1, $p_\xi = 3$; ${}^{m2}\phi_h$, $({}^{m1}\phi_h)_{new}$, $({}^{m1}\phi_h)^{is}_{new}$ and their derivatives up to second order; Figures 3.47-3.49

(c) C^1, $p_\xi = 15$; ${}^{m1}\phi_h$, ${}^{m2}\phi_h$, $({}^{m1}\phi_h)_{new}$ and their derivatives up to second order; Figures 3.50-3.52

(d) C^1, $p_\xi = 15$; ${}^{m2}\phi_h$, $({}^{m1}\phi_h)_{new}$, $({}^{m1}\phi_h)^{is}_{new}$ and their derivatives up to second order; Figures 3.53-3.55

Since at $p_\xi = 3$ the solution ${}^{m1}\phi_h$ is not converged, it has errors and hence its map ${}^{m2}\phi_h$ is expected to have errors as well and the maps of the errors in the two cases will also be different. In Figure 3.44, the solution map is in fair agreement with ${}^{m1}\phi_h$, however the correct solution for $m2$ is $({}^{m2}\phi_h)_{new}$ which does not agree with the map. The differences between the mapped solution ${}^{m2}\phi_h$ and $({}^{m2}\phi_h)_{new}$ are more pronounced in Figures 3.45 and 3.46 showing graphs of the first and second derivatives, respectively. From Figures 3.47-3.49, showing graphs of ${}^{m2}\phi_h$, $({}^{m2}\phi_h)_{new}$, and $({}^{m1}\phi_h)^{is}_{new}$ and their derivatives up to second order, we observe perfect agreement between $({}^{m2}\phi_h)_{new}$ and $({}^{m2}\phi_h)^{is}_{new}$ and their derivatives up to second order. Even though ${}^{m2}\phi_h$ is in error, using ${}^{m2}\phi_h$ as an initial solution, it is possible to obtain the correct solution for the rediscretization $m2$. This is a significant merit of the proposed approach using ${}^{m2}\phi_h$ as an initial solution for the BVPs described by non-linear differential operators. Solutions of class C^1 at $p_\xi = 15$ (Figures 3.50-3.55) further substantiate the usefulness and merit of this approach. From these figures, we note that even though ${}^{m2}\phi_h$ and their derivatives are erroneous, $({}^{m2}\phi_h)^{is}_{new}$ is in perfect agreement with $({}^{m2}\phi_h)_{new}$ and their derivatives of up to second order. The findings reported here also hold when the local approximations are of higher classes.

Table 3.9: Burgers equation (BVP): $C^{1,1}$ p-version hierarchical local approximations.

Solution	Mesh	p-level	I	$\|\phi_h\|_{L_2}$	$\left\|\frac{d(\phi_h)}{dx}\right\|_{L_2}$	$\left\|\frac{\partial^2(\phi_h)}{dx^2}\right\|_{L_2}$
${}^{m1}\phi_h$	5	3	0.105577e0	0.829991e0	0.183169e1	0.131250e2
${}^{m2}\phi_h$	7	3	-	0.830241e0	0.183269e1	0.130113e2
$({}^{m2}\phi_h)_{new}$	7	3	0.799813e-1	0.850746e0	0.199550e1	0.155220e2
$({}^{m2}\phi_h)^{is}_{new}$	7	3	0.799813e-1	0.850746e0	0.199549e1	0.155220e2
${}^{m1}\phi_h$	5	15	0.113703e-10	0.959166e0	0.288675e1	0.322748e2
${}^{m2}\phi_h$	7	15	-	0.963128e0	0.317969e1	0.495645e2
$({}^{m2}\phi_h)_{new}$	7	15	0.154861e-12	0.959166e0	0.288675e1	0.322748e2
$({}^{m2}\phi_h)^{is}_{new}$	7	15	0.155708e-12	0.959166e0	0.288675e1	0.322748e2

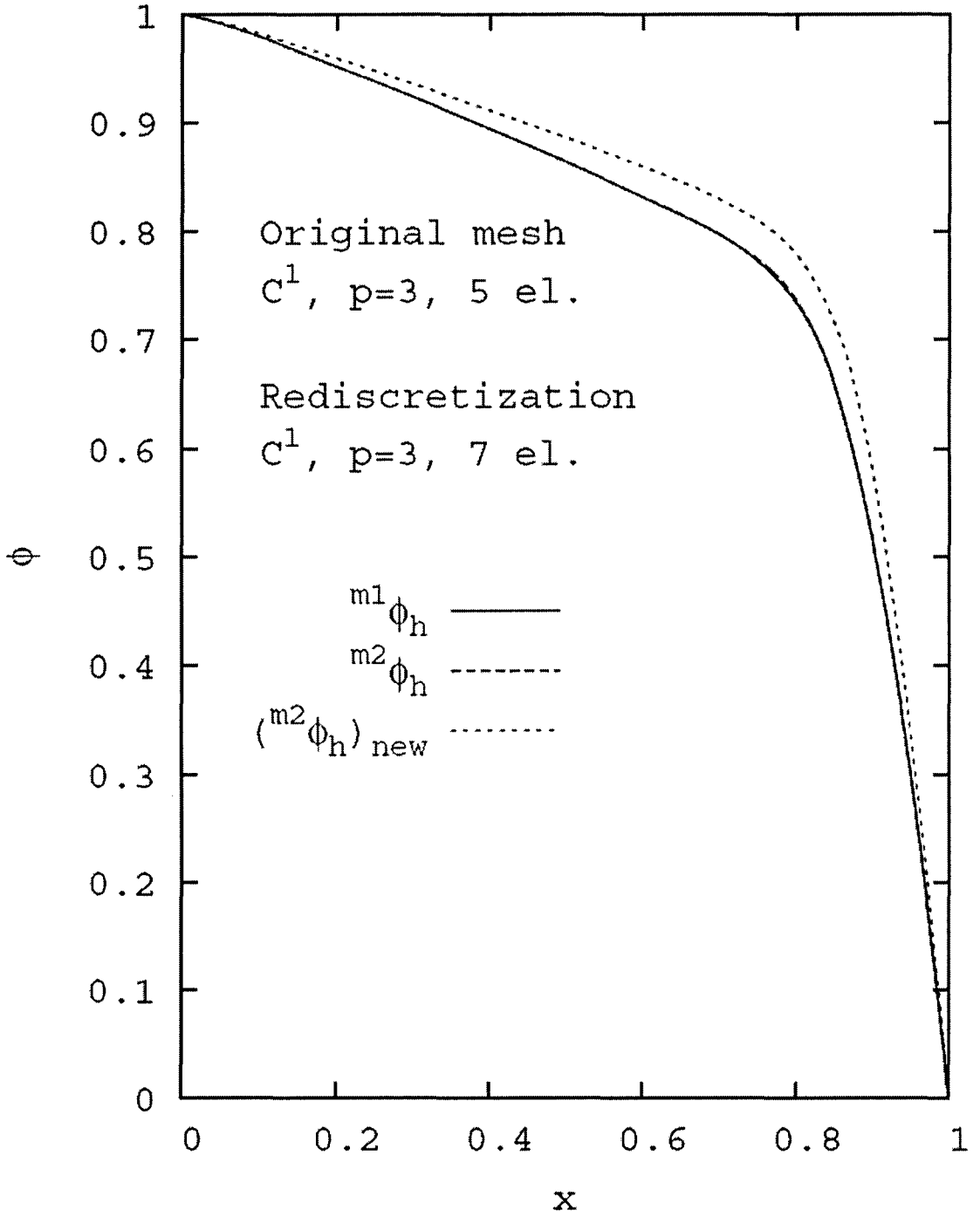

Figure 3.44: Burgers equation (BVP): ϕ versus x for original, mapped and new solutions.

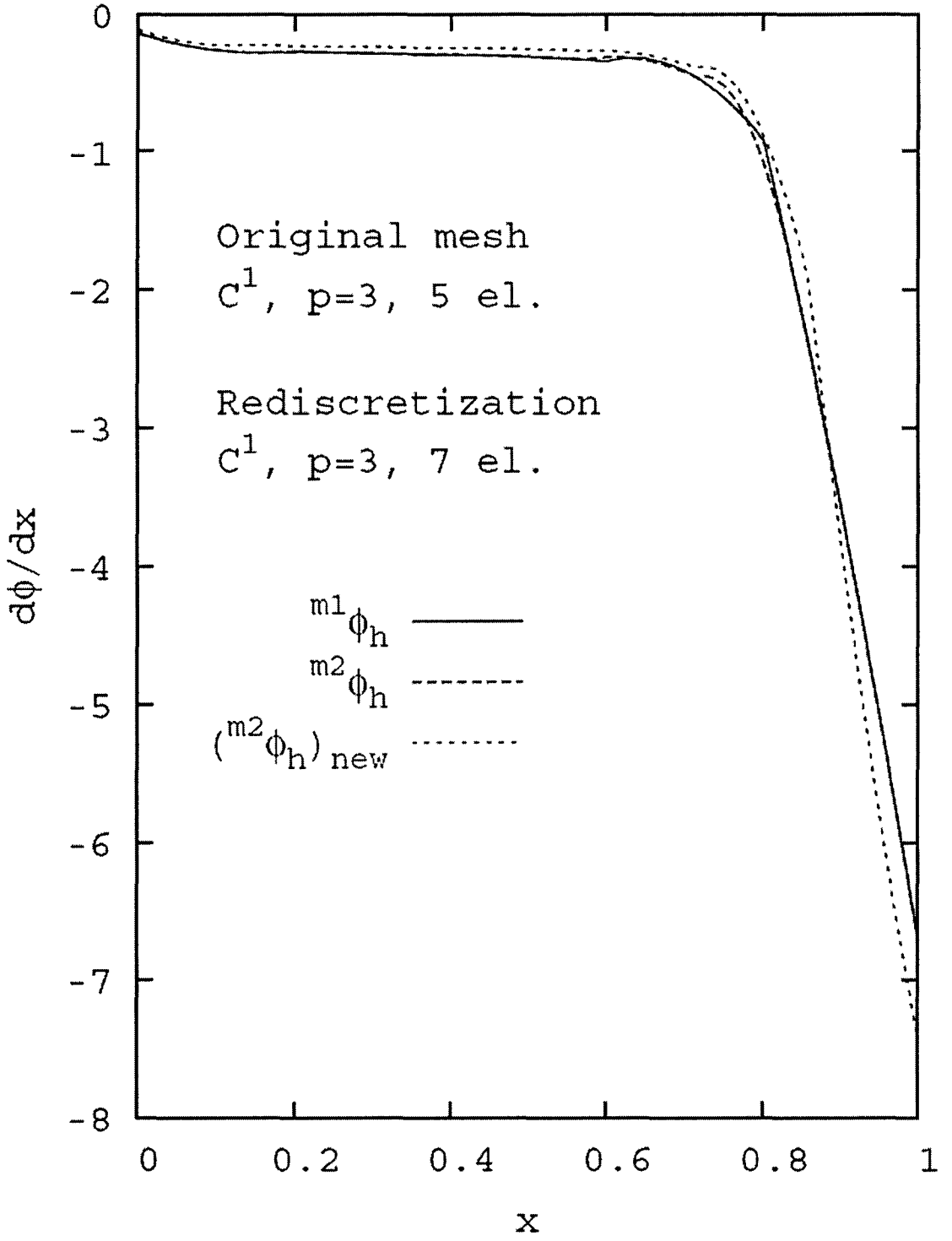

Figure 3.45: Burgers equation (BVP): $\frac{d\phi}{dx}$ versus x for original, mapped and new solutions.

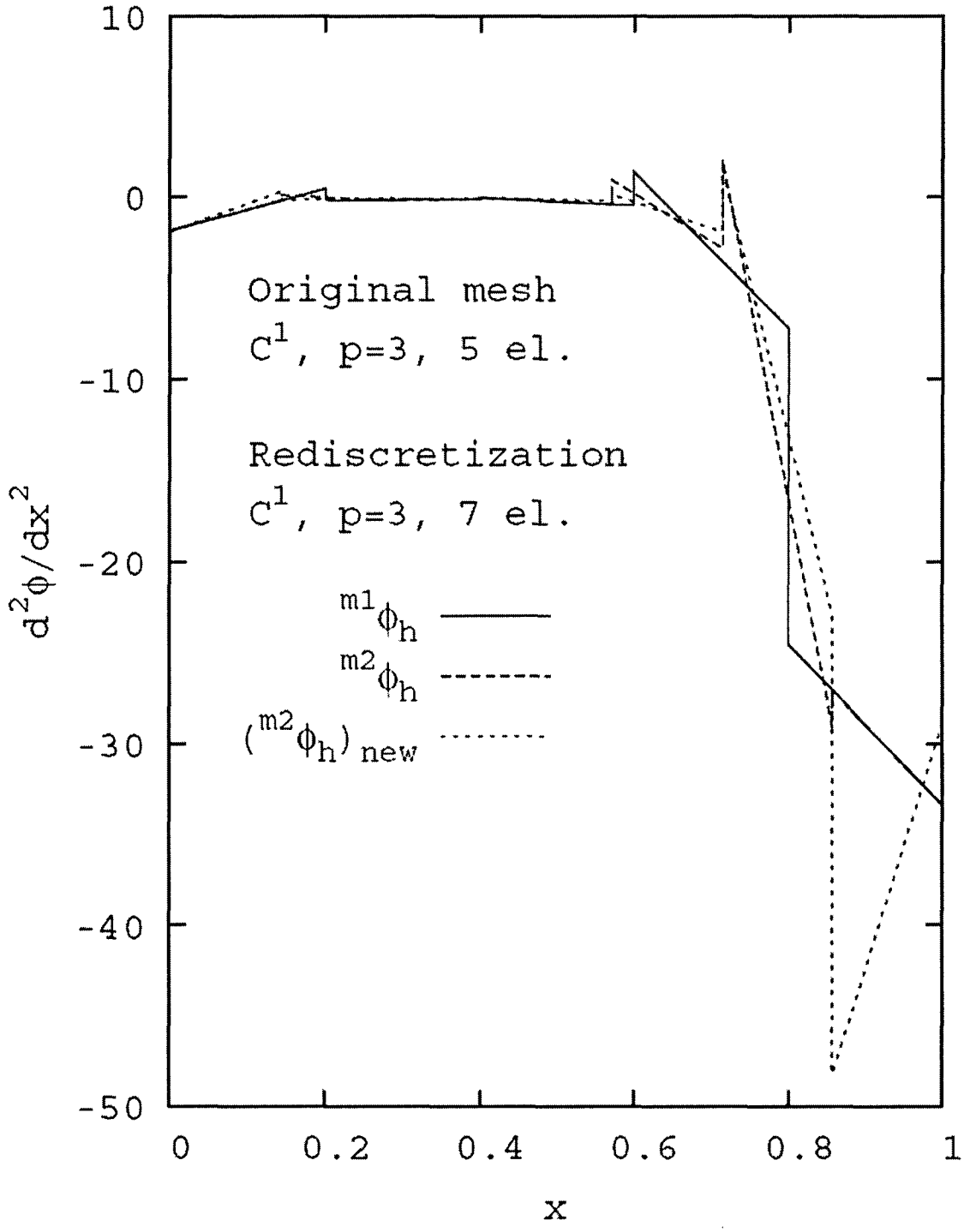

Figure 3.46: Burgers equation (BVP): $\frac{d^2\phi}{dx^2}$ versus x for original, mapped and new solutions.

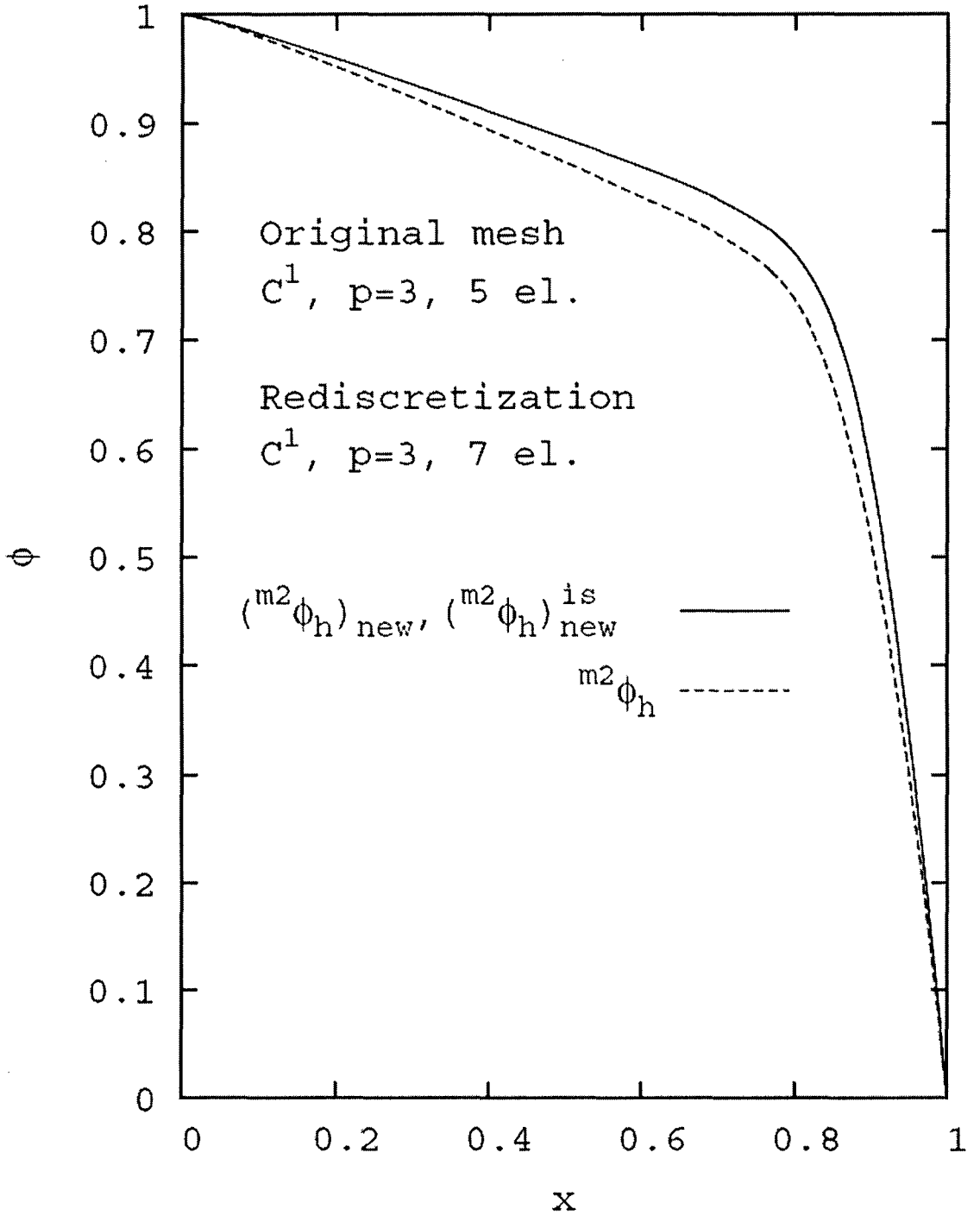

Figure 3.47: Burgers equation (BVP): ϕ versus x for mapped, new and new with initial solution.

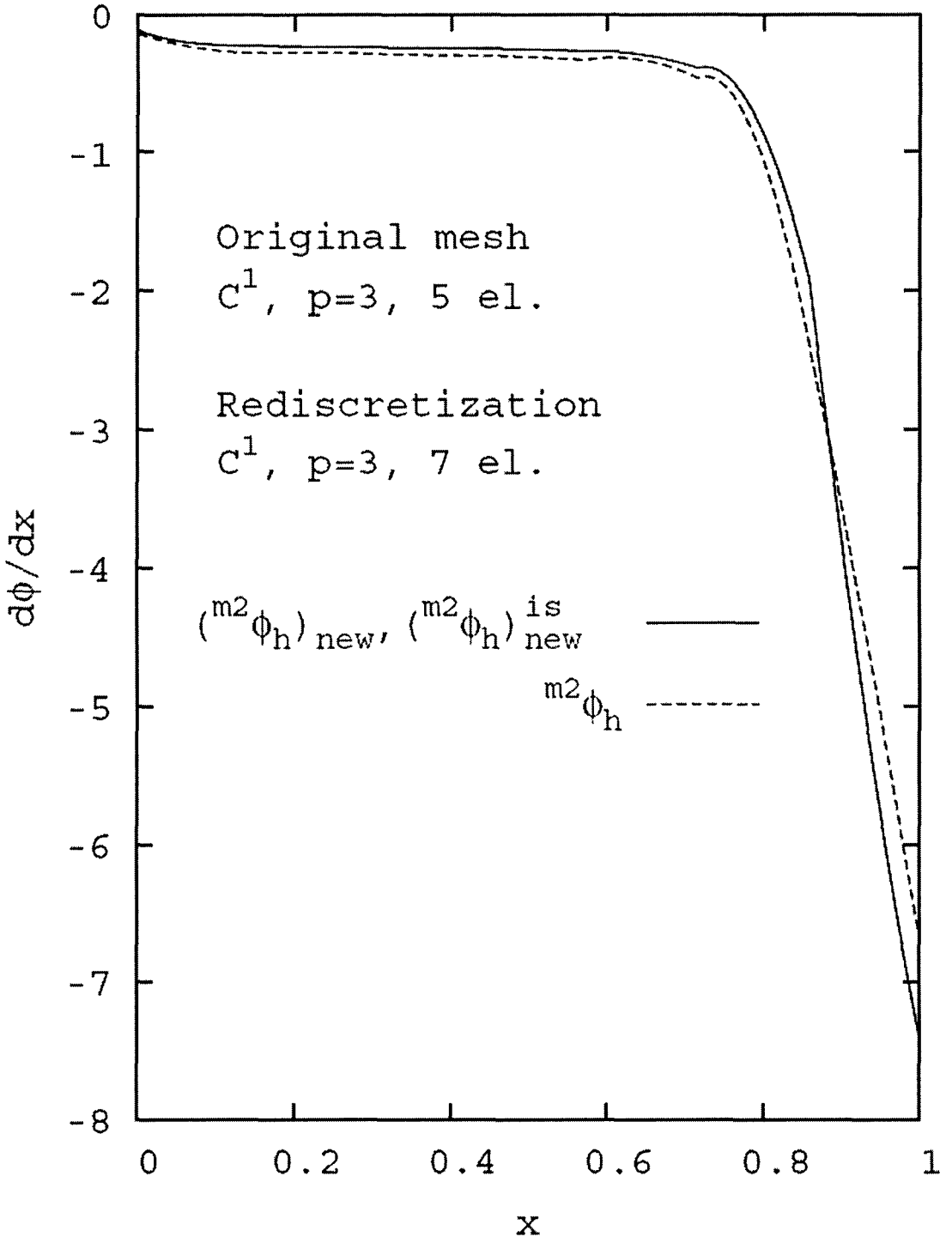

Figure 3.48: Burgers equation (BVP): $\frac{d\phi}{dx}$ versus x for mapped, new and new with initial solution.

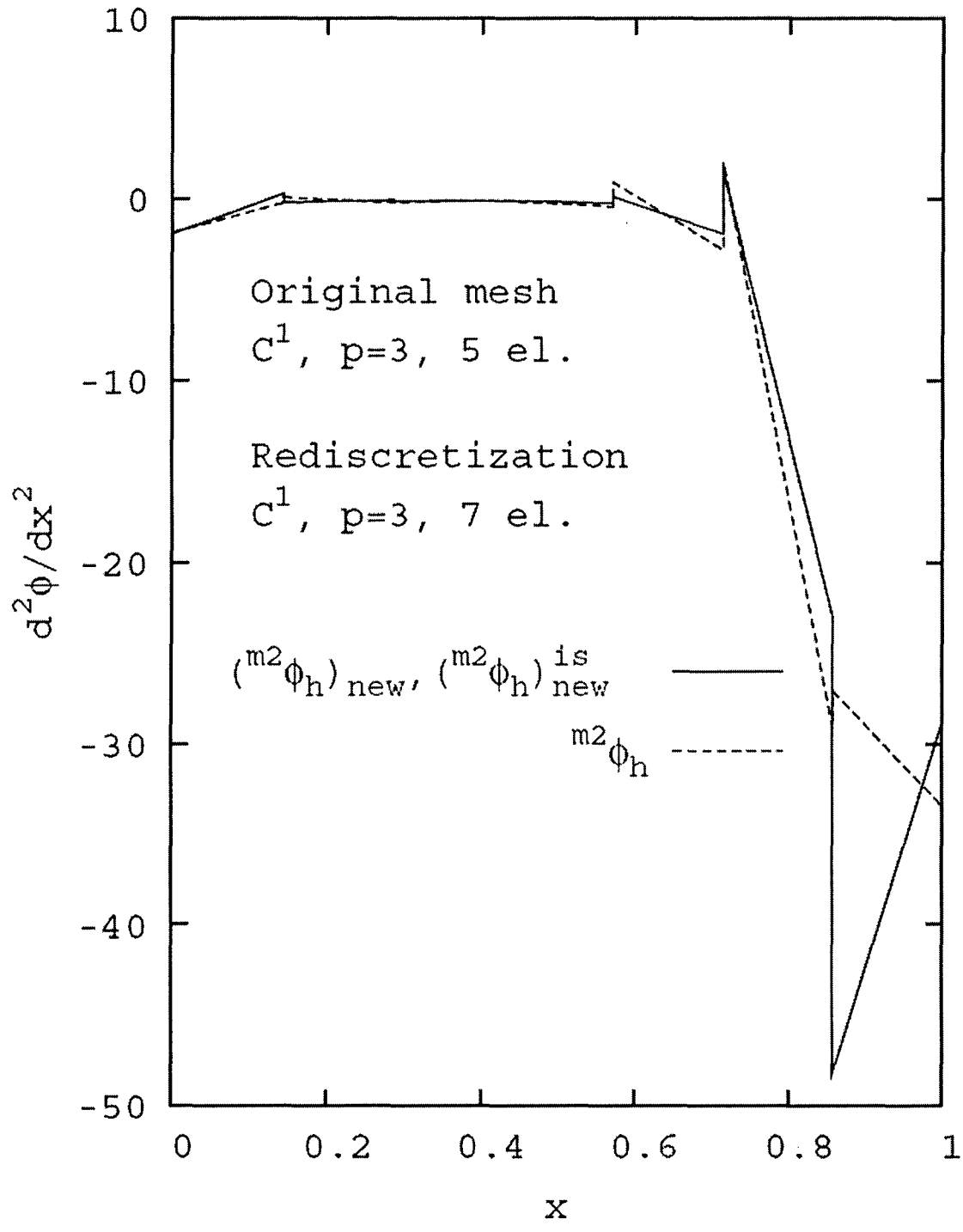

Figure 3.49: Burgers equation (BVP): $\frac{d^2\phi}{dx^2}$ versus x for mapped, new and new with initial solution.

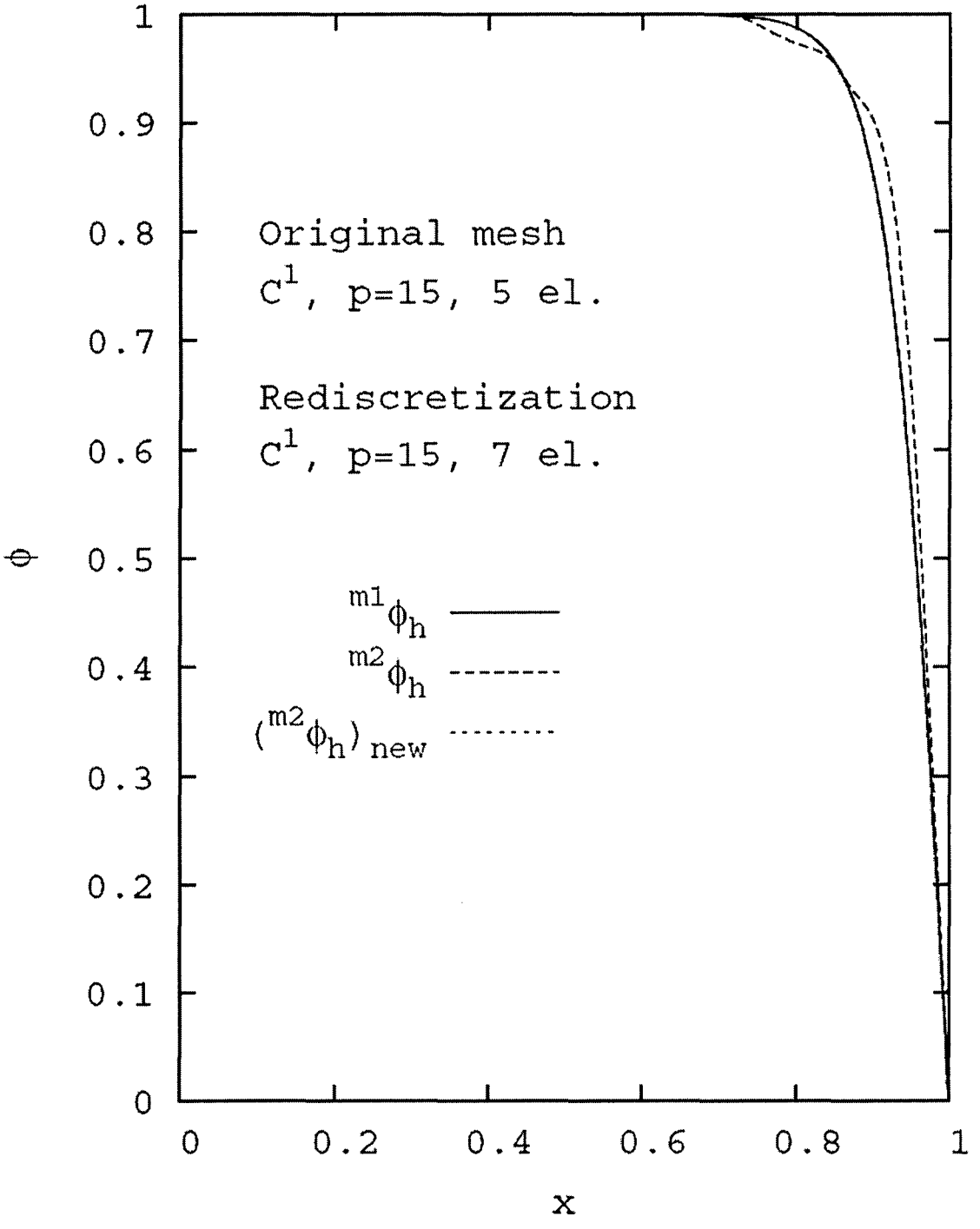

Figure 3.50: Burgers equation (BVP): ϕ versus x for original, mapped and new solutions.

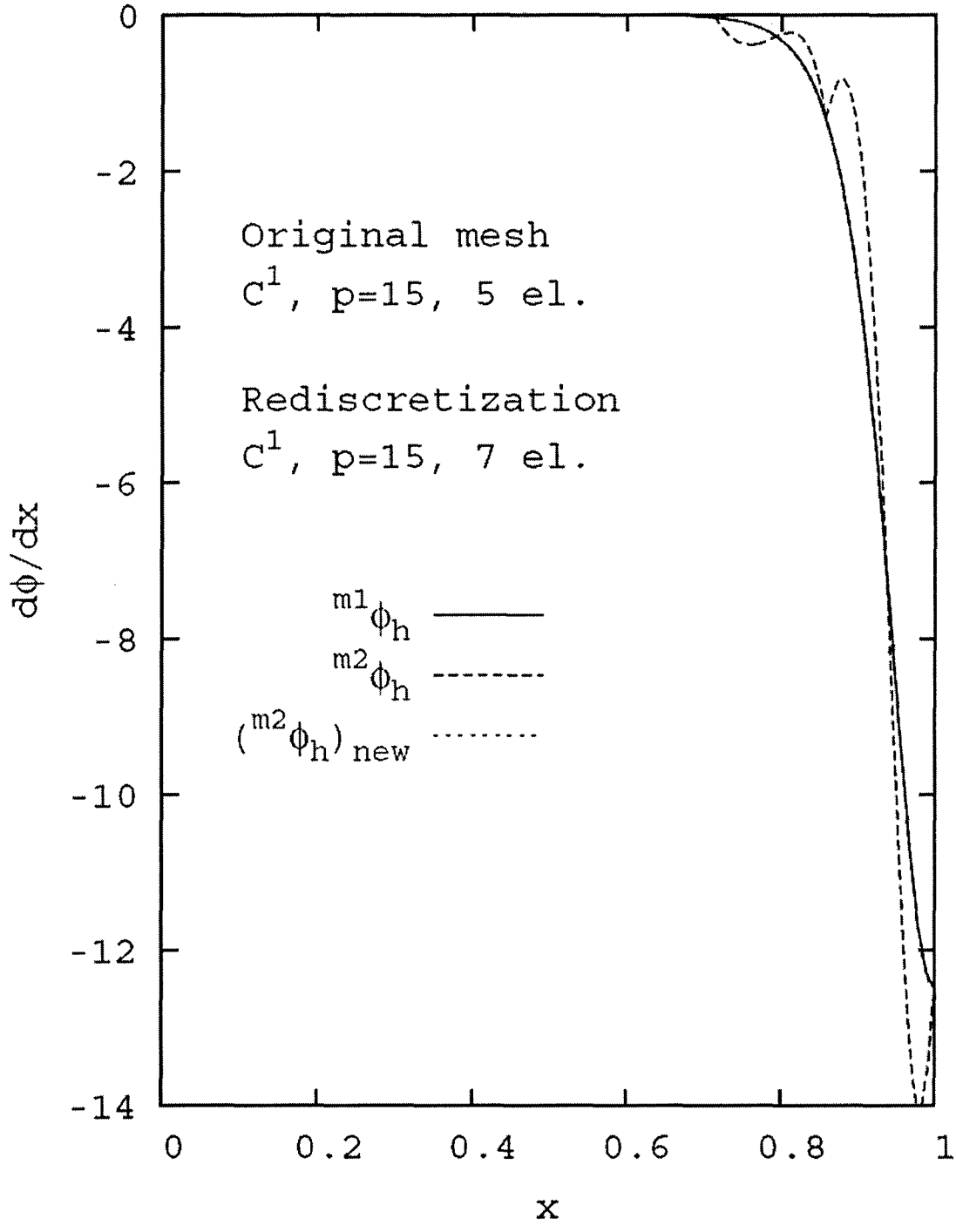

Figure 3.51: Burgers equation (BVP): $\frac{d\phi}{dx}$ versus x for original, mapped and new solutions.

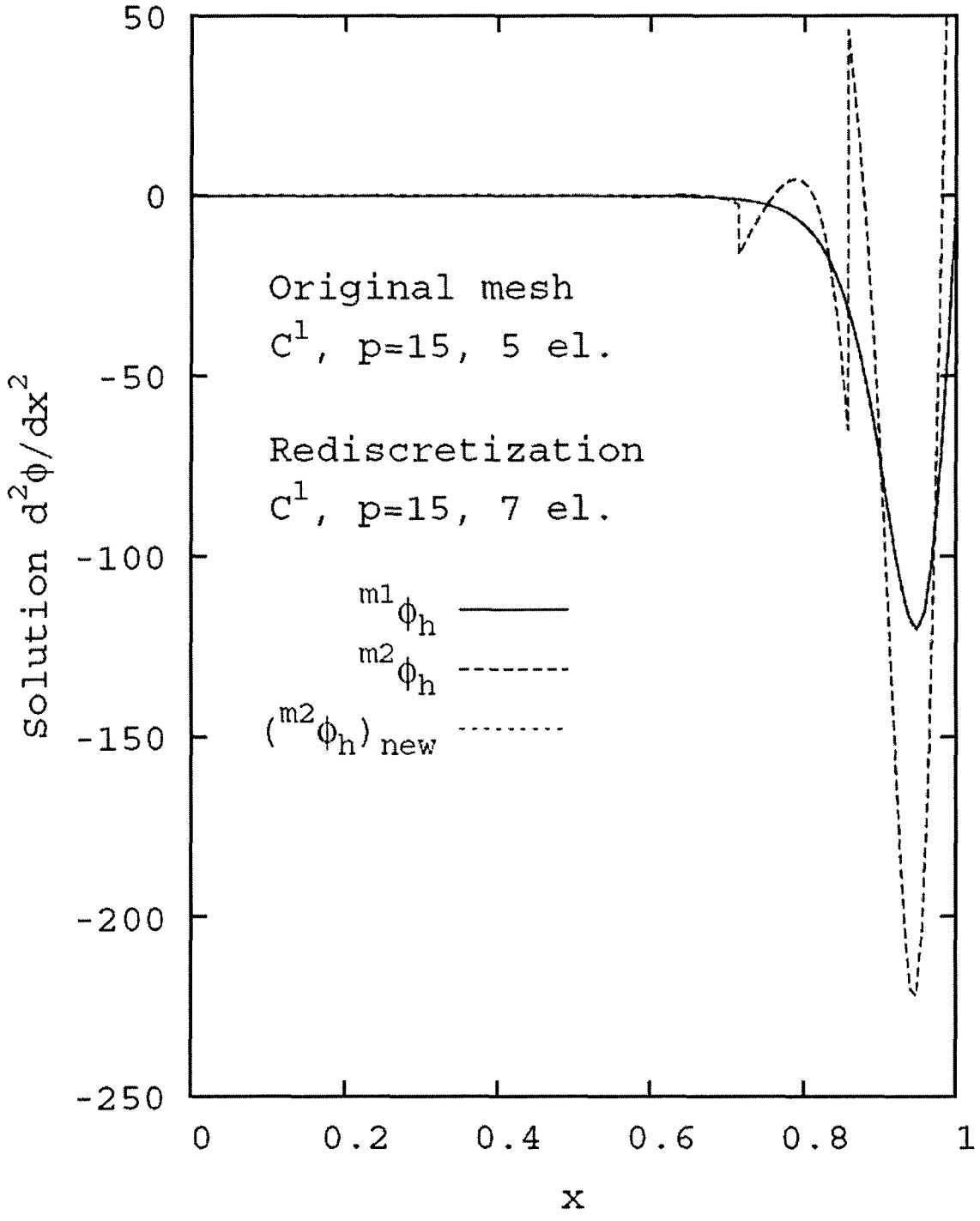

Figure 3.52: Burgers equation (BVP): $\frac{d^2\phi}{dx^2}$ versus x for original, mapped and new solutions.

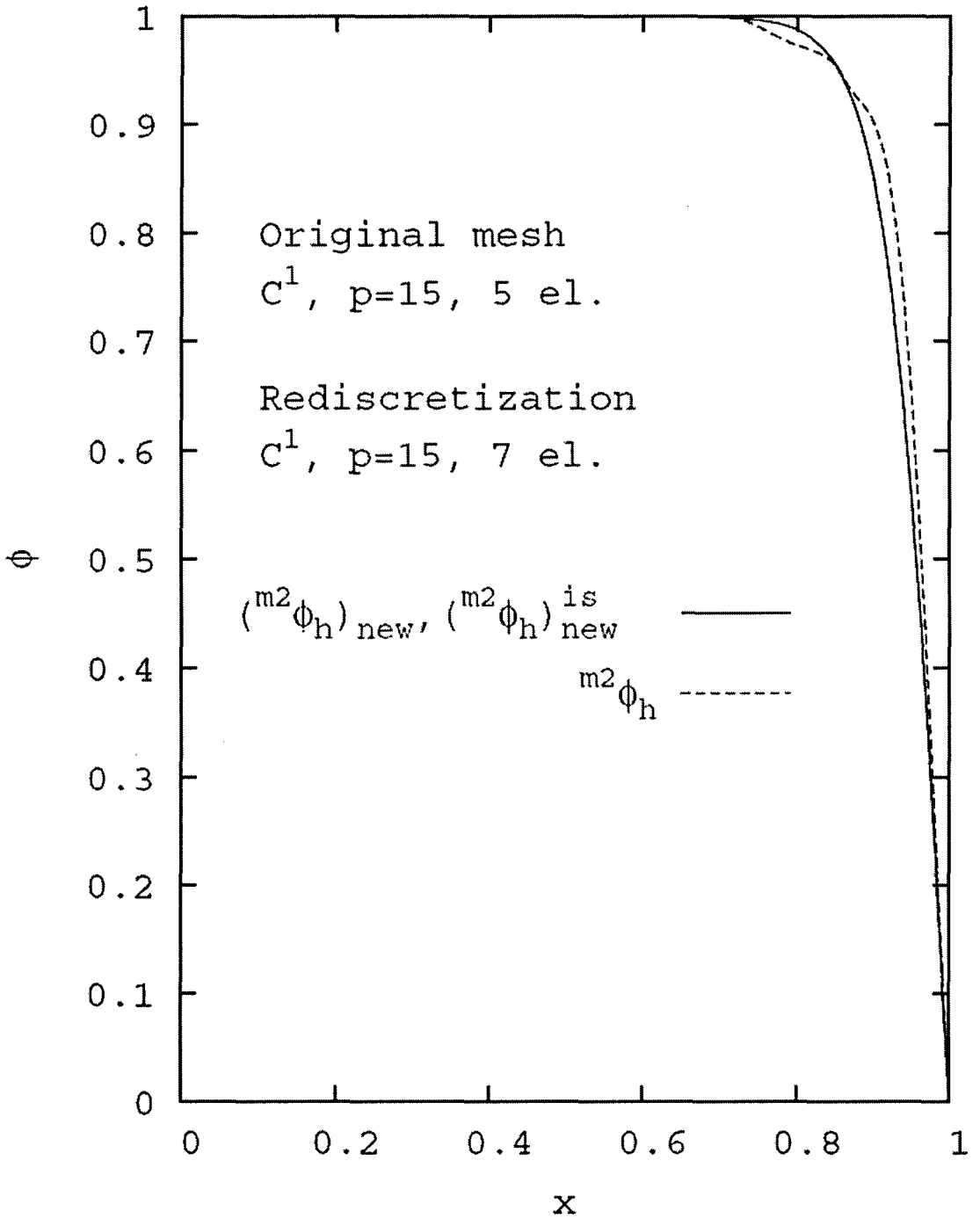

Figure 3.53: Burgers equation (BVP): ϕ versus x for mapped, new and new with initial solution.

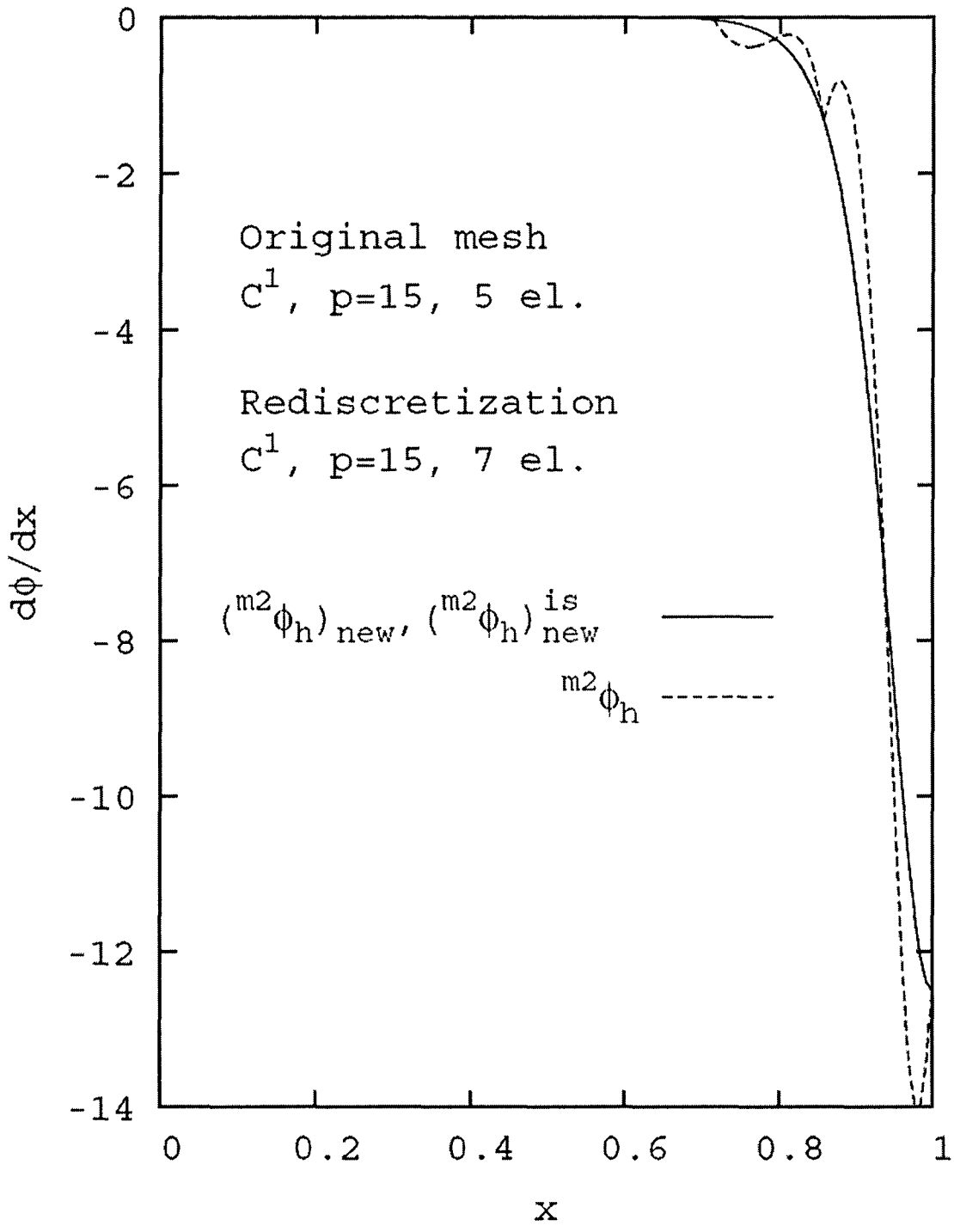

Figure 3.54: Burgers equation (BVP): $\frac{d\phi}{dx}$ versus x for mapped, new and new with initial solution.

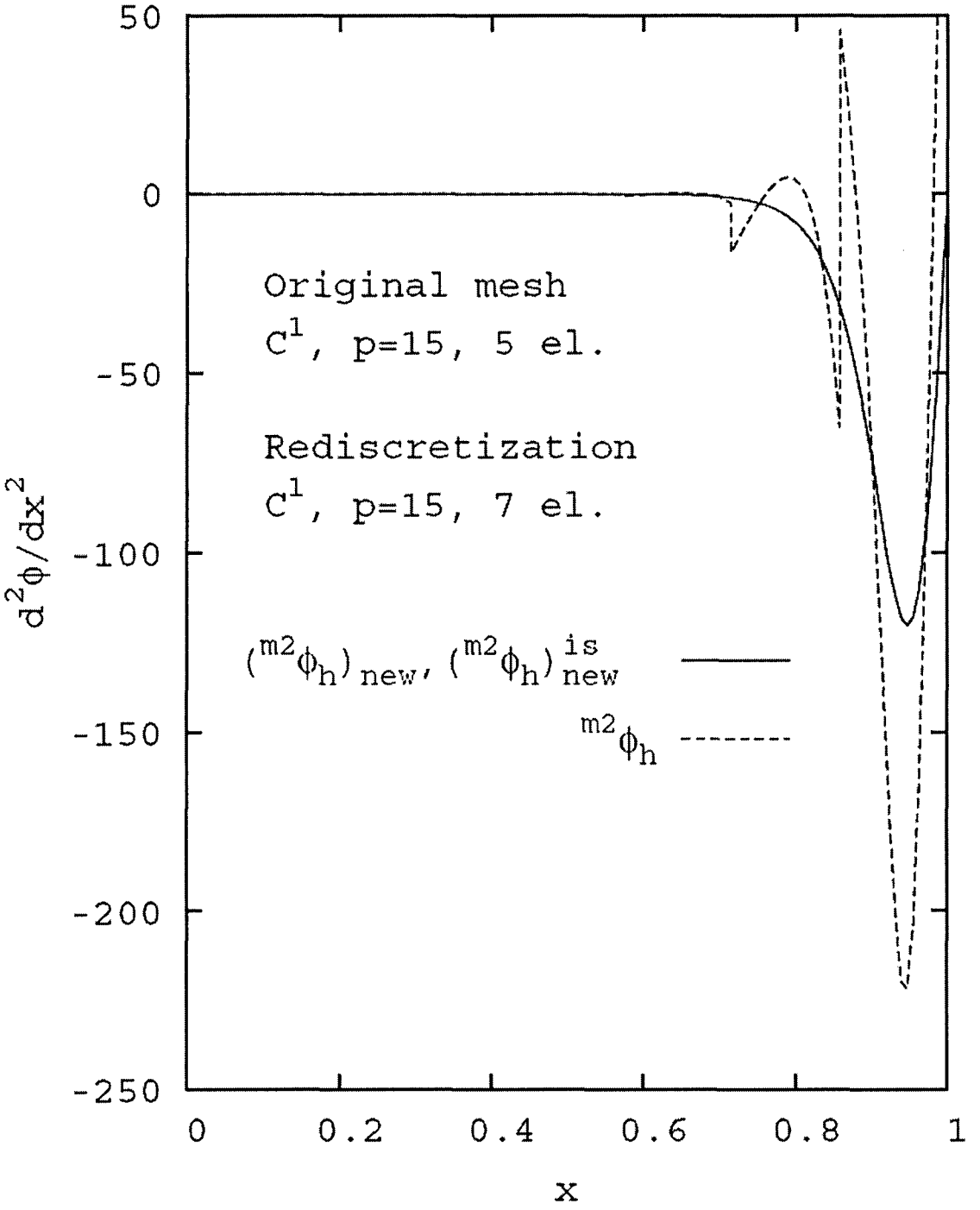

Figure 3.55: Burgers equation (BVP): $\frac{d^2\phi}{dx^2}$ versus x for mapped, new and new with initial solution.

3.6 Moving Mesh 1D IVP: Transient Convection Diffusion Equation ($Pe = 10^6$)

We consider the following transient convection diffusion equation

$$\frac{\partial \phi}{\partial x} + \frac{\partial \phi}{\partial t} - \frac{1}{Pe}\frac{\partial^2 \phi}{\partial t^2} = 0 \quad in \quad \Omega_x \times \Omega_t = (0,1) \times (0,\tau) \tag{3.4}$$

with

$$\phi(0,t) = 0 \; \phi'(0,t) = 0$$

$$\phi(x,0) = exp(-\frac{(x-x_0)^2}{2\sigma_0^2}) \tag{3.5}$$

where x_0 and σ_0 are the mean and standard deviation of the Gaussian distribution and are chosen to be 0.2 and 0.03, respectively. We consider the first and subsequent space-time strips shown in Figure 3.56. Discretization details for the first and subsequent space-time strips are also shown in Figure 3.56. The spacial discretization in zone B is chosen such that the initial conditions described by the Gaussian distribution are resolved accurately. Upon evolution, this disturbance (I.C.) moves into zone C in which the discretization is of the same refinement as in zone B and hence will yield time accurate evolution. A time step Δt of 0.02 is considered. For the second space-time strip the discretization is moved in the spatial direction by $\Delta x = 0.02$, which is in conformity with the speed of propagation of the disturbance. The solution from the open boundary of the first space-time strip is mapped as I.C. for the second space-time strip and the time evolution is computed. This process is continued for each increment of time until $t = \tau$ is reached ($\tau = 6\Delta t = 0.12$). Since the local approximations are of class $C^{1,1}$ with p-level of three in space and time, there are no hierarchical dofs at the mid-side and center nodes of the space-time elements, and furthermore, since the solution for the first space-time strip is converged, we expect the I.C. map of the solution for all space-time strips to be good. Time evolution of the solutions is shown in Figure 3.57. At $Pe = 10^6$, the physical diffusion is insignificant and hence we expect the Gaussian distribution to march in time without amplitude decay or base elongation as shown in Figure 3.57.

Remarks

(a) The moving mesh procedure permits relatively coarser discretization for $\bar{\Omega}_x$ of $\bar{\Omega}_{xy} = \bar{\Omega}_x \times \bar{\Omega}_t$.

(b) Highly refined meshes in the area of high solution gradients and relatively coarser meshes elsewhere are more practical and are in conformity with what is necessitated by the physics.

(c) In this approach, a micro disturbance and its propagation can be resolved over a macro domain without excessive computational effort.

(d) The approach requires accurate mapping of the I.C. regardless of the nature of the differential operator. The initial solution approach presented for non-linear BVPs to improve the mapped solution cannot be used for IVPs and moving mesh approach due to the fact that I.C. are fixed and hence cannot be altered during evolution. This does present a problem when p-levels higher than minimally conforming for the chosen order of the approximation space are used due to inaccuracies in the map of the hierarchical dofs. Further work to alleviate this problem is in progress. Initial studies are promising.

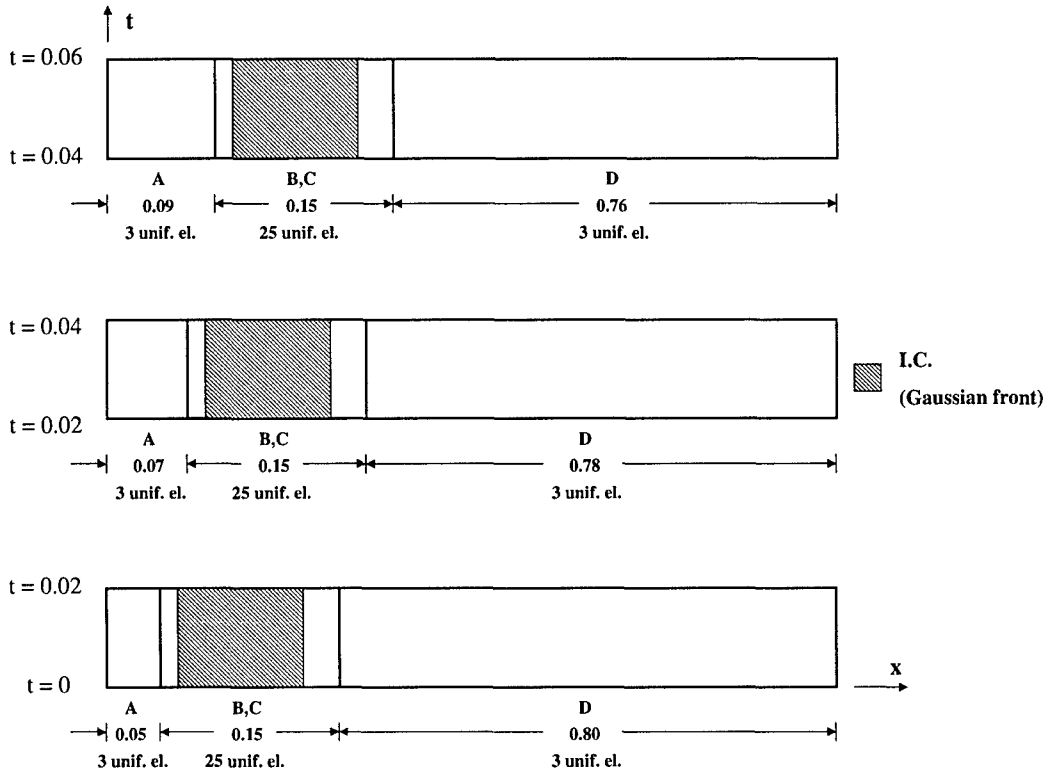

Figure 3.56: First three moving mesh space-time strips for transient convection diffusion equation.

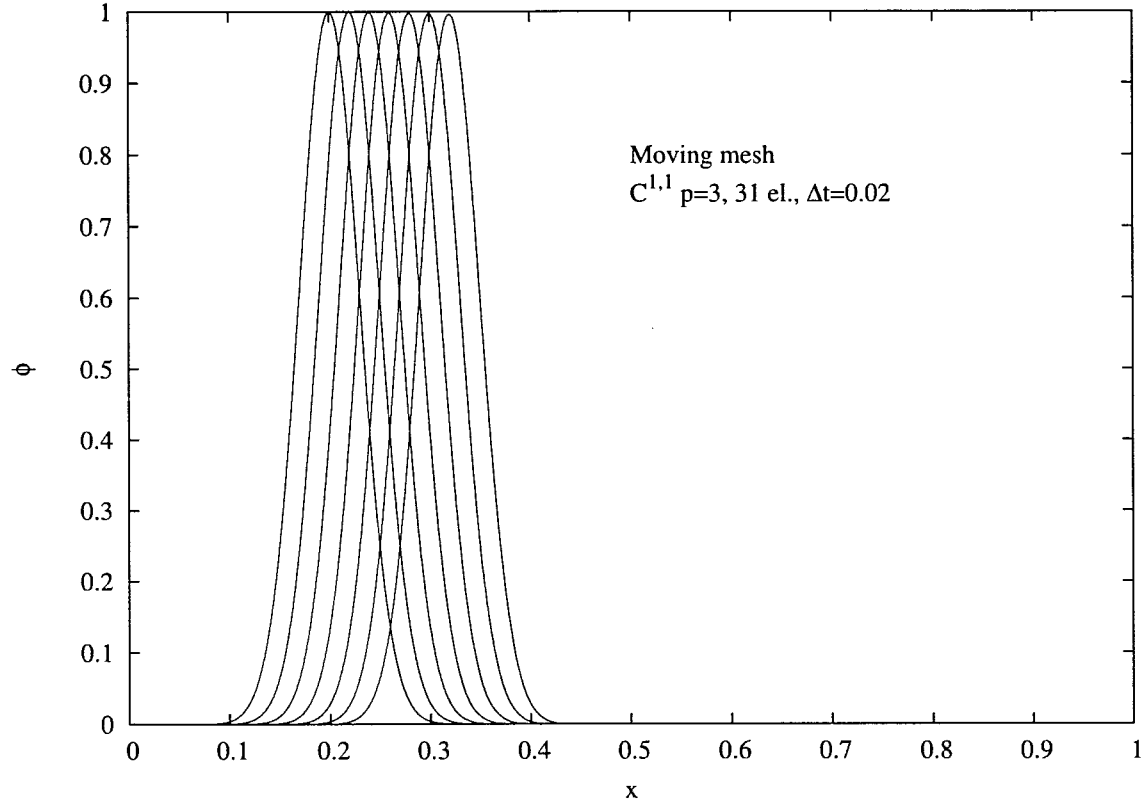

Figure 3.57: Transient convection diffusion equation (IVP): ϕ versus x for first six increments of time.

Chapter 4

Summary and Conclusions

Rediscretization, moving mesh and solution mapping approaches are presented for BVPs and IVPs. These methodologies essentially require two basic steps. In the first step, the geometry of the new discretization is mapped onto the existing discretization . In the second step, the solution from the existing discretization is mapped onto the new discretization or rediscretization using the geometry map form step one. In the following, we summarize the work presented here and draw some conclusions.

(1) In the case of BVPs, rediscretization requires a total map of the new discretization onto the existing mesh and then a total map of the solution from the current or existing discretization to the new discretization or rediscretization.

(2) In the case of IVPs, using space-time strips and space-time time marching, only a map of the geometry of the boundary requiring initial conditions onto the the open boundary of the previous or existing space-time strip is required. Using this map, the computed solution at the open boundary of the current space-time strip is mapped onto the boundary of the moved space-time strip that requires initial conditions.

(3) Except the basic difference discussed in (1) and (2), the mapping procedures for the geometry and the solution for rediscretization (for BVPs) and moving meshes (IVPs) are the same.

(4) First we consider rediscretization for BVPs.

(a) Mapping of the rediscretization geometry onto the existing discretization is always exact and unique when quadratic mapping is assumed for the subdomains between the physical coordinate space $x, (x, y)$ or (x, y, z) and $\xi, (\xi, \eta)$ or (ξ, η, ζ)

(b) Accuracy of the map of the solution from the existing discretization onto the rediscretization depends upon the type of local approximations.

(b1) When local approximations are of class C^0 Lagrange type in which only function values are nodal degrees of freedom, the solution mapping procedure presented here is good and free of any assumptions or approximations. If an unconverged solution is mapped, then the error maps in the two discretizations are not unique. More specifically, in the case of C^0 local approximations, magnitudes of inter-element jumps in the solution derivatives normal to the inter-element boundaries and their locations in the two maps are different. Thus, inter-element flux problems exist in both solutions as widely reported in the literature. We clearly observe that inter-element flux problems in the mapped solution are to to the inter-element flux problems in the solution for the original discretization. When weakly converged solutions are mapped, maps of the solution and its first derivative remain good, implying a lack of serious inter-element flux problems. These findings hold true for $p = 1$ as well as higher p-level Lagrange elements in 1D as well as 2D.

(b2) When the local approximations are of class C^0 p-version hierarchical, the solution map onto the rediscretizations require mapping of higher order derivatives with respect to ξ and η (1D and 2D BVPs). Due to the C^0 nature of the global approximations, direct mapping of the degrees of freedom using local approximations of the subdomains of the original discretization leads to substantial inaccuracies in the mapped solution. These inaccuracies or errors increase with increasing p-level (corresponding to higher order derivatives with respect to ξ and η). An alternative procedure has been proposed to overcome this difficulty, in which the solution is first mapped onto the corresponding C^0 Lagrange configurations that only requires function values and then the hierarchical dofs are recovered from these configura-

tions. With this procedure, we expect solution maps for C^0 p-version hierarchical local approximations to be good.

(b3) In the case of C^j; $i = 1, 2, \ldots$ higher order continuity 1D local approximations, there are no problems with the solution map when minimally conforming p-levels are used. p-levels higher than minimally conforming yield inaccurate solution maps due to inaccuracies in the mapping of hierarchical dofs. This problem can also be corrected using the corresponding C^0 Lagrange configurations (work in progress). In the case of 2D higher-order continuity local approximations, preliminary studies indicate that for $C^{1,1}$ solutions, the mapping inconsistencies in $\frac{\partial \phi}{\partial x \partial y}$ at the corner nodes are minimized when minimally conforming p-levels are used. However, for $C^{2,2}$ and higher order continuity approximations, these inconsistencies occur in more dofs at the corner nodes even when minimally conforming p-levels are used. Further work is needed to resolve these issues (work in progress).

(5) In the case of moving meshes, the computations work exceptionally well when

(i) Only converged solutions from the current space time strip are used to determine initial conditions for the subsequent space-time strip in which the mesh has been moved spatially.

(ii) The solution mapping process is free of errors and inaccuracies.

(iii) The initial conditions are resolved accurately and sufficient resolution is provided ahead of the front for its accurate time evolution over the space-time strip.

(6) When the mapping procedure for BVPs results in errors in the mapped solution caused by using non-weakly converged solutions or due to inaccurate maps of the hierarchical dofs, the situation is critical when the differential operators are self-adjoint or non-self adjoint due to the fact that in both bases the differential operators are linear and there is no further mechanism to improve the mapped solution. When the differential operators are non-linear, the inaccurate mapped solution can be used as a starting or initial solution for the rediscretization and the Newton's method with line search can be used to obtain the new or 'correct'

solution for the rediscretization. This solution always identical to the solution that one would obtain if new computations were done for the rediscretization. This feature is powerful in the sense that it permits us to eliminate the mapping errors in the solution map onto the rediscretization. In the case of IVPs, the situation is slightly different due to the fact that there appears to be no such mechanism to eliminate the inaccuracies in the map of the hierarchical dofs for the initial conditions due to the fact that initial conditions are fixed. Thus, for IVPs an accurate map of the initial conditions for the moved mesh is essential for accurate time evolutions.

(7) Benefits of higher-order continuity local approximations are clearly demonstrated. When local approximations of class C^j are weakly converged, the solution maps contain accurate values of the solution and its derivatives up to order $j+1$. This is only possible in the h-p-k framework.

(8) Numerical studies presented for 1D and 2D BVPs and 1D IVPs demonstrate various features of rediscretizations and moving mesh procedures proposed in this work. Possible remedies have been suggested to overcome the mapping inaccuracies in hierarchical dofs and higher-order continuity local approximations. Preliminary studies are promising. With the procedures proposed here, large deformation large strain studies for solid mechanics can be done accurately using the total Lagrangian approach. Moving fronts for IVPs can be simulated using coarser spatial discretizations. Lastly, it is envisioned that simulations of moving micro fronts on a macro scale will be possible using the moving mesh procedure proposed here. Simulation of moving shocks in a Riemann shock tube of actual physical dimensions is an example of such physics.

Bibliography

[1] K.S. Surana, S. Allu and J.N. Reddy, *The k-version of the finite element method for initial value problems: mathematical and computation framework* Computational Methods in Engineering Science and Mechanics, (in review).

[2] K.S. Surana, A.R. Ahmadi and J.N. Reddy, *The k-version of the finite element method for self-adjoint operators in BVPs*, Int. J. Comp. Eng. Sci., vol. 3, no. 2, 155-218, 2002.

[3] K.S. Surana, A.R. Ahmadi and J.N. Reddy, *The k-version of the finite element method for non-self-adjoint operators in BVPs*, Int. J. Comp. Eng. Sci., vol. 4, no. 4, 737-812, 2003.

[4] K.S. Surana, A.R. Ahmadi and J.N. Reddy, *The k-version of the finite element method for self-adjoint operators in BVPs*, Int. J. Comp. Eng. Sci., vol. 5, no. 1, 133-207, 2004.

[5] *Computational Methods for Transient Analysis*, vol. 1, North-Holland, 1992, edited by T. Balytschko and T.J.R. Hughes.

[6] Keith Miller and Robert N. Miller, *Moving finite elements I*, SIAM J. Num. Anal., vol. 18, 1019-1032, 1981.

[7] Keith Miller and Robert N. Miller, *Moving finite elements II*, SIAM J. Num. Anal., vol. 18, 1033-1057, 1981.

[8] M.J. Baines, *Moving Finite Elements*, Clarendon Press, Oxford, 1994.

[9] J.N. Reddy, *An Introduction to Finite Element Methods*, second edition, McGraw-Hill, New York, 1993.

[10] K.S. Surana, S.R. Petti, A.R. Ahmadi and J.N. Reddy, *On p-version hierarchical interpolation functions for higher order continuity finite element models*, Int. J. Comp. Eng. Sci., vol. 2, no. 4, 653-673, 2001.

[11] A.R. Ahmadi, K.S. Surana and J.N. Reddy, *Higher order global differentiability approximations for 2D distorted element geometries*, Presented at the 7^{th} World Congress on Computational Mechanics, Los Angeles, California, 2007.

[12] B.A. Finlayson, *Numerical methods for problems with moving fronts*, Ravenna Park Publishing Inc., Seattle, Washington 1992.